

2025 Conference 4th - 5th June 2025





2025 Conference 4TH - 5TH JUNE 2025

PROGRAMME

DAY 1 04 June

WEDNESDAY

09:00 – 09:30	Registration	
09:30 - 09:45	Welcome by Local Organizer and Opening Speech University of the Basque Country	Radmila Tomovska
09:45 – 10:00	Introduction by Action Chair HISTRATE - A route to certification-by-analysis for impact- loaded aeronautical composite structures	Patricia Verleysen
10:00 - 10:45	Keynote Speech Crashworhiness of Fuselage Hybrid Structure	Michel Mahe Laurent Risse
10:45 – 11:15	COFFEE BREAK	
11:15 – 12:45	Session 1 - Novel simulation methods and best practices for composites under high strain rates (WG4)	Chair: Nenad Djordjevic
11:15 – 11:30	High Strain Rate Behaviour of Ceramic - Polymer Sandwich Composite Systems; Numerical and Experimental Study	Ali Rashed, online
11:30 – 11:45	Optimisation of AS4 8552 Woven Composite Lamina Under Out of Plane Impact Loading	Ezgi Bakır
11:45 – 12:00	Strain Rate Dependent 3D Shear Characteristics of Thermoplastic FRC - Experiments, modelling and analysis by machine learning	Andreas Hornig
12:00 – 12:15	Modeling the High Strain Rate Behavior of Graphene Epoxy Nanocomposites Using Viscoplasticity Theory and Mori Tanaka Homogenisation	Özgen Çolak Çakır
12:15 - 12:30	Lessons Learned from Virtual Certification of an Aircraft Structure Against Birdstrike	Michele Meo
12:30 - 12:45	Modeling and Characterisation of UD Thermoplastic	Nenad Djordjevic

12:45 – 14:00 LUNCH BREAK











2025 Conference 4TH - 5TH JUNE 2025

PROGRAMME

DAY 1 04 June

WEDNESDAY

14:00 – 15:00	Poster session with 3 minute pitches	Chair: Hatice Sinem Şaş Çaycı
15:00 – 16:00	COFFEE BREAK with POSTER SESSION	
16:00 – 18:00	Session 2 - Novel composite materials for high strain rate applications (WG3)	Chair: Mauro Zarrelli / Thanasis Kotzakolios
16:00 – 16:15	Fracture Toughness of Survey of CF - LMPAEK Thermoplastic Composite via High-Speed Wedge Insert Fracture Method towards Stiffened Panel Design and Verification	Thomas Zaragkas
16:15 – 16:30	Effect of Rubber Interleaving on the Charpy Impact Properties of Basalt Fiber Reinforced Polymers	Çağatay Yılmaz
16:30 – 16:45	Enhancing Impact Resistance in Recycled Composite Materials for Aerospace Applications: The Role of Strand Morphology and Sandwich Structures	Hatice Sinem Şaş Çaycı
16:45 – 17:00	Enhanced Impact Resistance of 3D Spacer Composite by Hybridisation with CF Sheets	Volkan Eskizeybek
17:00 – 17:15	Charpy Impact Performance of S2 Glass/Basalt Fiber Reinforced Hybrid Composites	Sara S. A. Eltahir, online
17:15 – 17:30	Span Length Effect on Strain Rate and Flexural Performance of Natural Fibre Reinforced In-Situ Polymerisable Composite	Mohamad Alsaadi
17:30 - 17:45	Hydrothermal Ageing Effects on Basalt Fibre-epoxy Composites Modified with Star-like Polymers	Tatjana Glaskova- Kuzmina
 17:45 - 18:00	Effect of Carbonaceous Fillers on Interlaminar and Compression After Impact (CAI) Properties of Aeronautical CFRP	Mauro Zarrelli

CONFERENCE DINNER







19:30





2025 Conference

PROGRAMME

4TH - 5TH JUNE 2025

DAY 2 05 June

THURSDAY

08:45 - 09:00 Registration

09:00 - 10:30 Industry Session on Certification of Composite Products Chair: Michele Meo & Jens

Meo & Jens Wiegand

09:00 - 09:45 **Keynote speech -** Developing Composite (and other advanced manufactured) product certification - a regulator's perspective

Simon Waite -ONLINE

09:45 – 10:15 **Invited Speaker -** Powerplant Extreme Events Simulations: Impact on Certification

Giuseppe Zumpano -ONLINE

10:15 - 10:30 Thoughts and Examples on Certification by Analysis in Impact Loading of Composite Structures

Andre Haufe

10:30 - 11:00

COFFEE BREAK

11:00 – 12:15 Session 3 - Multi-modal sensing for impact detection and

Chair: Rohan Soman

damage characterisation (WG5)

Thanasis

11:00 – 11:15 Hybrid AI for Impact Detection in Polymeric Plate

Kotzakolios

11:15 – 11:30 Impact Damage Identification in GFRP Structures Using the Effective Boundary Approach

oarar / urmaer

11:30 – 11:45 Full Wave Field Analysis of Damage Severity for the Impacted

Pawel Malinowski

thermoplastic Composite

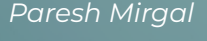
11:45 – 12:00 Identification of Impact damage in Sandwich Composite

Andrzej Katunin

Structures Using High-Speed 3D Digital Image Correlation and
Wavelength Analysis

12:00 - 12:15 Impedance Based Structural Health Monitoring for Multi-Impact

Damage Classification in PLA Plates





UNIVERSITY OF THE BASQUE COUNTRY, SAN SEBASTIAN, SPAIN

radmila.tomovska@ehu.es









2025 Conference

PROGRAMME

4TH - 5TH JUNE 2025

DAY 2 05 June

THURSDAY

12:15 – 13:00	Session 4 - Advanced testing and instrumentation for composites under high strain rates (WG6)	Chair: Andrei Anisimov
12:15 – 12:30	Integration of Optical Measurements in Standard Hopkinson bar Data Treatment	Marco Peroni
12:30 – 12:45	Common Path Polarisation Electronic Speckle Pattern Interferometry for Dynamic Deformation Analysis	Violeta Madjarova
12:45 – 13:00	Next Generation Dynamic Testing of Composites: A Review	Briek Luyten
13:00 – 14:00	LUNCH	
14:00 – 14:30	Session 4 - Advanced testing and instrumentation for composites under high strain rates (WG6) - continued	Chair: Tatjana Glaskova- Kuzmina
14:00 – 14:15	Elements for a Roadmap for Standardisation of High Strain Rate Testing of Composite Materials	Andrei Anisimov
14:15 – 14:30	Overview of Available Standards on High Strain Rate Testing	Marco Peroni
14:30 - 15:00	COFFEE BREAK with POSTER SESSION	
15:00 - 16:00	HISTRATE Use Cases	Chair: Michele Meo
15:00 – 15:15	Use Case 1: Infrared Curing of Composites	Thanasis Kotzakolios
15:15 - 15:30	Use Case 2: Thermoplastic Composites with in-situ Consolidation	Svetlana Risteska (online)
15:30 – 15:45	Use Case 3: Tailored Interlaminar Composite Properties	Andreas Hornig
15:45 - 16:00	Use Case 4: Bird Strike	Michele Meo
16:00 - 16:15	SUMMARY AND FAREWELL	Elena Stoykova





Radmila Tomovska







2025 Conference

PROGRAMME

4TH - 5TH JUNE 2025

Poster Presentations

Büşra Osma Investigation of Strength Properties of Polymer Based Carbon fiber-reinforced plastic (online) (CFRP) and glass fiber-reinforced plastic (GFRP) Composites as Experimental and

Numerica

Sara Srebrenkoska The effect of laser assisted tape placement processing conditions on flexural strength of insitu carbon fibre/PEEK laminates

Aleksandre Development of Basalt Based Fiber-Metal Laminates and Analysis of Their Mechanica Vanishvili Properties

Sevtlana Risteska Influence of some technological parameters in the content of voids on the in-situ

Vineta Ballistic strength of polyethylene composites based on directional and unidirectional fibres Srebrenkoska under the high-speed ballistic impact

Nikoloz Chikhradze Response of sandwich structure containing aluminum honeycomb to the contact

Matej Micusik Elastomer composites with hybrid carbon fillers

Ana Cristina Thermo-reversible Diels-Adler polyurethane adhesives for sustainable composite bonding Restrepo Montoya

Jadranka New Composite Materials with enhanced mechanical properties Blazhevska Gilev

Abdulkadir Sezai Thermomechanical properties of electrospun polyacrylonitrile nanofibers with embedded Saraç magnetic nanoparticles in a magnetic field

Rohan Soman Impact localisation in a CFRP plate with unknown material properties

Maciej Radzienski Delamination detection in complex composite laminates using guided wave conversion

Tomasz Rogala Detection of subsurface damage caused by impact in CFRP composites using an eddy

Elena Stoykova Numerical simulation tool for speckle-based NDT systems: ESPI, shearography and laser speckle photometry

Yüksel Çakır A study on specimen dimension for standardisation of the split Hopkinson pressure bar test











2025 Conference

PROGRAMME

4TH - 5TH JUNE 2025

Speakers*

NAME ORGANISATION

Radmila Tomovska	University of Basque Country	
Patricia Verleysen	Ghent University	Tat
Michel Mahe	Airbus France	
Laurent Risse	Airbus France	
Ali Rashed	Sabancı University	
Ezgi Bakır	Istanbul Technical University	
Andreas Hornig	TUD Dresden University of Technology	
Özgen Çolak Çakır	Yıldız Technical University	
Michele Meo	University of Southampton	
Nenad Djordjevic	Brunel University	
Thomas Zaragkas	University of Patras	
Çağatay Yılmaz	Abdullah Gül University	
Hatice Sinem Sas	University of Sheffield	
Volkan Eskizeybek	Canakkale Onsekiz Mart Üniversitesi	
Saeed Abdulrahman Eltahir	Abdullah Gül University	
Rohan Soman	Polish Academy of Sciences	

^{*} listed per order of talks

Sara

UNIVERSITY OF THE BASQUE COUNTRY, SAN SEBASTIAN, SPAIN

NAME ORGANISATION

Mohamad Alsaadi	Technological University of the Shannon
atjana Glaskova-Kuzmina	University of Latvia
Mauro Zarrelli	CNR - National Research Council of Italy
Simon Waite	EASA
Giuseppe Zumpano	Rolls Royce UK
André Haufe	DYNAmore GmbH, an Ansys Company
Thanasis Kotzakolios	University of Patras
Jafar Amrei	Silesian University of Technology
Pawel Malinowski	Polish Academy of Sciences
Andrzej Katunin	Silesian University of Technology
Paresh Mirgal	Polish Academy of Sciences
Marco Peroni	European Commissiin
Violeta Madjarova	Bulgarian Academy of Sciences
Briek Luyten	Ghent University
Andrei Anisimov	TU Delft
Svetlana Risteska	Goce Delcev University
Elena Stoykova	Bulgarian Academy of Sciences











2025 Conference

4TH - 5TH JUNE 2025

PROGRAMME

Speakers*

NAME

Büşra Osma

Sara Srebrenkoska

Aleksandre Vanishvili

Sevtlana Risteska

Vineta Srebrenkoska

Nikoloz Chikhradze

Matej Micusik

Ana Cristina Restrepo Montoya

Jadranka Blazhevska Gilev

Abdulkadir Sezai Saraç

Rohan Soman

Maciej Radzienski

Tomasz Rogala

Elena Stoykova

Yüksel Çakır

ORGANISATION

Yıldız Technical University, Türkiye

Goce Delcev University, Macedonia

Grigol Tsulukidze Mining Institute, Georgia

Goce Delcev University, Macedonia

Goce Delcev University, Macedonia

Grigol Tsulukidze Mining Institute, Georgia

Slovak Academy of Sciences

University of the Basque Country

Ss. Cyril Methodius University in Skopje

Istanbul Technical University

Polish Academy of Sciences

Polish Academy of Sciences

Silesian University of Technology

Bulgarian Academy of Sciences

Istanbul Technical University









Preface

We present the Book of Abstracts for the Second HISTRATE Conference — Advanced Composites under HIgh STRAin rates Loading: A Route to Certification-by-Analysis, held from June 4 to 5, 2025, in San Sebastian, Spain. Following the enthusiastic response to the first edition of HISTRATE conference, this year's event reaffirms its role as a dedicated forum for specialists working at the intersection of composite materials, dynamic loading, and computational certification methodologies. Nestled between the rolling green hills of the Basque Country and the sparkling waters of the Bay of Biscay, San Sebastián offers a stunning setting for intellectual exchange.

As advanced composite materials play an increasingly central role in industries such as aerospace, automotive, defense, marine, and renewable energy where lightweight, high-performance, and impact-resistant structures are vital. The accurate understanding of their behavior under high strain rate conditions has become both a scientific and engineering imperative. In parallel, the concept of certification-by-analysis is gaining momentum as an efficient, reliable, and cost-effective alternative to traditional testing regimes. This shift relies fundamentally on the development of validated, high-fidelity numerical models capable of predicting material and structural responses under dynamic events with confidence.

The HISTRATE conference series was started to bring together an international community of researchers, engineers, industry representatives, and regulatory stakeholders to exchange knowledge, share new methodologies, and discuss both the advances achieved and the hurdles yet to be overcome in the domain of composites. The 2025 edition focuses particularly on integrating experimental, numerical, and analytical approaches to support and accelerate the transition towards certification-by-analysis for composite structures subjected to high strain rate loading.

This Book of Abstracts reflects the diversity, depth, and forward-looking spirit of the conference. It compiles contributions from 35 universities, 11 academic research centers, and 5 industrial research centers, covering a broad spectrum of topics. These include innovative experimental techniques for dynamic characterization, advances in constitutive modeling and failure criteria under high strain rates, multiscale simulation approaches, novel composite architectures for improved dynamic performance, and strategies for integrating numerical predictions into certification pathways. Emerging themes such as the use of artificial intelligence and machine learning in high-strain-rate material modeling, and the role of uncertainty quantification in predictive simulations, are also represented. The conference united authors from Belgium (2), Bulgaria (2), Czech Republic (3), Cyprus (1), France (1), Georgia (2), Germany (3), Greece (3), Ireland (1), Italy (5), Latvia (2), Lithuania (1), The Netherlands (2), North Macedonia (5), Poland (7), Slovakia (2), Turkiye (12), UK (9). One third of the corresponding authors are early career researchers.

The conference program features keynote lectures by experts from industry, technical sessions and poster presentations organized around thematic tracks in the COST CA21155 Working groups and the Action use cases, including research from early-career scientists. This dynamic format is designed to foster both formal and informal exchanges, encouraging collaborations that extend beyond the conference itself.

We wish to thank all the authors for their valuable contributions, the reviewers for their thorough evaluations, and the members of the organizing and scientific committees for their tireless work in shaping this conference. Special recognition is also due to our host from University of the Basque Country for their organizing efforts and generous support.

We believe this collection of abstracts will serve not only as a useful reference but also as a lasting record of the ongoing efforts to push the boundaries of composite material technology and certification practices under dynamic loading conditions.

The HISTRATE 2025 Organizing Committee



2025 Conference 4th – 5th JUNE 2025

Session 1 - Novel simulation methods and best practices for composites under high strain rates (WG4)





High Strain Rate Behavior of Ceramic – Polymer Sandwich Composite Systems; Numerical and Experimental Study

Ali Rashed 1*, Mojtaba Yazdani 2

¹ Faculty of Engineering and Natural Sciences, Sabanci University, Tuzla, Istanbul, Turkey, 34956

Abstract: In this research, we have studied the high-strain-rate behavior of ceramic-polymer sandwich-composites under impact conditions. The research includes numerical study in Ansys-APDL and LS-Dyna; and experimental manufacturing technique of aqueous gel-casting for ceramics, and finally, testing of the sandwich-target with gas-gun steel projectiles. Various criteria are introduced to measure the impact resistance of the panel such as DOP, residual velocity, effective crushed mass, projectile erosion length, projectile stop-time, etc. The numerical and experimental results show that among various ceramic layups and polymer types, for specific mass or thickness, the equal-thickness dual-layered ceramic sandwich has the highest efficiency against impact load.

1. Introduction

The use of sandwich composites is of high interest in the field of impact engineering as it combines various properties of lightweight materials and produces impact resistant structures with high efficiency. Advanced ceramics are novel materials used for this purpose as the mechanism of the conical fracture of it enables the load distribution in larger area damping the intense impact load and converting from local to global response of the target. On the other hand, the polymeric layers are widely used materials as interlayers which transfer the load to the supporting blocks. In previous studies, the mechanism of ceramic sandwich structure was not investigated and the fracture conoid expansion was not analyzed in detail. Besides, the advanced manufacturing technique of aqueous gel-casting for ceramic production for any shape for high velocity impact purposes is not performed before. We have used both the materials in a sandwich composite to take advantage of them to increase the efficiency of the target. For this purpose, ceramic layers are sandwiched between the polymeric layers to transfer the impact wave step by step to backing layers causing impact force to distribute in larger areas and the fall of pressure magnitude gradually.

2. Numerical Simulation

In this paper, Finite element 2D-axisymmetric Lagrangian approach with Johnson-Holmquist constitutive model for ceramics, Mie-Gruneisen equation of state for polymers, and Johnson-Cook constitutive model for projectile are used [1-3]. We have proposed a simple naming code to easily identify the layup of the target. For example E(1.5-0.2) C(12-8-4) defines a sandwich panel with Epoxy interlayers of 0.2mm and Epoxy Backing layer of 1.5mm and Ceramic tiles of 12mm, 8mm, and 4mm from back to front plate (projectile impact plate), so the 4mm plate will be the first tile to be hit by the projectile. In Fig. 1, the fracture conoid mechanism of a sample ceramic tiles are depicted which is getting larger by extending to back layers.

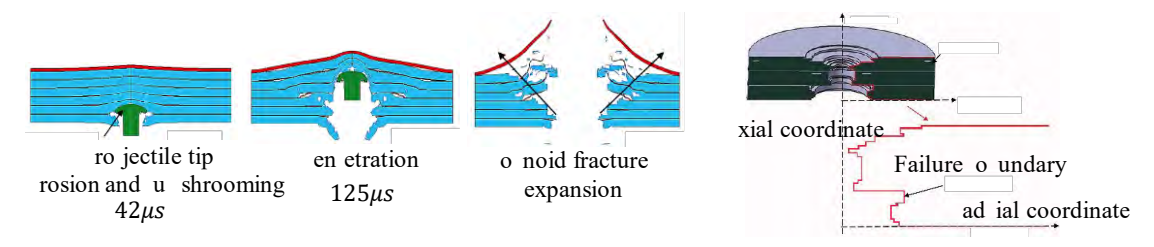


Fig. 1. Different stages of projectile impact to sandwich composite: a) projectile erosion and mushrooming, b) penetration, c) fracture conoid expansion in ceramic-polymer layers extending from layer to layer, d) fracture conoid boundary decreasing from front to mid, then increasing from mid to back (expansion mechanism).

The polymeric interlayers transfer the impact wave to back layers causing fracture in larger area. The failure boundary decreases to some extent then increases to larger area until back layer.

3. Manufacturing and Testing

The manufacturing part consists of Alumina ceramics produced with aqueous gel-casting method (Fig. 2). In this method, ceramic is formed in a gelation state which has the advantage of forming to flexible shapes, then it is sintered in high temperatures to reach high stiffness and hardness [4]. For the polymeric interlayers, we chose epoxy with hardener and glued it to the ceramic interfaces.

² Dynamic Behavior of Materials Research Laboratory, Tabriz university of technology (Sahand), P.O. Box 51335-1996, Tabriz, Iran *Email: rashed@sabanciuniv.edu

Fig. 2. q ueous gel-casting process of alumina ceramic

In the testing stage, the ceramics are prepared in one tile block and dual tiles block (each with half thickness of one tile block to maintain equal thickness) and then we tested them by gas-gun with flat steel projectile (Fig. 3).



Fig. 3. The illustration of a) ceramic blocks and epoxy specimen, b) testing gas-gun, c) impact chamber with speed camera, and d) back layer view of fractured block

4. Results and Conclusion

Various numerical studies are performed for sandwich blocks with 30 different layups with equal total thickness. The ballistic performance criteria are categorized with priority of residual velocity, then Depth of Penetration, Projectile eroded length, effective crushed mass of the target, and lastly, the stopping time of the projectile. In any similar case of residual velocity, 2nd criteria of DOP, and in the case of equality of that, the 3rd criteria and so on are used for ballistic measurement. The numerical and experimental tests show the highest efficiency of dual layered ceramic target with 0.2mm polymeric interlayers (Table 1).

Item	L yup	thick (mm)	$\rho_a \left(\frac{kg}{m^2}\right)$	$V_i\left(\frac{m}{s}\right)$	$V_r\left(\frac{m}{s}\right)$	T_s (ms)	DOP (mm)	L_e (mm)	M _{eff} (%)
1	E(1.5-0.2) C(4)6	26.5	94.16	830	129	-	-	15.46	-
2	(1.5-0.2) $(4)7$	30.7	109.6	830	0	0.3	27.31	18.95	
3	(1.5-0.2) (6)4	26.1	93.69	830	0	0.12	16.75	17.21	6.97
4	(1.5-0.2) $(8)3$	25.9	93.45	830	0	0.097	11.84	18.95	6.55
5	(1.5-0.2) (4-8-12)	25.9	93.45	830	0	0.08	10.21	19.83	5.99
6	(1.5) (24)	25.5	92.97	830	0	0.95	9.62	21.57	4.45
7	(1.5-0.2) $(12)2$	25.7	93.21	830	0	0.057	6.71	23.01	6.83

Table 1. Impact measurement results of sandwich targets with various criteria

References

- [1] a shed, . , Yazdani, ., a baluo, ., and Hajizadeh arvin, ., 2016, "Investigation on High-Velocity Impact Performance of Multi-Layered Alumina Ceramic Armors with olymeric Interlayers," J. o mpos. ater., 50(25), pp. 3561–3576. https://doi.org/10.1177/0021998315622982.
- [2] Johnson, G. R., Stryk, R. A., Holmquist, T. J., et al., 1997, Numerical Algorithms in a Lagrangian Hydrocode, Wright Laboratory, Ohio, pp. 1–193.
- [3] ro nin, D. S., u i, K., Kaufmann, . , et al., 2003, "Implementation and Validation of the Johnson-Holmquist Ceramic Material Model in LS-Dyna," roc. 4th u r. LS-Dyna Users Conf., Canada, Material I, pp. 47–60.
- [4] Babaluo, A. A., Kokabi, M., Manteghian, M., and Sarraf-amoory, . , 2004, "odified odel for lu mina embranes Formed by Gel-Casting Followed by Dip-o ating," J. ur. e ram. Soc., 24, pp. 3779–3787.

Optimization of AS4 8552 Woven Composite Lamina Under Out of Plane Impact Loading

Ezgi Bakır^{1*}, Oğuzcan İnal², Zahit Mecitoğlu³, and Vedat Ziya Doğan²

Abstract: This study aims to optimize the thickness of an AS4 8552 woven composite laminate under impact loading, high strain rate, by minimizing both the maximum stress and mass. The optimization is approached using a metamodel-based multi-objective function, where a surrogate Kriging model is developed from LS-Dyna generated FEM data. The Kriging model approximates the system's behavior, significantly reducing computational costs. A genetic algorithm (GA) is employed to solve the multiobjective optimization problem, targeting the minimization of stress and mass. The optimization process demonstrates the effectiveness of using GA and surrogate models to efficiently explore the design space.

1. Ls-Dyna Impact Analysis Model

The laminate dimensions are 100 mm by 100 mm, with thickness as the key design variable, which depends on the number of laminae. To simulate out-of-plane impact loading, finite element analysis (FEA) is performed using LS-Dyna. The lamina is modeled with 2D quad elements to reduce analysis time. Boundary conditions with 3 DOF (x, y, z) constraints are applied to all edges. A spherical rigid ball, modeled with 3D hex elements, impacts the center of the plate at 10 m/s, as shown in Fig. 1.

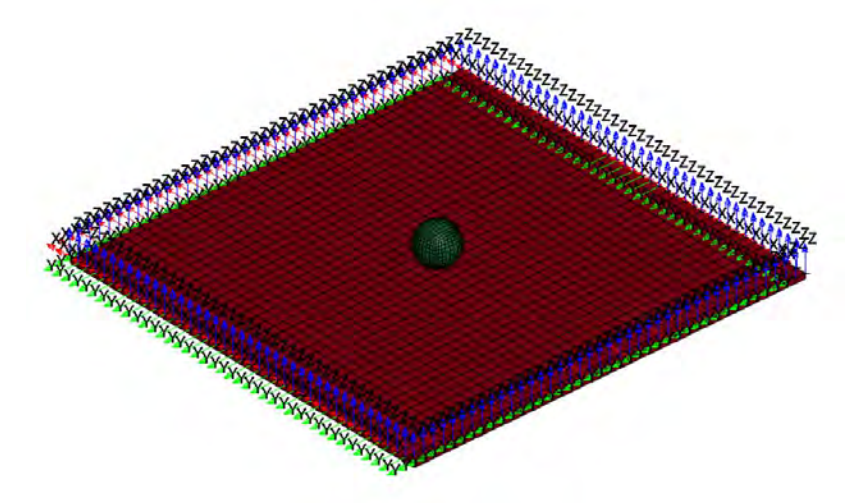


Fig. 1. Lamina Under Impact Loading Model in LS-Dyna Software

2. Metamodel Based Multiobjective Optimization

To optimize a model, the mathematical expression of the objective function should be obtained. If it is a complicated problem that cannot be expressed with an objective function, or due to the extended duration of the optimization process, a metamodel can be used. Another important point is the multi-objective function. If the optimization has two objective functions, these functions are combined. To combine these objective functions, a weighted function is used. If the weights of each objective function are equal, the importance of each objective function for the optimization is also equal.

2.1. The Surrogated Model (The Metamodel)

To optimize the problem, a surrogate Kriging model is used due to the complexity of the mathematical expression for composite plate under out of plane impact analysis. Kriging is a commonly applied technique in computational engineering which is found by Krige to solve the issue of combining results from limited locations in gold mining. Kleijnen (2017) explained that the approach relies on a stationary Gaussian process, where the mean, variance,

Department of Aeronautics and Astronautics Engineering, Graduate School, İstanbul Technical University, İstanbul, 34467, Türkiye

² Department of Aeronautical Engineering, İstanbul Technical University, İstanbul, 34467, Türkiye

³ Department of Astronautical Engineering, İstanbul Technical University, İstanbul, 34467, Türkiye

^{*} bakirez16@itu.edu.tr

and covariances depend only on the distances between points in 3D space, defining a multivariate normal distribution [1]. The model is trained with simulation data from LS-Dyna, relating the number of laminae to the maximum normal stress of the lamina and total mass.

2.2. The Optimization

The optimization process, focused on minimizing both stress and mass, is approached through a weighted multiobjective function. A genetic algorithm (GA) is then used to find efficient, near-optimal solutions, with population size impacting the overall performance. Saraswat and Sharma (2013) demonstrated that MATLAB effectively implements genetic algorithms for optimization problems, providing quick, high quality solutions. Their experiments showed that increasing the population size improves performance, while the crossover rate has little impact on solution quality.[2]

3. Results

A metamodel-based multi-objective function is provided for the optimization of the AS4 8552 woven composite laminate under high strain rate impact loading. The objective functions are to minimize in-plane stress and total mass by varying the ply number. Additionally, this approach can be applied with different parameters, such as stacking sequences, different high strain rate composite materials, and varying impactor dimensions.

References

- [1] Kleijnen, J. P. C. (2007). Kriging metamodeling in simulation: A review. European Journal of Operational Research, 192(3), 707-716. https://doi.org/10.1016/j.ejor.2007.10.013
- [2] Saraswat, M., & Sharma, A. K. (2013). Genetic algorithm for optimization using MATLAB. *International Journal of Advanced Research in Computer Science*, 4(3), 155–159. Available at http://www.ijarcs.info.

Strain rate dependent 3D shear characteristics of thermoplastic FRC – Experiments, modelling and analysis by machine learning

Johannes Gerritzen¹, Maik Gude¹ and Andreas Hornig^{1,2,3,*}

* andreas.hornig@tu-dresden.de

Abstract: A glass fibre reinforced thermoplastic textile composite material is characterized in terms of its strain rate dependent 3D shear deformation behaviour. However, the highly non-linear material response prevents an evaluation by means of established, brittle nature based composite material parameters. Besides the attempt to extract engineering constants at fixed strain values (moduli, strengths), a data-driven approach is deducted enabling the modelling of the stress-strain response at different shear strain rate levels. It is used to generate virtual data to train a machine learning model capable of extracting modelling parameters from experimental results.

1. Experiments

1.1. Methodology

The investigated composite consists of commingled hybrid E-glass fibre polypropylene (GF/PP) rovings in a multi-layered weft knitted fabric textile architecture. The determination of the shear properties has been performed with the Iosipescu shear testing setup in accordance with ASTM D 5379 at shear rates of $2 \cdot 10^{-4} - 3 \cdot 10^{0}$ 1/s. Figure 1 illustrates the alignment of each shear specimen configuration: 12- (in-plane), 13- and 31-configuration (out-of-plane). The load is applied with a servo-hydraulic test system Instron VHS 160/20. Deformation measurements and subsequent strain analysis were performed using high speed DIC, based on the stochastic grey

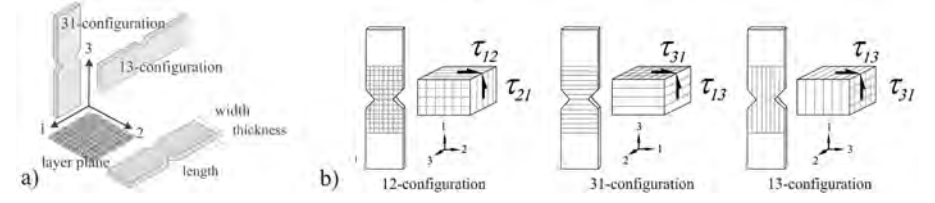


Fig. 1. Specimen configurations with respect to the fibre reinforcement plane (a) and the corresponding stress states during IOSIPESCU testing (b) [1].

1.2. Experimental Results

The effects of the shear strain rate on the material parameters within the considered strain rate range are investigated. Exemplary stress–strain results are illustrated in Figure 2. The curves exhibit an almost linear behaviour at very low strain. With increasing strain, the curves become strongly nonlinear until a relinearisation occurs for 12- and 13-configuration. A strong shear-rate sensitivity can be observed for the stress-strain curves (Figure 2a), shear modulus (Figure 2b) and shear strength (Figure 2c).

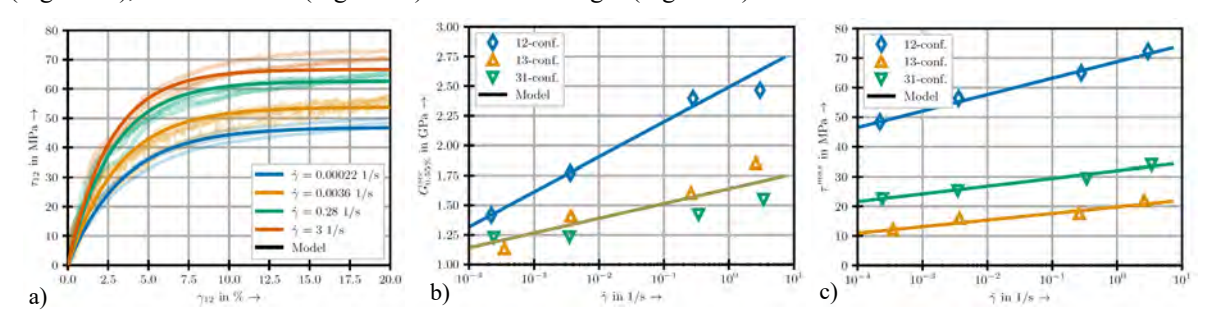


Fig. 2. Shear-strain dependent results and model predictions: a) stress-strain curves (12-configuration), b) shear modus, c) shear strength [2].

2. Modelling

Due to the highly nonlinear nature of the stress–strain curves, the identification of single representative stiffness or failure parameters analogous to materials of brittle characteristic is not possible. However, slopes, referred to as shear moduli $G_{0.55\%}^{sec}$ (Figure 2b), given by

¹ Institute of Lightweight Engineering and Polymer Technology (ILK), TUD Dresden University of Technology, Holbeinstrasse 3, Dresden, 01307, Germany

² Department of Engineering Science, Solid Mechanics and Materials Engineering, University of Oxford, Oxford, OXI 3PJ, United Kingdom

³ Center for Scalable Data Analytics and Artificial Intelligence Dresden/Leipzig (ScaDS.AI), TUD Dresden University of Technology, Strehlener Straße 12-14, Dresden, 01069, Germany

$$G_{0.55\%}^{sec} = \frac{\tau_{0.55\%} - \tau_{0.15\%}}{0.004} \tag{1}$$

as well as maximum stress levels, referred to strengths τ^{max} (Figure 2c), are determined. In order to incorporate the increase of those parameters with the strain rate, a model originally proposed by JOHNSON and COOK [3] is chosen, which is widely used in literature to model the strain rate dependency of model parameters, is chosen:

$$G_i^{sec}(\dot{\gamma}) = G_{i,ref}^{sec} \left(1 + A^G \ln \frac{\dot{\gamma}}{\dot{\gamma}_{ref}} \right) \qquad \tau^{max}(\dot{\gamma}) = \tau_{ref}^{max} \left(1 + A^T \ln \frac{\dot{\gamma}}{\dot{\gamma}_{ref}} \right)$$
 (2)

Alternatively, a data driven modelling approach was investigated. It has been found, that a closed formulation describing the entire experimental curves by coherent formulae (Figure 2a) with the determining parameters being the material's characteristics yields in

$$\tau(\gamma) = \frac{G_0^{tan}}{a} \left(1 - \exp(-a\gamma) \right) \quad \text{with} \quad G_0^{tan}(\dot{\gamma}) = G_{0,ref}^{tan} \left(1 + A^G \ln \frac{\dot{\gamma}}{\dot{\gamma}_{ref}} \right) \quad a(\dot{\gamma}) = a_{ref} \left(1 + A^a \ln \frac{\dot{\gamma}}{\dot{\gamma}_{ref}} \right) \quad (3)$$

3. Data driven analysis and machine learning

Based on the findings it can be demonstrated how Machine learning (ML) techniques can be employed to externalize the knowledge and time intensive process of material parameter identification. A convolutional neural network (CNN) based model architecture [4] is trained to predict material modelling parameters using the input of experimental stress-strain curves [5]. Hyperparameters were determined on a subset of the training data using the hyperparameter optimization tool OmniOpt [6]. The closed form stress-strain relation (Eq. 3) enables generating representative virtual training data. A sequential model is found to work well on both artificial and experimental shear strain rate dependent data [7]. It is capable of extracting well suited parameters from the artificial data under realistic conditions. For the experimental data, the model performance depends on the composition of the experimental curves, varying between excellently suiting and reasonable predictions.

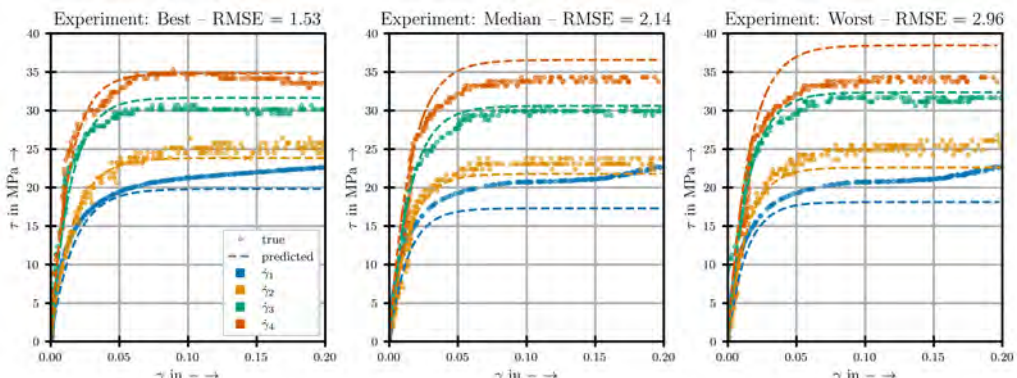


Fig 3. Resulting stress-strain-curves from predictions of the sequential model for experimental data [7]

Funding

This research was funded by the Deutsche Forschungsgemeinschaft (DFG, German Research Foundation) – Project-ID 418701707 - TRR 285/2 - sub-project A03.

References

- [1] Hufenbach, W., Langkamp, A., Hornig, A., Zscheyge, M., & Bochynek, R. (2011). Analysing and modelling the 3D shear damage behaviour of hybrid yarn textile-reinforced thermoplastic composites. Comp. Struct., 94(1), 121–131. https://doi.org/10.1016/j.compstruct.2011.07.010
- [2] Gerritzen, J., Hornig, A., Gröger, B., & Gude, M. (2022). A Data Driven Modelling Approach for the Strain Rate Dependent 3D Shear Deformation and Failure of Thermoplastic Fibre Reinforced Composites: Experimental Characterisation and Deriving Modelling Parameters. Comp. Sci., 6(10), 318. https://doi.org/10.3390/jcs6100318
- [3] Johnson, G. R., & Cook, W. H. (1985). Fracture characteristics of three metals subjected to various strains, strain rates, temperatures and pressures. Eng. Frac. Mech., 21(1), 31–48. https://doi.org/10.1016/0013-7944(85)90052-9
- [4] Meißner, P., Hoppe, T., & Vietor, T. (2022). Comparative study of various neural network types for direct inverse material parameter identification in numerical simulations. Applied Sciences, 12(24), 12793. https://doi.org/10.3390/app122412793
- [5] Gerritzen, J., Hornig, A., Winkler, P., & Gude, M. (2024). A methodology for direct parameter identification for experimental results using machine learning Real world application to the highly non-linear deformation behavior of FRP. Comput. Mat. Sci., 244, 113274. https://doi.org/10.1016/j.commatsci.2024.113274
- [6] Winkler, P., Koch, N., Hornig, A., & Gerritzen, J. (2021). OmniOpt a tool for hyperparameter optimization on HPC. In Lecture notes in computer science (pp. 285–296). https://doi.org/10.1007/978-3-030-90539-2 19
- [7] Gerritzen, J., Hornig, A., Winkler, P., & Gude, M. (2024). Direct parameter identification for highly nonlinear strain rate dependent constitutive models using machine learning. In Proceedings of the 21st European Conference on Composite Materials - ECCM (Vol. 3, pp. 1252-1259). https://doi.org/10.60691/yj56-np80

Modeling the High Strain Rate Behavior of Graphene Epoxy Nanocomposites Using Viscoplasticity Theory and Mori-Tanaka Homogenization

Okan Bakbak and Ozgen Colak*

Yıldız Technical University
Department of Mechanical Engineering, Turkey
* ozgen@yildiz.edu.tr

Abstract

Cooperative viscoplasticity theory based on overstress (C-VBO) is developed to describe the rate-dependent mechanical response of graphene epoxy nanocomposites. The model integrates the Mori-Tanaka homogenization scheme to account for the effective properties of the nanocomposite, considering the dispersion and interfacial interactions of graphene nanoplatelets within the epoxy matrix. The C-VBO framework enables the prediction of strain-rate sensitivity, and inelastic deformation mechanisms under high strain rates. The model parameters are calibrated using experimental data obtained from Split Hopkinson Pressure Bar (SHPB) tests.

1. Introduction

Accurate modeling of nanocomposites under dynamic loading requires an approach that captures both time-dependent and rate-sensitive deformation mechanisms. C-VBO provides a robust framework for describing the inelastic and rate-dependent behavior of these materials. Additionally, the Mori-Tanaka homogenization scheme allows for the effective modeling of nanocomposite properties by considering the dispersion and interaction of graphene within the epoxy matrix.

In this study, newly developed C-VBO model incorporating the Mori-Tanaka method to predict the high strain rate response of graphene epoxy nanocomposites is introduced. The model is calibrated and validated using experimental data obtained from SHPB tests, ensuring accurate representation of the material's dynamic behavior. This approach provides a valuable predictive tool for optimizing the performance of graphene-based nanocomposites in high-strain-rate applications.

2. Cooperative Viscoplasticity Theory Based on Overstress (C-VBO) for Nanocomposites

C-VBO is a constitutive modeling framework designed to describe the rate-dependent inelastic behavior of materials under dynamic loading conditions. For finite deformation, the deviator of the rate of total deformation tensor (d) is given by equation (1).

$$\boldsymbol{d} = \boldsymbol{d}^e + \boldsymbol{d}^{vp} = \frac{1+v}{CE} \boldsymbol{s}^o + \frac{3}{2} \dot{\boldsymbol{\gamma}}^{vp} \frac{\boldsymbol{s} - \boldsymbol{g}}{\Gamma}$$
 (1)

where s and d are the deviators of the Cauchy stress tensor, σ , and the rate of deformation tensor, D, respectively, and g is the deviatoric part of the equilibrium stress. s^o is the objective rate of Cauchy stress.

Temperature and strain rate-dependent elasticity modulus is given in equation (2).

$$E(\theta, \dot{\varepsilon}) = (E_1(\dot{\varepsilon}) - E_2(\dot{\varepsilon})) \exp\left[\left(-\frac{\theta}{T_\beta(\dot{\varepsilon})}\right)^{m_1}\right] + (E_2(\dot{\varepsilon}) - E_3(\dot{\varepsilon})) \exp\left[\left(-\frac{\theta}{T_g(\dot{\varepsilon})}\right)^{m_2}\right] + E_3(\dot{\varepsilon}) \exp\left[\left(-\frac{\theta}{T_f(\dot{\varepsilon})}\right)^{m_3}\right]$$
(2)

where $E_i(\dot{\varepsilon})$ is the stiffness of the material at the beginning of each transition *i*. These transitions are β , α (glass transition) transitions and flow. m_i is the Weibull moduli corresponding to the statistics of bond breakage and the transition temperatures T_{β} , T_{g} , and T_{f} found by dynamic mechanical analysis (DMA).

To model nanocomposites, the C-VBO formulation is coupled with the Mori-Tanaka homogenization scheme, which estimates the effective macroscopic properties based on the behavior of the matrix (epoxy) and inclusions (graphene nanoplatelets). In the development of the nanocomposite material model from C-VBO model, the reference instantaneous stiffness's at three main transitions (E_i^{ref}) are replaced by the effective moduli, (\bar{E}_i^{ref}).

$$\bar{E}_i = \bar{E}_i^{ref} \left(1 + s \log \left(\frac{\varepsilon}{\varepsilon^{ref}} \right) \right) \tag{3}$$

where \bar{E}_i^{ref} is the value of the effective transition moduli, \bar{E}_i obtained for a reference strain rate value (\mathcal{E}^{ref}).

Here, only three equations are given about the model. For details of the C-VBO model for nanocomposites, the work by Bakbak and Colak [1] is recommended.

3. Simulation Results

Mechanical behavior of graphene-epoxy nanocomposite at quasi static and high strain rate behavior are depicted in Fig. 1.

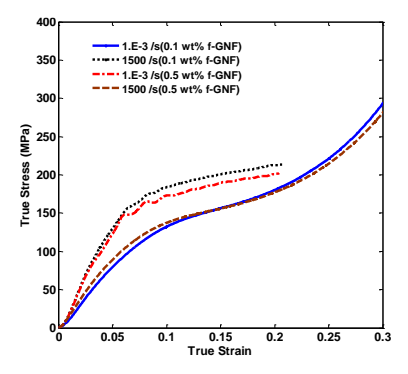
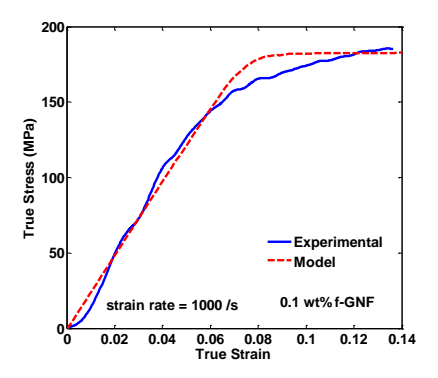


Fig.1. Comparison of stress-strain behavior of nanocomposites containing 0.1 and 0.5 wt% f-GNF at 1.E-3/s and 1500/s strain rates [1, 2]

Adiabatic heating occurs at high strain rates. Therefore, thermal strain is incorporated in simplified C-VBO to model the high strain behavior of nanocomposites. The stress-strain behavior of graphene epoxy nanocomposite with the content of 0.1 %wt f-GNF at high strain rates of 1000 and 1500/s is predicted and depicted in Fig.2.



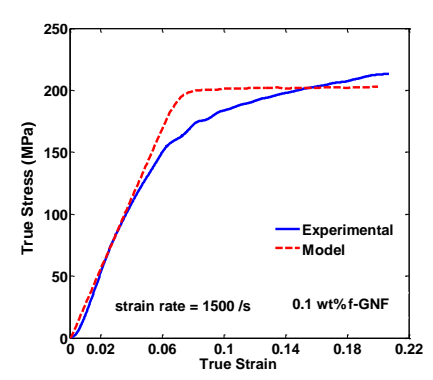


Fig.2. Comparison of model predictions with experimental data at the strain rate of 1000 and 1500/s, [1].

Including thermal strain into the model leads us to model high strain rate behavior of the nanocomposites in addition to quasi static loading.

4. Conclusions

The proposed approach provides a robust predictive tool for understanding and optimizing the behavior of graphene epoxy nanocomposites under extreme loading conditions, contributing to their design for advanced structural applications.

5. References

[1] Bakbak, O and Colak O., 2022, "Simplified cooperative viscoplasticity theory based on overstress model for nanocomposites", Journal of Applied Polymer Science, 139, pp.2-18.

[2] Colak, O., Birkan, E., Bakbak, O., Acar, A. and Uzunsoy, D., 2023, "Functionalized graphene-epoxy nanocomposites: experimental investigation of viscoelastic and viscoplastic behaviors", Mech. Time-Depend. Mater., 27, pp.185-205

Lessons Learned from Virtual Certification of an Aircraft Structure Against Birdstrike

Michele Meo

Department of Aeronautical and Astronautical Engineering,
University of Southampton, UK
m.meo@soton.ac.uk

Abstract: This paper provides key insights from the numerical certification of aircraft structures against birdstrike, a critical issue for aviation safety. Traditionally, birdstrike certification has required costly and time-intensive full-scale physical testing of aircraft components to meet stringent regulatory requirements. In this study, advanced numerical simulations, specifically finite element analysis (FEA), were employed to reduce the reliance on full-scale testing. Only one full-scale birdstrike test was conducted for validation, while the bulk of the predictions were based on smaller component testing and detailed simulations, demonstrating a more efficient path to certification [1,2].

1. Overview

The research focuses on the lesson learned on the design, manufacturing, and testing of a birdstrike-resistant leading-edge structure made from fiber-metal laminate (FML) and composite materials in collaboration with a large aircraft manufacturer company.

FML combines the strength of aluminum alloys with the flexibility and energy absorption properties of fiber-reinforced composites, offering improved resistance to high-speed impacts. Using state-of-the-art simulation tools and adopting both Lagrangian and Eulerian modeling approaches, multiple birdstrike scenarios were simulated [1-6]. This allowed for the optimization of the structural design and provided crucial data to ensure compliance with Federal Aviation Administration (FAA) and European Aviation Safety Agency (EASA) certification standards [4,5].

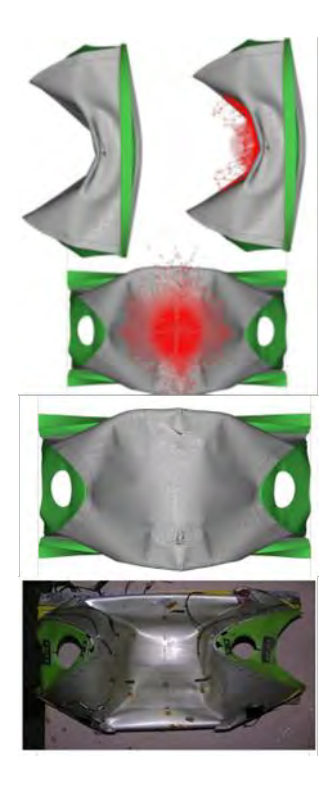


Fig. 1. Birdstrike numerical and experimental result on a section of a FML leading edge.

One of the significant lessons learned was the efficiency of using numerical simulations and small-scale component testing to predict full-scale behavior. This approach greatly reduced the need for expensive, large-scale physical tests, with only one final full-scale test required to confirm the numerical models' accuracy. These simulations proved invaluable in predicting impact loads, material failure, and deformation under birdstrike conditions. Additionally, the study highlights the superior performance of FML compared to traditional aluminum configurations in terms of energy absorption and resistance to catastrophic damage [1,4].

The findings underscore the importance of accurate material modeling, as well as the value of advanced numerical methods in reducing certification costs while ensuring safety. The simulations captured critical aspects of birdstrike events, such as handling large deformations, tracking the interaction between the bird and aircraft surfaces, and predicting localized material failure.

The lessons learned from this approach provide a framework for improving future aircraft designs, making numerical certification an effective tool in the design of birdstrike-resistant structures [1-6].

2. References

- [1] Guida, Michele; Marulo, Francesco; Meo, M; Riccio, M; , Analysis of bird impact on a composite tailplane leading edge , Applied Composite Materials , 15 , , 241-257 , 2008 , Springer Netherlands
- [2] Guida, Michele; Marulo, Francesco; Polito, Tiziano; Meo, Michele; Riccio, Massimo; , Design and testing of a fiber-metal-laminate bird-strike-resistant leading edge , Journal of Aircraft , 46 , 6 , 2121-2129 , 2009 ,
- [3] Guida, Michele; Marulo, Francesco; Meo, Michele; Grimaldi, A; Olivares, G; , SPH-Lagrangian study of bird impact on leading edge wing, Composite Structures, 93, 3, 1060-1071, 2011, Elsevier
- [4] Guida, Michele; Marulo, Francesco; Meo, Michele; Russo, S; , Experimental tests analysis of fiber metal laminate under birdstrike, Mechanics of Advanced Materials and Structures, 19, 5, 376-395, 2012, Taylor & Francis Group
- [5] Guida, Marulo; Marulo, Francesco; Meo, M; Russo, S; , Certification by birdstrike analysis on C27J fullscale ribless composite leading edge , International Journal of Impact Engineering , 54 , , 105-113 , 2013 , Pergamon

Modelling and Characterisation of UD Thermoplastic Laminates under Dynamic Loading

Nenad Djordjevic^{1,2*}, Rade Vignjevic¹, Svetlana Risteska^{3**}, Vineta Srebrenkoska³ and Sara Srebrenkoska⁴

¹ Brunel University London, Centre for Assessment of Structures and Materials under Extreme Conditions, London UB83 PH, UK

² Institute for Information Technology Kragujevac, Jovana Cvijića bb 34000 Kragujevac, Serbia

³ Faculty of Technology, Goce Delcev University, Krste Misirkov, No. 10-A Stip, Republic of North Macedonia.

³ Faculty of Mechanical Engineering, Goce Delcev University, Krste Misirkov, No. 10-A Stip, Republic of North Macedonia.

*nenad.djordjevic@brunel.ac.uk; **svetlana.risteska@ugd.edu.mk

Abstract: This paper describes work-in-progress on modelling and characterisation of an AS4/PEEK UD composite undergoing compression at the range of loading rates from $1 \times 10^{-3} \, s^{-1}$ to $2 \times 10^{3} \, s^{-1}$. The material at quasistatic rates was tested by using a servo hydraulic test machine, whilst the high strain rate testing was conducted by using Split Hopkinson Pressure bar (SHPB) rig. Simulation programme was conducted with LS Dyna explicit solver where the composite was modelled at quasi-continuum and micro scale with linear hexahedral solid elements. A selection of experimental results was compared to simulation results and the results agree well in terms of measured maximum stress at failure and effective laminate stress obtained in the simulation.

Keywords: AS4/PEEK UD composite, thermoplastic composite, LS Dyna models, finite element methods;

1. Introduction

Fibre reinforced polymers laminates are widely used in aerospace and automotive industry, because of their high specific stiffness and strength, with the growing interest in carbon-thermoplastic laminates. Design and materials characterisation under compression are still based on the experimental testing but these campaigns are very costly and time consuming [1-7]. Simulation methods, combined with appropriate constitutive models, including failure criteria, and realistic boundary conditions can enable engineers to predict performance and accelerate the components design. However, a limited number of publications is available on numerical investigations of the compression behaviour of carbon thermoplastic laminates [7-10], particularly at the elevated loading rates. Consequently, the objective of the work presented in this paper is modelling and characterisation of the AS4-PEEK composite laminate, where the material is tested at the range of loading, starting from the quasistatic up to the high rate loading and modelled by using LS-Dyna FEM solver [11].

2. Experimental characterisation at a range of strain rates

Using a servo-hydraulic testing machine to characterise the mechanical properties of composites under static and quasi-static loading conditions provide a comprehensive understanding of their strength, stiffness, failure modes and fatigue behaviour. The precision and versatility of servo-hydraulic testing machines enable the testing under various mechanical conditions and help optimise designs for reliability, durability, and performance.

The material tested here is unidirectional AS4/PEEK preprag laminate, which consists of 32 plies and the stack sequence $[0/45/-45/90]_{4s}$. The quasistatic loading was conducted with the specimen shown in Fig. 1a, on the 200kN servo hydraulic machine with max loading rate 200 mm/s, shown in Fig. 1b. The quasistatic tests were conducted at the loading rates of 0.01mm/s, 1mm/s and 100mm/s, which correspond to the stain rates of $1\times10^{-3}\,s^{-1}$, $10^{-1}\,s^{-1}$ and $10\,s^{-1}$, respectively. PCO edge 5.5 camera and Veritas Constellation 120 lamps were used for first two tests, whilst equipment for the highest loading rate included: NI USB-6366 acquisition board, ultra-high speed laser displacement sensors Keyence LK-G5000 and sensor head LK-H157, piezoelectric load cell Kistler 9106A, Charge amplifier Kistler 5015, High speed camera IDT OS8-S3 and Veritas Constellation 120 lamps. Three tests were performed at each loading rate and the stress strain curves are given in Fig. 2.

The same material was also tested at higher strain rates using the SHPB setup, with cylindrical specimen. The apparatus consists of Maraging 300 bars Ø 25mm (striker 2m, Input bar 2m and output bar 4 m), Ohmic and semiconductor strain-gages, strain gage amplifier EFS SGA02 high-speed (cut-off frequency of 500 kHz) and fast transient recorder GAGE CSE8482-H2 (sample-rate 10 MHz). The strain gauges are mounted on the incident and transmission bars to measure the elastic strain waves generated at impact of the incident bar and determine the stress-strain response of the material. Two loading rates of 8000mm/s and 18000mm/s, which

respectively correspond to strain rates of $800s^{-1}$ and $1800s^{-1}$, were testes with three samples to check for the repeatability. The average test results for the two loading rates are given in Table 1.

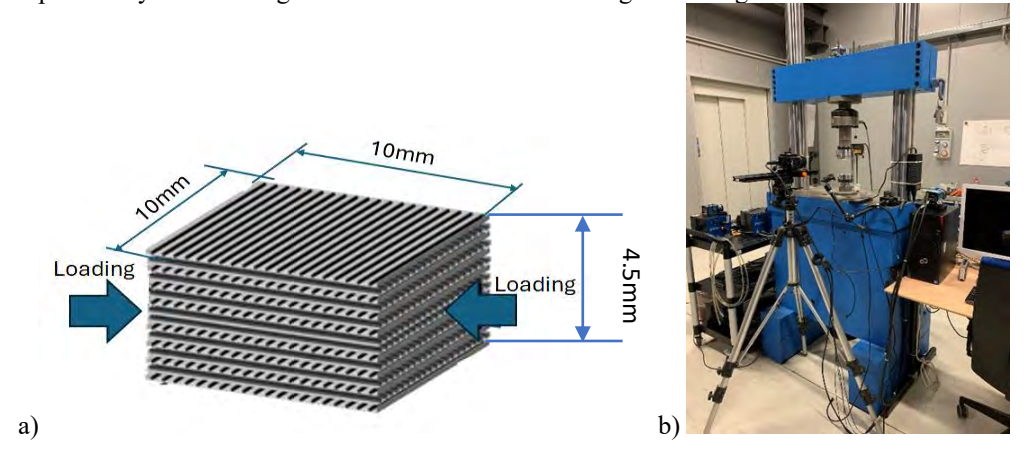


Fig. 1 a) AS4/PEEK laminate for compression testing b) Servo-hydraulic testing machine

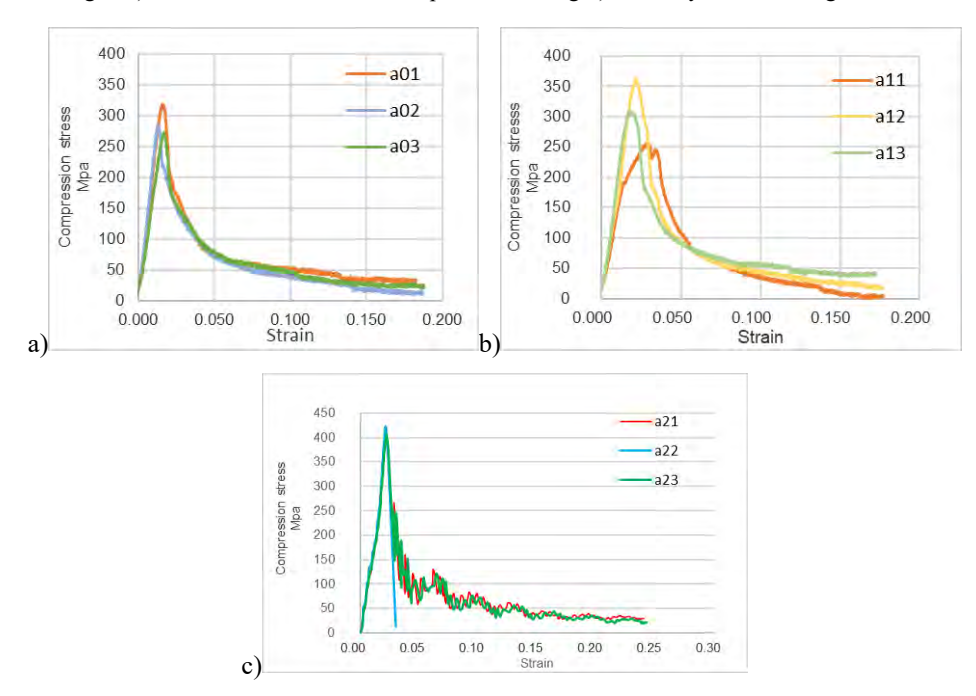


Fig. 2 Stress – Strain curves obtained with UD AS4-PEEK under compression at loading rates: a) v=0.01 mm/s, b) v=1 mm/s and c) v=100 mm/s

Table 1 Loading strain rates and maximum compression stress obtained in SHPB tests.

Specimens	Thermoplastic	Velocity	Strain	loading	Compression
	resin	mm/s	Rates (/s)	directions in the	stress MPa
				compression test	
Avg	PEEK	8 000	800	In-plane loading	400,2
Avg	PEEK	18 000	1 800	In-plane loading	460,2

3. Modelling of compression tests

The finite element models of the samples used in the quasistatic testing are developed by using LS Dyna and linear solid hexahedral elements available there in. Two discretisation methods were developed: a) quasicontinuum approach, where the plies are modelled individually by using three elements through thickness and element aspect ratio one, shown in Fig. 3a); and b) micromechanical approach, where the matrix and fibres are modelled individually. Only the bottom part of the laminate was modelled with symmetry boundary conditions applied on the Z plane so that the quasi continuum model consists of 1,920,000 solid elements. The composite

material was modelled by using material type 59 [11], based on Tsai – Wu ellipsoidal failure surface criteria. The simulation results for the stress strain curves obtained in each individual ply are shown in Fig. 3b) for the loading rate of 1mm/s. The effective laminate stress calculated from this result based on the load balance through the thickness of the laminate agrees well with the experimental results in terms of maximum stress at failure being within 10% of the average experimental value.

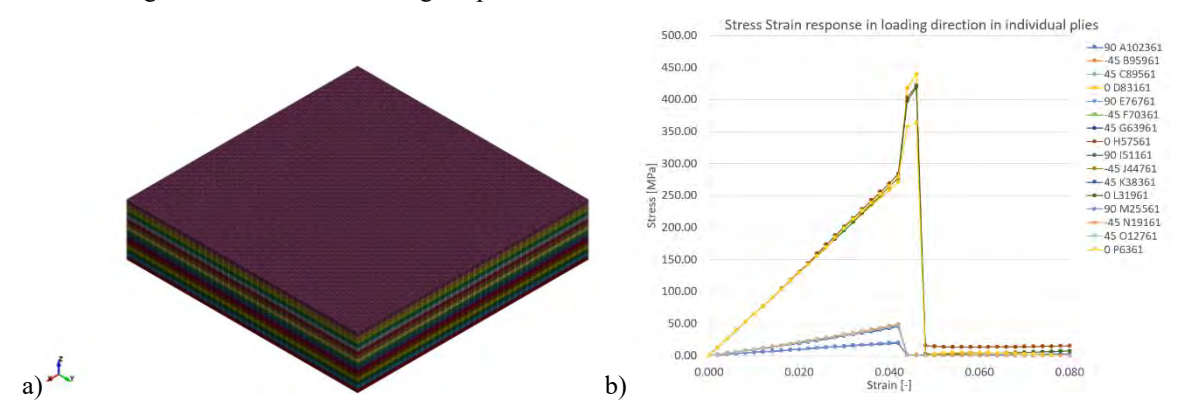


Fig. 3 a) FEM Model developed for analysis AS4/PEEK laminate under compression loading b) Stress strain curves in the laoding direction obtained in the individual plies in the simulaiton at v=1 mm/s

4. Conclusions

The AS4/PEEK UD laminate has been characterised for the range of the loading rates relevant for automotive and aerospace applications and the high fidelity models of the tests have been developed. The first simulation results agree well with the experimental results. The future work will include a comprehensive simulation programme both at the quasi continuum and micromechanical scale. The latter will allow for analysis of the matrix dominated rate effects onto the overall material response and calculation of the smeared material properties, which will significantly reduce the size and computational costs of the real world/component models.

References

- [1] Khondker, O.A., Leong, K.H., Herszberg, I., Hamada, H., "Impact and compression-after-impact performance of weft-knitted glass textile composites", Composites: Part A, 2005, Vol. 36, pp. 638 648.
- [2] Petit, S., Bouvet, C., Bergerot, A., Barrau, J. J., "Impact and compression after impact experimental study of a composite laminate with cork thermal shield.", Composites Science and Technology, 2007, Vol. 67, pp.3286 3299.
- [3] Feraboli, P., "Some Recommendations for Characterization of Composite Panels by Means of Drop Tower Impact Testing." Journal of Aircraft, 2006, Vol. 43.
- [4] Arhant, M.; Davies, P. 2-Thermoplastic matrix composites for marine applications. In Marine Composites; Pemberton, R., Summerscales, J., Graham-Jones, J., Eds.; Woodhead Publishing: Cambridge, UK, 2019; pp. 31–53.
- [5] Huiran Zou, Weilong Yin, Chaocan Cai, Bing Wang, Ankang Liu, Zhen Yang, Yibin Li and Xiaodong He, The Out-of-Plane Compression Behavior of Cross-Ply AS4/PEEK Thermoplastic Composite Laminates at High Strain Rates, Journal Materials 2018, Vol11, 2312; doi:10.3390/ma11112312
- [6] Lisa Feuillerat, Olivier De Almeida a, Jean-Charles Fontanier , Fabrice Schmidt, Effect of poly(ether ether ketone) degradation on commingled fabrics consolidation, Journal Composites Part A 149 (2021) 106482 https://doi.org/10.1016/j.compositesa.2021.106482
- [7] Boon, Y.D.; Joshi, S.C.; Bhudolia, S.K. Review: Filament Winding and Automated Fiber Placement with In Situ Consolidation for Fiber Reinforced Thermoplastic Polymer Composites. Polymers 2021, v 13, pp1951.
- [8] Gama, B. A., Travis A. Bogetti, and Gillespie, J. W., "Finite Element Modeling of Impact, Damage and Penetration of Thick-Section Composites," International Journal of Impact Engineering, 2010. doi:10.1016/j.ijimpeng.2010.11.001.
- [9] Tucci, F.; Rubino, F.; Pasquino, G.; Carlone, P. Thermoplastic Pultrusion Process of Polypropylene/Glass Tapes. Polymers 2023, 15, 2374. https://doi.org/ 10.3390/polym15102374
- [10] Maja Stefanovska, Blagoja Samakoski, <u>Svetlana Risteska</u>, Gari Maneski, "Influence of Some Technological Parameters on the Content of Voids in Composite during On-line Consolidation with Filament Winding Technology"ICMTM Berlin 2014International Conference on Metallurgy Technology and Materials.
- [11] Livermore Software Techology, "LS-Dyna," Sep. 24, 2021, LIVERMORE SOFTWARE TECHNOLOGY (LST), ANSYS COMPANY, Livermore, California 94551: R13.



2025 Conference 4th – 5th JUNE 2025

Session 2 - Novel composite materials for high strain rate applications (WG3)





Fracture Toughness Survey of CF-LMPAEK Thermoplastic Composite via High-Speed Wedge Insert Fracture Method towards Stiffened Panel Design and Verification

Thomas Zaragkas, 1*

Georgios Kotsinis¹, George Sotiriadis, ¹ Theodoros Loutas, Vassilis Kostopoulos, ¹ and Spyridon Psarras^{1,*}

¹ Applied Mechanics Laboratory, Department of Mechanical Engineering and Aeronautics, University of Patras, Patras University Campus, GR-26504 Rio-Patras, Greece

* thomaszaragkas@ac.upatras.gr

Abstract: In this work the TC1225 thermoplastic composite material utilizing T700S fibers and the recently developed highly engineered LMPAEK matrix undergoes Dynamic Mode I test via the Wedge Insert Fracture (WIF) method using a DCB specimen on a novel pressure gun set up monitored by 2D DIC system, to examine the effect of high speed in intralaminar fracture. This survey is part of a global test campaign towards the experimental building block approach for the design of a thermoplastic composite fuselage stiffened panel. Furthermore, due to the existence of the adhesive joints between the thermoplastic composite skin and the epoxy stiffener (Cycom 977-2) the dynamic tests are also surveying the affection of the steep crack opening at the adhesive film (FM300k). The experimental findings are straightly compared to comprehensive Finite Elements Models in terms of Dynamic Energy Release Rate and the material response, incorporating both 2D planar schemes with cohesive elements or VCCT method and 3D methodology employing cohesive surfaces. Numerical strategies, material properties and failure criteria are already verified by the authors through the material characterization, static fracture and upperlevel component tests (CAI, bolted joints, adhesive joints, panel level) elsewhere.

1. Introduction

1.1. TC1225 Thermoplastic Composite Material

Thermoplastic composites were overshadowed by thermosets due to the lack of processing technologies in the Aerospace industry. Yet lately this has changed due to the development of technologies such as Consolidation, Automated Fiber placement etc. that enable the fast production and reduced costs, tackling the problems arise with the high processing temperature. Thermoplastic composites present numerous advantages towards the decarbonization era and green development since they can melt and re-shape, be recycled and also can be welded. Epigrammatically, some other advantages are the high production rates, lower assembly costs, high fracture toughness as was also proved from this test campaign, enhanced fatigue strength, suitable for hygrothermal conditions and Fire-Smoke-Toxicity environments since they don't absorb humidity and have great chemical resistance. Furthermore, there is no concern about expiration and cold room storage and the glass transition temperature is not affected by hygrothermal conditions [1].

The TC1225 material with commercial name CETEX® which constitutes from T700S carbon fibers and the recently developed highly engineered thermoplastic matrix LMPAEK is already participating in several primary structural applications such as A380 leading edge and A350 pylon cover and shear clips. But more importantly, NASA has been studying the present material under a wide range of tests and applications towards the Hi-Rate Composites Aircraft Manufacturing (HiCAM) project for usage on the next space missions. Specifically, the TC1225 undergoes thermal and structural tests (also high strain rate impacts) for employing to: a) Nancy Grace Roman Telescope as primary structural component which will be launched on 2026 [2] and to the b) Tall Lunar Tower Project as truss joint with in-space manufacturing capabilities [3].

1.2. High Speed Fracture Testing

A.J. Smiley and R. B. Pipes [4] were the first to investigate the effect of strain rates on interlaminar fracture toughness under Mode I opening scheme and found that the PEEK thermoplastic composite matrix show a 76.7% decrease in the value of fracture toughness which was similar to an epoxy composite, yet the thermoplastic composite has significant higher initial value. The investigation was carried with rates to be deviating from pseudostatic conditions to 0.67m/s. They also have proposed a data reduction scheme, with several restrictions. Similarly, Chen et al. [5] have clarified the expression given by Smiley and Pipes and the restrictions that it introduces, such as the neglection of kinetic and strain energy induced by beam vibrations and the constant loading rate. Chen et

al have proposed a brief mathematical model for Energy Release Rate (SERR) calculations including beam vibration characteristics under the Euler Bernoulli kinematics. Additionally, G. Kotsinis and T. Loutas [6] have also considered shear components and rotations as prescribed by Timoshenko beam theory.

The WIF method utilizing DCB specimen is carried out recently by G. Kotsinis et al. [7] towards the investigation of fracture toughness of metal to composite dissimilar joints, incorporating an analytical-experimental hybrid method through DIC kinematics, Timoshenko beam theory and Lagrangian contact formulation. They have proven the succession of the present experimental set-up and the effectiveness of their hybrid method.

2. Methodology

Aim of this study is to investigate the performance of TC1225 material under high speed utilizing the Mode I WIF test on a pressure gun configuration and the data reduction scheme given by A.J. Smiley and R. B. Pipes [4] and Chen et al. [5] for interlaminar fracture toughness extraction. This investigation is taking place for both interlaminar characterization but also for dissimilar adhesive joints representing the skin-to-stiffener joint of the fuselage stiffened panel. A triple methodology with Finite Elements employing 2D VCCT, 2D cohesive elements and 3D cohesive surfaces is utilized for benchmark study. This approach is part of a general building block approach design methodology towards a fuselage panel design and verification unlocking thermoplastic composite capabilities and highlighting literature and standard voids, due to the dominance of thermoset composites in Aerospace Industry.

3. Results

The static tests for both TC1225 laminate and the dissimilar adhesive joints have been conducted following the Airbus standards for Static Mode I fracture toughness property extraction. The CF-LMPAEK composite material has an enhanced fracture toughness and one of the highest found in Literature [1]. On the contrary, the FM300k adhesive film is failed under brittle adhesive mode presenting the stick-slip phenomenon, unsteady and sudden crack propagations and low fracture toughness, considering the participation on primary structural joint. This has resulted due to the low surface capabilities and slickness of the thermoplastic matrix, and it is evident in many loading schemes of the test campaign. For example, static tests which require tabs attachment have failed several times due to debonding issues. For this reason, a surface treatment prior secondary bonding is suggested, such as laser ablation technique.

Target Group	Static Fracture Toughness	Coefficient of Variation
TC1225	1.99	3.51%
FM300k Adhesive	0.29	10 19%

Table 1. Static Fracture Toughness Extraction

References

- [1] Krueger, R. and A. Bergan, Advances in Thermoplastic Composites Over Three Decades–A Literature Review. 2024.
- [2] Miller, S., et al. Manufacture, Characterization, and Fusion Welding of Thermoplastic Composites for Space Applications. in 2nd ASME Aerospace Structures, Structural Dynamics, and Materials Conference (SSDM). 2024.
- [3]Tiffin, D. and M. Mahlin, Tall Lunar Towers: Systems Analysis of Lunar-Surface-Assembled Power, Communication, and Navigation Infrastructure. 2023.
- [4] Smiley, A.J. and R.B. Pipes, Rate Effects on Mode I Interlaminar Fracture Toughness in Composite Materials. Journal of Composite Materials, 1987. 21(7): p. 670-687
- [5] Chen, T., et al., Dynamic interfacial fracture of a double cantilever beam. Engineering Fracture Mechanics, 2020. 225: p. 106246.
- [6] Kotsinis, G. and T. Loutas, Strain energy release rate under dynamic loading considering shear and crack tip root rotation effects. European Journal of Mechanics A/Solids, 2022. 92: p. 104435.
- [7] Kotsinis, G., et al., Interlaminar fracture toughness of metal/composite bonded joints under high-speed mode I loading considering the elastic vibration. Composites Science and Technology, 2024. 258: p. 110858.

Effect of Rubber Interleaving on the Charpy Impact Properties of Basalt Fiber Reinforced Polymers

Çağatay Yilmaz,1,* and Sara S. A. Eltahir,2

¹ Department of Mechanical Engineering, Abdullah Gül University, Kayseri/Türkiye

² Department of Advanced Materials and Nanotechnology, Abdullah Gül University, Kayseri/Türkiye *yilmaz.cagatay@agu.edu.tr

Abstract: Basalt fiber-reinforced polymers (BFRPs) offer a balance between the high performance of carbon fibers and the cost-effectiveness of E-glass fibers. However, their poor adhesion to epoxy matrices limits their impact resistance. This study investigates the dynamic behavior of BFRPs with interleaved rubber foil, which enhances adhesion and damping properties. Basalt fiber composites with and without rubber foil are fabricated using the vacuum-assisted hand lay-up technique and tested via Charpy impact. The results provide insights into the effectiveness of rubber interleaving in improving the impact resistance of BFRPs.

1. Introduction

The use of fiber-reinforced polymers (FRPs) in structural components continues to grow, with various types of fiber reinforcements, such as carbon fibers and glass fibers, being incorporated into polymer matrix composites. Carbon fibers, known for their superior mechanical properties, are relatively expensive, while glass fibers, such as E-glass, are cost-effective but offer lower mechanical performance. To bridge the gap between the two, basalt fibers have emerged as a promising reinforcement candidate. Basalt fibers, like E-glass, are affordable, yet they exhibit higher mechanical properties compared to E-glass fibers.

Despite some studies on the quasi-static mechanical properties of basalt fiber-reinforced polymers [1–3], limited research has been conducted on their dynamic properties. The literature suggests that basalt fibers have relatively poor adhesion to epoxy matrices, likely due to their ceramic nature. This study aims to investigate the dynamic behavior of basalt fiber-reinforced polymers, incorporating an innovative approach by interleaving rubber foil between basalt fiber layers. The rubber foil serves dual purposes: acting as an adhesion promoter and a damper to prevent delamination during impact.

The dynamic properties of basalt fiber-reinforced polymers will be assessed through Charpy impact tests. Two types of basalt fiber-reinforced polymers will be fabricated using the vacuum-assisted hand lay-up technique, and the influence of interleaved rubber foil on the impact resistance of these composites will be analyzed.

2. Material and Testing

Basalt fiber-reinforced polymeric material is produced by stacking ten layers of 200 gsm plain weave basalt fabric mats on top of each other with and without rubber foils. The rubber foils used has a thickness of 0.2 mm and the surface is treated for bonding. As a matrix material, Biresin CR 122 epoxy resin is mixed with CH122-5 hardener with a weight ratio of 100:30. Thereafter, the mixture is degassed for 10 minutes to remove the entrapped air bubbles introduced to the resin-hardener mixture during mechanical stirring. S2-glass fabric stack is impregnated by the resin mixture and then followed by curing at 90 °C for 18 hours. Curing is completed on a heated plate and the consumables used in the curing is given in Figure 1. The produced plate is cut into test coupons as per the dimensions given in ASTM D790 by using a three-axis CNC milling machine.

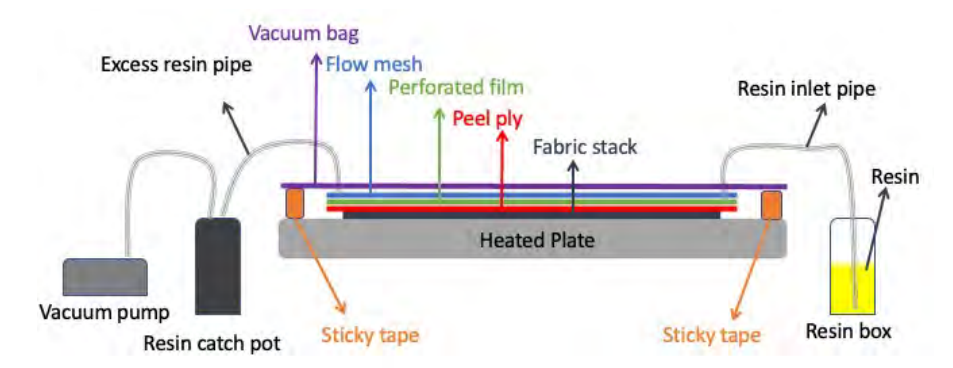


Figure 1: Schematic of the vacuum-influsion process and order of consumables used in the production of the composite test plate

The Charpy impact test will be performed with the Charpy Impact test fixture to study the impact properties of basalt fiber reinforced polymer with and without rubber interleaves. For each group, at least five specimens are tested to get an average result of the impact performance of basalt fiber-reinforced polymer. Once the impact test is completed, fractured samples are analyzed with an optical microscope to reveal the fracture mechanism of the tested samples.

3. References

- [1] Liu Q, Shaw MT, Parnas RS, McDonnell A. Investigation of basalt fiber composite mechanical properties for applications in transportation. Polym Compos 2006;27:41–8.
- [2] Manikandan V, Jappes JTW, Kumar SMS, Amuthakkannan P. Investigation of the effect of surface modifications on the mechanical properties of basalt fibre reinforced polymer composites. Compos B Eng 2012;43:812–8.
- [3] Ralph C, Lemoine P, Archer E, Mcilhagger A. Mechanical properties of short basalt fibre reinforced polypropylene and the effect of fibre sizing on adhesion. Compos B Eng 2019;176:107260.

Enhancing Impact Resistance in Recycled Composite Materials for Aerospace Applications: The Role of Strand Morphology and Sandwich Structures

Yağız Özbek^{1,2}, Abdulrahman Al-Nadhari^{1,2}, Sinem Elmas^{1,2}, Volkan Eskizeybek³, Mehmet Yıldız ^{1,2}, Hatice S.

¹Sabanci University Integrated Manufacturing Technologies Research and Application Center & Composite Technologies Center of Excellence, Teknopark Istanbul, 34906, Pendik, Istanbul, Türkiye

²Faculty of Engineering and Natural Sciences, Sabanci University, 34956, Tuzla, Istanbul, Türkiye

³Department of Materials Science and Engineering, Faculty of Engineering, Çanakkale Onsekiz Mart University, 17100, Çanakkale, Türkiye

⁴School of Mechanical, Aerospace and Civil Engineering, The University of Sheffield, S1 3JD, UK

* hatice.sas@sabanciuniv.edu

Abstract: This study investigates the impact resistance of recycled composite materials tailored for aerospace applications. By analyzing the influence of strand size and morphology on mechanical performance and integrating randomly oriented strand (ROS) composites into sandwich structures with atmospheric plasma activation (APA), we aim to enhance material toughness. Mechanical evaluations, including impact testing, demonstrate that these strategies offer sustainable, cost-effective solutions for secondary load-bearing aerospace structures.

1. Introduction

The aerospace industry continually seeks materials that offer superior performance while aligning with sustainability goals. Composite materials, particularly fiber-reinforced polymers (FRPs), have become integral in aerospace applications due to their high specific strength, stiffness, and corrosion resistance. These attributes contribute to significant weight reductions and enhanced fuel efficiency in aircraft design. However, the environmental impact of traditional composite manufacturing, which often relies on non-renewable resources and energy-intensive processes, has prompted a shift towards more sustainable practices. This transition includes the development and utilization of recycled composite materials, which not only mitigate waste but also reduce the carbon footprint associated with production [1]. A critical factor in the adoption of these recycled composites is their impact resistance—a measure of a material's ability to withstand sudden forces or shocks without significant degradation. In aerospace applications, where materials are subjected to dynamic loads and potential impacts, ensuring adequate impact resistance is paramount to maintaining structural integrity and safety [2]. This study investigates strategies to enhance the impact resistance of recycled composite materials for aerospace applications. Specifically, it examines the influence of strand morphology on mechanical performance and explores the integration of randomly oriented strand (ROS) composites into sandwich structures. By optimizing these parameters, the research aims to develop sustainable, cost-effective materials suitable for secondary load-bearing components in aircraft.

2. Material and Methods

Recycled CFRP composites are sourced from decommissioned aerospace components. The recycling process involved mechanical shredding and sieving to obtain strands of varying lengths and aspect ratios. For the sandwich structures, lightweight core materials such as Nomex honeycomb and foam cores are employed to enhance impact resistance while maintaining structural integrity. To assess the influence of strand morphology on mechanical performance, recycled carbon fibers are categorized based on length and aspect ratio [3]. Composite skins are fabricated with different strand configurations. Randomly oriented strand (ROS) composites are manufactured by distributing recycled strands in the epoxy matrix, followed by curing under controlled temperature and pressure conditions. For sandwich structures, ROS composite skins are bonded to core materials using a high-strength adhesive (Fig. 1). Prior to bonding, atmospheric plasma activation (APA) is applied to the ROS skins to enhance surface energy and improve adhesion [4]. The ROS composite surfaces are exposed to plasma for a specified duration to modify surface chemistry and increase wettability, thereby enhancing the bond strength between the skins and core materials. Mechanical testing included low-velocity impact tests performed using a drop-weight impact tester, adhering to ASTM D7136 standards. Specimens are subjected to controlled impact energies to evaluate damage resistance and energy absorption capabilities. Post-impact damage assessment is conducted using non-destructive evaluation (NDE) techniques such as ultrasonic Digital Image Correlation (DIC) to detect internal delamination and fractures. Scanning electron microscopy (SEM) is utilized to examine the fracture surfaces of impacted specimens, providing insights into failure mechanisms, fiber-matrix interactions, and the effectiveness of atmospheric plasma activation (APA) treatment in enhancing interfacial bonding.

3. Results and Discussion

First, the impact resistance of CFRP composites is significantly influenced by the morphology of the recycled carbon fiber strands. Composites reinforced with longer strands exhibit higher energy absorption during impact testing compared to those with shorter strands. This enhancement is attributed to the increased load transfer efficiency and improved stress distribution associated with longer fibers, which effectively bridge cracks and hinder crack propagation [3]. These findings are consistent with previous studies that have demonstrated the positive correlation between fiber length and impact resistance in composite materials [2]. Furthermore, integrating recycled CFRP composites into sandwich structures with lightweight cores, such as Nomex honeycomb and foam cores, results in a notable improvement in impact resistance. The sandwich structures absorb higher impact energies and exhibit reduced damage areas compared to monolithic composites. This improvement is due to the ability of the core materials to dissipate impact energy and prevent damage propagation through the thickness of the structure. Similar observations have been reported in studies where sandwich configurations enhance the energy absorption and shock resistance properties of composite materials [5].

The application of atmospheric plasma activation (APA) treatment to the surfaces of recycled CFRP composites prior to bonding in sandwich structures significantly enhances interfacial adhesion between the skins and core materials. This enhanced adhesion contributes to improved impact resistance, as evidenced by higher energy absorption and reduced delamination observed during impact testing. The APA treatment increases the surface energy of the composite skins, promoting better bonding with the adhesive and core materials. This finding aligns with existing literature that highlights the role of surface treatments in enhancing the interfacial properties and overall performance of composite structures [4,6].

Post-impact evaluations reveal that both the strand morphology and sandwich structure configuration influence the residual mechanical properties of the composites. Specimens with longer fiber strands and those configured as sandwich structures retain higher residual flexural strength and stiffness after impact [6]. This retention is attributed to the improved damage tolerance provided by longer fibers and the energy-dissipating characteristics of the sandwich core materials.

4. Conclusion

In summary, tailoring the strand morphology and employing sandwich structures with appropriate surface treatments can significantly enhance the impact resistance and post-impact performance of recycled CFRP composites. These results highlight the importance of optimizing fiber morphology and structural design to enhance the durability and service life of recycled CFRP composites in applications subject to impact loading.

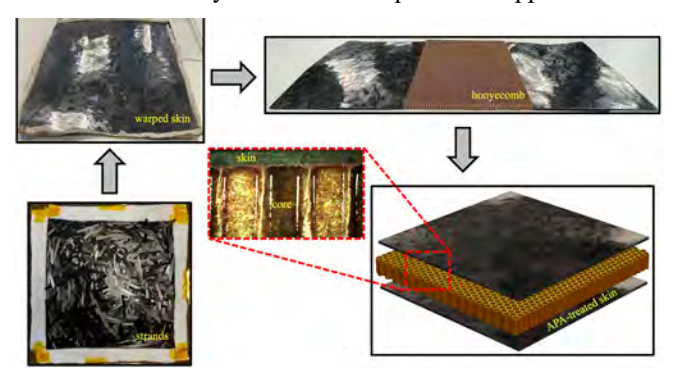


Fig. 1. Manufacturing of sandwich composites from ROS using APA-treatment.

5. References

- [1] Qiao, Yao, et al. "A review of the fabrication methods and mechanical behavior of continuous thermoplastic polymer fiber—thermoplastic polymer matrix composites." Polymer Composites 44.2 (2023): 694-733.
- [2] Pedroso, Judith M., et al. "Comparative study of friction and wear performance of PEK, PEEK and PEKK binders in tribological coatings." Polymers 14.19 (2022): 4008.
- [3] Özbek, Yağız, et al. "İnfluence of Strand Size and Morphology on the Mechanical Performance of Recycled CF/PEKK Composites: Harnessing Waste for Aerospace Secondary Load-Bearing Applications." Composites Part B: Engineering (2025): 112232.
- [4] Ozbek, Yagiz, et al. "Enhancing adhesive bonding and mechanical properties of composite sandwich panels through atmospheric plasma activation." Polymer Composites (2024).
- [5] Zaharia, Sebastian Marian, et al. "Mechanical properties and fatigue performances on sandwich structures with CFRP skin and nomex honeycomb core." Mat. Plast 54 (2017): 67.
- [6] Özbek, Yağız, et al. "Feasibility and performance evaluation of randomly oriented strand recycled composite skins in sandwich structures: A green cost-effective solution for aerospace secondary load-bearing applications." Polymer Composites (2025).

Enhanced impact resistance of 3D spacer composite by hybridization with CF sheets

Ferhat Yıldırım, ¹ Volkan Eskizeybek, ^{2*}

Abstract: The increasing demand for lightweight and high-strength battery pack enclosures in electric vehicles motivates the exploration of advanced composite materials as an alternative to conventional metal enclosures. In this study, carbon fiber face sheet reinforced single and double-layer 3D glass spacer composites were produced and their low velocity impact performance was investigated. The peak force increased 97.7 % compared to the neat 3D composite for double-layer 3D glass spacer composites with the addition of a carbon fabric interlayer. Comparative analysis confirms its suitability for enhancing battery safety and efficiency, making it a promising solution for next-generation energy storage systems.

1. Introduction

1.1. Required Elements

Battery pack enclosures (BPE) mechanically support vehicle stability while protecting the batteries from impact, moisture, dust, electromagnetic interference, and thermal runaway. Additionally, they play a crucial role in thermal management and represent the structural foundation on which electric vehicles are built [1]. Therefore, although they are one of the most significant weight contributors to the vehicle, weight alone cannot be the only design consideration for battery enclosures [2]. Efforts to reduce the overall weight of structural components have focused on low-density materials such as aluminum alloys and composite materials [3; 4]. Composite materials offer a potential solution due to their high specific strength, low weight, and thermal and chemical resistance. Wang et al. replaced designated body parts of a metal-framed electric vehicle with polymer-reinforced carbon fiber (CFRP) components. Their analyses and experimental applications showed that the vehicle's chassis could be made over 30% lighter compared to its metal counterpart (469 kg for steel parts vs. 322 kg for composite equivalents) while still passing crash tests without any loss of safety [5]. Glass fiber-reinforced polymer (GFRP) composites demonstrate superior impact resistance compared to CFRP due to their improved energy absorption capacity. Consequently, GFRP can endure prolonged stress before failure, making it a more effective reinforcement option. To address the impact resistance and energy absorption limitations of CFRP, a method has been developed that combines carbon fiber (CF) and glass fiber (GF) within a composite material. This technique, commonly referred to as fiber hybrid composite, is designed to overcome these challenges. Hosseinzadeh et al. [6] stated that fiber hybrid composites maintain suitable behavior under both low-speed and high-energy impacts, as GF and CF complement each other's inherent limitations. These specialized composites also exhibit high tolerance and significant damage resistance. In this study, single and double-layer 3D composites were produced as hybrids with CF and their low velocity impact properties were investigated.

2. Materials and Methods

As a main reinforcement, we used 3D E-glass spacer woven fabric (Parabeam BV., Netherlands) with a thickness of 3.3 mm and a density of 782 g m $^{-2}$. Used carbon fiber fabric as the hybridization reinforcement material in the study has 7 μ m diameter and 240 g m $^{-2}$ density with twill woven. The epoxy matrix with two components commercially available as known MGS LR285/LH285 and both materials was purchased from Dost Kimya, Türkiye.

The partial vacuum infusion method was used for the neat 3D composites manufacturing according to the previous studies of our research group [7; 8]. For hybridization process of single layer 3D composites, one layer of carbon fabric was laid under the 3D fabric and one layer on top, and all the fabrics were taken under vacuum. When the fabrics were completely wet, the vacuum bag was removed before the curing to provide the crushed plies of the fabric spring back and allowing the material to regain its 3D spacer form [7; 8]. For obtaining double layered 3D hybrid composite, carbon fabric was positioned at the bottom, 3D fabric was placed on it, then another 3D fiber was positioned at a 90 degree angle, and finally the second carbon fabric was positioned again on top. When all layers were prepared, the fabrics were taken under vacuum again and impregnated with epoxy. When the wetting process was completed, the vacuum bag removed again for allowing to spring back. Finally, the single- and double-layer hybrid 3D woven composites were cured for 18 h at room temperature.

¹ Department of Machinery and Metal Technologies, Çanakkale Onsekiz Mart University, Çanakkale 17202, Turkey

² Department of Materials Science and Engineering, Çanakkale Onsekiz Mart University, Çanakkale 17020, Turkey

*veskizeybek@comu.edu.tr

Low-velocity impact (LVI) tests were conducted following the ASTM D-7136 standard with a sample size of 100×100×3 mm, by using Instron Ceast 9350 test device. The impactor with a semi-spherical tip (20 mm diameter) and impact energy was set as 15 Joule according to the older studies [8].

3. Results and discussions

Figure 1 represents force-time responses of the 3D composites according to hybridization variety. The continuous oscillation of the force-time curves in Fig. 1 is caused by the main shock pulse, high-frequency oscillation, and free vibration of the laminate at LVI [9]. When the neat 3D composites' graph is investigated, firstly, the elastic deformation on the 3D composite occurs and the kinetic energy of impactor is converted into elastic deformation. With the gradual increase of absorbed energy, matrix microcracks and fractures appear on the composite. When the load on the composite reaches the peak force, the material absorbs all the kinetic energy. Then the elastic energy of the composite is converted into the kinetic energy of the impactor, and the displacement of the impactor begins to return. The occured linearity on curves at the 6 ms is due to the deformation sizes. While the force decreases with a steep slope in other samples, the neat sample has a more horizontal curve because it has undergone a lot of deformation. Compared to the neat, the rising incline of the curve of the carbon fabric faced samples (S1) indicates the difference in reaction based on hardness between carbon and glass. After the energy transformation with the same formation, the force increases to a maximum and then decreases again.

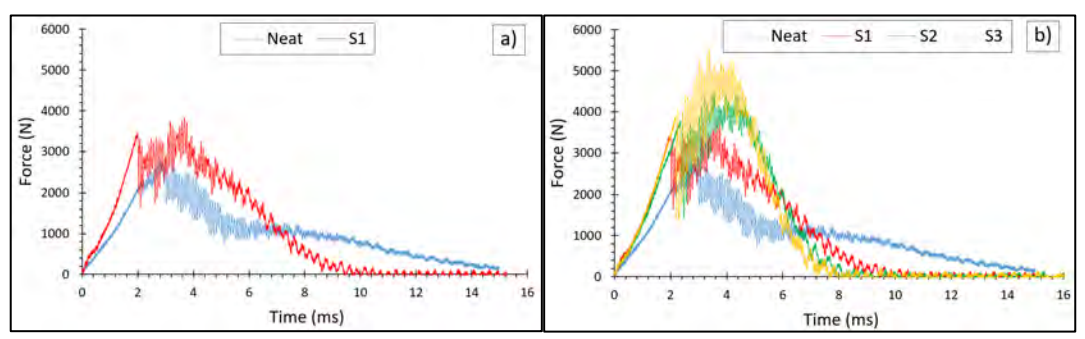


Figure 1. Force Time results, a) Single layer samples, b) All samples comparisons

The double-layer designed 3D composites show greater peak forces compared to the single-layer composites. The measured fmax value for S2 sample was 4447.21 N and development rates achieved nearly 58.7% compared to the neat 3D composite. Here, in accordance with the literature, it is seen that carbon with high bending stiffness and brittleness and glass fabrics with lower properties can be ideally combined [10]. As known, carbon and glass can be arranged in different sequences ways, but here they are located in the outer layers of the 3D and composite due to the special spacer structure. Hybrid samples are designed in this way and the effect of the hard carbon fabric is clearly seen. For S2 samples, besides the carbon surface coating, the added second 3D glass layer has an important role for obtained impact force improvement. Differences between the peek forces of S1 and S2 resulted due to the effect of second 3D glass fabric. The peak force value of S3 samples containing an additional carbon fabric layer between 2 3D glasses increased even more. The measured fmax value for sample S3 was 5538.59 N and the improvement ratio reached 97.7 % compared to the neat 3D composite. It is also higher than 43.6% and 24.5% versus S1 and S2, respectively. When comparing the S2 and S3 samples, it can be said that the added carbon fabric directly affected this result.

References

- [1] Shui, L., Chen, F., Garg, A. et al., 2018, "Design optimization of battery pack enclosure for electric vehicle. Struct Multidisc Optim" 58, pp. 331–347.
- [2] Höhne, C.C., Blaess P, Ilinzeer,, S., Griesbaum, P., 2023, "New approach for electric vehicle composite battery housings: Electromagnetic shielding and flame retardancy of PUR/UP-based sheet moulding compound", Composites Part A: Applied Science and Manufacturing, 167,107404.
- [3] Arora, S., Shen, W., Kapoor, A., 2016, "Review of mechanical design and strategic placement technique of a robust battery pack for electric vehicles, Renew. Sustain," Energy Rev., 60, pp. 1319–1331.
- [4] Kaleg, S. and Amin, 2016, "1P15S lithium battery pack: Aluminum 5052–0 strength of material analysis and optimization," International Conference on Sustainable Energy Engineering and Application (ICSEEA), IEEE, 2016, pp. 1–5.
- [5] Wang, Z., Käferböck, M., Zhao, H., Chen, H., 2021, "First Body-in-White Made from Composites for a Chinese Electric Car," ATZ Worldw, 123(3), pp. 16-21.
- [6] Hosseinzadeh, R.; Shokrieh, M.M.; Lessard, L., 2006, "Damage Behavior of Fiber Reinforced Composite Plates Subjected to Drop Weight Impacts," Compos. Sci. Technol. 66, pp. 61–68.

- [7] Yildirim F, Aydin M, Avci A., 2021, "Improved mechanical performance of three-dimensional woven glass/epoxy spacer composites with carbon nanotubes," Journal of Reinforced Plastics and Composites, 40(13-14), pp.533-549.
- [8] Yıldırım F, Tatar AC, Eskizeybek V, Avcı A, Aydın M., 2021, "Impact response of nanoparticle reinforced 3D woven spacer/epoxy composites at cryogenic temperatures," Journal of Composite Materials, 55(28), pp. 4231-4244.
- [9] Found, M.S., Howard, I.C., Paran, A.P., 1998, "Interpretation of signals from dropweight impact tests," Compos. Struct, 42(4), pp. 353–363.
- [10] Huang, Y., Liu, Y., Liu, H., Zhang, S., Hu, J., Zhao, J., 2025, "Low-velocity impact and compression-after-impact behaviors of carbon/glass fiber hybrid composite laminates based on thin-ply carbon fiber prepreg and unidirectionally arrayed chopped strand," Thin-Walled Structures, 211:113075.

Charpy Impact Performance of S2 Glass/Basalt Fiber-Reinforced Hybrid Composites

Sara Saeed Abdulrahman Eltahir, ¹ Çağatay Yılmaz ^{2,*}

¹ Department of Advanced Materials and Nanotechnology, Abdullah Gül University, Kocasinan 38080, Kayseri/Türkiye

² Department of Mechanical Engineering, Abdullah Gül University, Kocasinan 38080, Kayseri/Türkiye

*yilmaz.cagatay@agu.edu.tr

Abstract: This study contributes to the mechanical performance of S2 Glass/Basalt Fiber-Reinforced Hybrid Composites under high strain rate loading - Charpy impact testing. The composite laminates are produced using vacuum vacuum-infused process in four fiber stacking sequences. Using CNC milling machine the specimens are produced following ISO 179 standard and tested in an impact testing machine subjected to both edgewise and flatwise loading. Charpy's impact energy is aimed to be obtained, consequently, post-fracture analysis is conducted using scanning electron microscopy (SEM) to examine failure surfaces.

1. Introduction

Fiber-reinforced polymers have gained significant attention due to their superior mechanical properties. S2 glass fibers offer enhanced properties compared to traditional glass fibers, having remarkable impact strength, tensile strength, chemical stability, gamma radiation resistance, and low density. Similarly, Basalt fibers demonstrate exceptional heat resistance, mechanical robustness, high failure strain, and corrosion resilience making them suitable for ballistic protection applications, reinforced concrete constructions, and fire-resistant fabrics [1]. Despite growing interest in fiber hybridization, limited research has focused on the Charpy impact strength of S2 glass/basalt hybrid composites. Dorigato et al. 2013 investigated the flexural and impact behavior of carbon/basalt fibers hybrid laminates [2]. Doğru et al. 2024 studied the ballistic impact resistance and flexural performance of natural basalt fiber with carbon and traditional glass fibers [3]. Similarly, Bonsu et al. 2022 investigated the mechanical degradation and failure Analysis of hybridized traditional glass fiber with basalt fiber in simulated marine condition [4]. Therefore, this paper aims to add to the literature the Charpy impact performance of S2 glass/basalt reinforced hybrid composites.

2. Material Preparation and Testing

The primary materials used are S2 glass fiber and basalt fiber plain-weave of 800 and 220 gsm, respectively, combined with Biresin CR122-5 epoxy resin. Composite laminates are fabricated using the vacuum infusion process with four different fiber stacking sequences: pure S2 glass, pure basalt, S2-B-S2, and B-S2-B laminates, displayed in Table 1. Unnotched specimens are prepared following the ISO 179 standard, with dimensions of 80 \times 10 mm and an approximate thickness of 3.3 mm. Specimen cutting is performed using a Hannsa YL 1000-B three-axis CNC milling machine and pyramid diamond cutting tool at a spindle speed of 1000 rpm and a feed rate of 0.1 mm/rev. A total of 40 specimens are produced, with 10 from each plate – 5 for edgewise and 5 for flatwise Charpy impact testing.

Charpy impact tests are conducted on an instrumental impact-testing machine and the specimens are tested under both edgewise and flatwise loading. The data is processed and Charpy's impact energy is computed in kJ/m2. After testing is concluded, post-fracture analysis is performed using scanning electron microscopy (SEM) to examine the fracture surfaces.

Table 1. Laminate Stacking Sequence

Laminate No.	Stacking Sequence	Composition
1	[S2] ₅	Pure S2 glass
		laminate
2	$[B]_{20}$	Pure B glass
		laminate
3	$[S2/S2/B/B]_{\rm s}$	Hybrid laminate
4	$[B/B/S2/S2]_s$	Hybrid laminate

3. References

- [1] A. C. Sayin, S. Danisman, E. Ersoy, C. Yilmaz, and S. Kesriklioglu, "Experimental and statistical damage analysis in milling of S2-glass fiber/epoxy and basalt fiber/epoxy composites," Polym Compos, Jul. 2024, doi: https://doi.org/10.1002/pc.28826.
- [2] A. Dorigato and A. Pegoretti, "Flexural and impact behaviour of carbon/basalt fibers hybrid laminates," J Compos Mater, vol. 48, no. 9, pp. 1121–1130, Apr. 2013, doi: 10.1177/0021998313482158.
- [3] M. H. Doğru, E. Yeter, İ. Göv, and K. Göv, "Ballistic impact resistance and flexural performance of natural basalt fiber with carbon and glass fibers in inter-ply hybrid composites," Polym Compos, vol. 45, no. 11, pp. 9785–9801, Aug. 2024, doi: https://doi.org/10.1002/pc.28438.
- [4] A. O. Bonsu, C. Mensah, W. Liang, B. Yang, and Y. Ma, "Mechanical Degradation and Failure Analysis of Different Glass/Basalt Hybrid Composite Configuration in Simulated Marine Condition," Polymers (Basel), vol. 14, no. 17, 2022, doi: 10.3390/polym14173480.

Span Length Effect on Strain Rate and Flexural Performance of Natural Fibre Reinforced In-situ Polymerisable Composite

Mohamad Alsaadi, 1,2 * Tomas Flanagan, 2 and Declan M. Devine 1

PRISM Research Institute, Technological University of the Shannon, Athlone, Ireland,
Éire Composites Teo., An Choill Rua, Indreabhán, H91 Y923 Galway, Ireland
*mohamad.alsaadi@tus.ie and m.alsaadi@eirecomposites.com

Abstract: This study aims to investigate the effect of the span-to-depth ratio on the strain rate and, thus, the flexural strength and flexural modulus of a natural basalt fibre-reinforced novel in-situ polymerisable thermoplastic resin composite. Composite samples were manufactured and tested in three-point bending according to ASTM D790 standards, using span-to-depth ratios of 40, 32, and 19. The varying span value can lead to a change in the rate of straining of the outer surface of the test composite specimen and flexural performance. The results indicated that span length can significantly affect the strain rate at the outer surface of the composite, and thus its flexural strength and modulus.

1. Introduction

The complex behaviour of composite materials, including their anisotropic nature and unique stress-strain relationships, underscores the importance of thorough and appropriate mechanical testing. These tests provide the necessary data to understand, predict, and optimise the performance of composite structures in various applications. For instance, the fibre orientation gives the composite anisotropic properties, i.e., the properties in fibre orientation are dominated by the fibre properties and are perpendicular to them, so the matrix properties are more pronounced. Therefore, the mechanical properties vary depending on the direction of the applied load. Knowledge of this anisotropic behaviour is required to design and produce these composite components. When the anisotropy of a material is unknown, it can lead to errors in measuring flexural performance and pose significant design problems for products made from fibre-reinforced composites. For example, plane surfaces can buckle, crack or break early [1]. The three-point bending test is analysed considering the shear and local deformation effects during load application and support. The advantages of the flexural three-point bending test are that it is a simple setup and provides knowledge of flexural stress-strain behaviour. At the same time, the limitations are high shear stresses near supports and the potential for localised damage at the loading point. Since shear effects influence bending tests when the span-to-depth ratio is not large. In unidirectional composites, the effect is significant when the test is carried out in the direction of the fibre since the ratio between longitudinal flexural modulus and shear modulus is greater than 20, while the isotropic materials, the maximum ratio between longitudinal modulus and shear modulus is 3, due to the maximum value of Poisson ratio being 0.5 [2]. The standard ISO 14125 [3] proposes a fixed strain range for modulus determination when shear effects are negligible. According to Mujika [2], the variation of span in three-point and four-point bending caused by bending rotations is related to the strain range used for determining flexural modulus. Correction factors have been proposed to consider the effect mentioned. According to the standard of flexural testing, the span-to-depth ratio shall be chosen such that failure occurs in the outer fibres of the samples and is due only to the bending moment. Hence, a support span-to-depth ratio of 16:1 is generally satisfactory when the ratio of the tensile strength to shear strength is less than 8. Still, the support span-to-depth ratio must be increased for composite laminates with high tensile strength parallel to the support span and low shear strength in the laminate plane. Therefore, a span-to-depth ratio higher than 16:1 is essential, such as 32:1 or 40:1. For some highly anisotropic composites, shear deformation can significantly influence modulus measurements, even at span-to-depth ratios as high as 40:1. Hence, the increasing of the span-to-depth ratio can lead to eliminating shear effects when modulus data are required [5]. Elium is a new acrylic-based, in-situ polymerisable, low-viscosity resin that functions as an infusible thermoplastic. It can be infused under vacuum at room temperature and post-cured at a low temperature below 60°C. This study investigated the effect of the span length on the strain rate of the outer composite fibre and the flexural strength and flexural modulus of a natural basalt fibre-reinforced novel thermoplastic resin composite. The span-to-depth ratio of 16:1 is unsatisfactory for our BF/Elium composite, as the tensile strength-to-shear strength ratio is approximately 20.

2. Materials and Testing

The basalt fibre (90% of its fibre in the 0° direction and 8.6% in the 90° direction, with the remaining 1.4% used for stitching) is used to reinforce Elium thermoplastic resin. The flexural properties were determined using the Zwick Roll machine (Z010, GmbH & Co. KG, Baden-Wurttemberg, Germany) (Figure 1). Flexural test samples were prepared according to ASTM D 790, with a size of 130×13 mm and span-to-thickness ratios of 19, 32, and 40, respectively. The samples' thickness was 2.63 ± 0.05 mm. The crosshead speed for the flexural test was 4

mm/min. At least three specimens were tested for each span-to-depth ratio, and the average value was dependent. The flexural stress (σ) , strain (ε) and modulus (E) were determined from the data of the testing machine by using the following equations:

$$\sigma = \frac{{}_{3}P_{max}L}{2bh^2} \left[1 + 6\left(\frac{D}{L}\right)^2 - 4\left(\frac{h}{L}\right)\left(\frac{D}{L}\right) \right], \quad \varepsilon = \frac{6Dh}{L^2}, \quad E = \frac{mL^3}{4bh^3}, \qquad Z = \frac{6Rh}{L^2}$$
 (1)

Where L, b and h are the span, width and depth of the specimen (mm), m is the slope of the tangent to the initial straight-line portion of the load–deflection curve, D is the maximum deflection before failure, P is the load at a given point on the load-deflection curve, R is the rate of crosshead motion (mm/min), and Z is the rate of straining of the outer fibre (mm/mm/min).

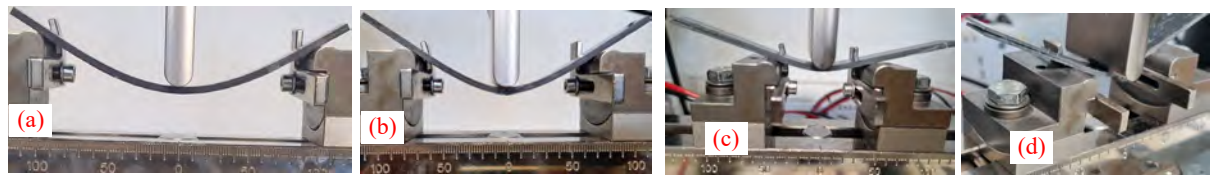


Fig. 1. Flexural samples during testing, with various span-to-depth ratios of (a) 40, (b) 32, (c) 19 and (d) 19.

Stress-strain responses of the three various span-to-depth tests are shown in Figure 2 and Table 1. As shown in Table 1, with a span-to-depth ratio of 32, the strain rate is 0.01, as specified by ASTM 790, which yields the best results without shear or delamination for the first failure, where the fibre pulls out from the matrix and breaks (Fig. 2 b). On the other hand, the flexural strength and modulus values were significantly reduced with a span-to-depth ratio of 40 (strain rate: 0.006) by 17% and 8%, respectively. Consequently, the sample slide, as evident at the end of the curve (Fig. 1a and 2a). The flexural strength and modulus values decreased by 8% and 25% due to the shear and delamination effect with the span-to-depth ratio of 19 (strain rate was 0.025) (Fig. 1c and d). It was noticed that the failure strain values were slightly affected when changing the span length.

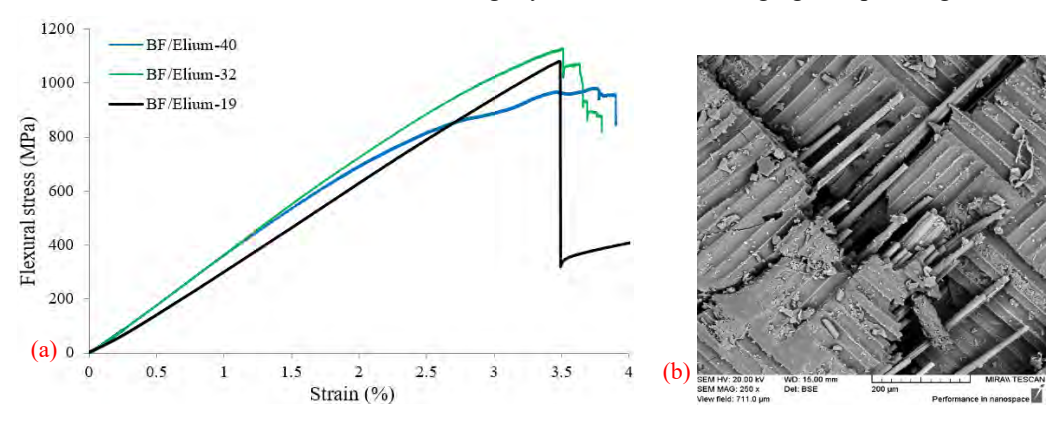


Fig. 2. (a) Flexural stress-strain behaviour of various span-to-depth ratios, (b) SEM of the 32 span-to-depth.

Table 1. Flexural properties

Sample No.	Strain rate, Z (mm/mm/min)	Span/depth (mm/mm)	Strength (MPa)	Reduction (%)	Modulus (GPa)	Reduction (%)
BF/Elium-40	0.006	40	932± 37	17	33.7±1.4	8
BF/Elium-32	0.01	32	1128+15	-	36.6 ± 1.5	-
BF/Elium-19	0.025	19	1036 ± 21	8	27.4 ± 1.7	25

3. References

- [1] NETZSCH, Why Knowledge About Anisotropy is Crucial when Designing High-Performance Composite Parts, https://analyzing-testing.netzsch.com/en/blog/2020/why-knowledge-about-anisotropy-is-crucial-when-designing-high-performance-composite-parts, Last Accessed 2025/22/02.
- [2] Mujika, F., 2007. On the effect of shear and local deformation in three-point bending tests. polymer testing, 26(7), pp.869-877
- [3] ISO 14125:1998, Fibre-reinforced plastic composites, Determination of flexural properties, 1998.
- [4] ASTM D 790-10. Standard Test Methods for Flexural Properties of Unreinforced and Reinforced Plastics and Electrical Insulating Materials; 2010.

Funding: This work is funded by the GreenCompos research project, with financial support from Research Ireland grant Number 23/IRDIFB/12098, and financial support for the HISTRATE Conference 2025.

Hydrothermal ageing effects on basalt fibre-epoxy composites modified with star-like polymers

Tatjana Glaskova-Kuzmina,^{1,*} Rochele Pinto,¹ Kristina Zukiene,² Gediminas Monastyreckis,¹ Vladimir Spacek,³ and Daiva Zeleniakiene¹

Abstract: The mechanical properties of basalt fibre-reinforced epoxy composites (BFRC) modified with star-like polymers (SLP) were evaluated after hydrothermal ageing (water absorption and desorption at 50 °C). BFRC with 1 wt.% SLP showed 49% higher fracture toughness, 26% higher critical load, and 195% greater absorbed energy in impact tests than the neat BFRC. However, increased water absorption led to significant decreases in critical load and fracture toughness — 14% and 33% for neat BFRC and 23% and 48% for SLP-modified BFRC. It was described by the improved wettability of SLP-modified epoxy on the surface of basalt fibres, testified using contact angle measurements.

1. Introduction

The demand for lightweight, energy-efficient materials in industries like wind, aerospace, and automotive is driving composite market growth. This raises concerns about plastic waste and depletion of petroleum, increasing interest in eco-friendly bio-based composites. However, natural fibre composites face challenges like lower mechanical properties, high water absorption, and limited durability [1]. BFRC offer a promising, cost-effective alternative to synthetic fibres, bridging the performance gap between glass (GFRC) and carbon fibre-reinforced composites (CFRC). Produced by melting volcanic basalt rock at 1450–1500 °C, basalt fibres require less energy and no additives than glass fibres. They offer low cost, good recyclability, and excellent mechanical, thermal, and flame-retardant properties [2]. BFRC also show superior resistance to water, acids, and chemicals, enhancing their durability in outdoor environments and making them a strong candidate for future structural materials [3,4].

The durability of fibre-reinforced composites depends on the degradation of the polymer matrix, fibres, and their interfacial bond [4]. Due to hydrothermal effects, epoxy resins used in fibre-reinforced composites (FRC) can undergo physical and chemical changes, leading to plasticization, chemical reactions, and post-curing [5]. However, experimental research on environmental impacts on FRC fracture toughness remains limited [6].

This study investigates the Mode I interlaminar fracture toughness of moisture-exposed, bioepoxy-based BFRC modified with SLP, aiming to assess the effect of water absorption and water-induced changes on their interlaminar fracture properties.

2. Materials and methods

Star-like polymers, specifically poly(n-butyl methacrylate)-(glycidyl methacrylate) block copolymer, were added to a biobased epoxy matrix reinforced with basalt fibres to improve the mechanical properties. The matrix, made from SR Greenpoxy 33 (Sicomin, France) and LITE 2401 (Cardolite, Belgium), contained approximately 33% bio content from biobased carbons and cashew nutshell liquid. The solid polymer was dissolved in a 51% tetrahydrofuran solution and mixed with the resin at 80 °C for 24 hours to create a 10 wt.% masterbatch [7]. This was then diluted to produce samples with 0.25, 0.5, and 1 wt.% concentrations, compared to the neat matrix. Unidirectional basalt fibre fabric (Basaltex, Belgium) was used to create laminate plates impregnated with the same polymer content as the epoxy.

Water absorption and desorption tests at 50 °C were conducted to assess the effect of star-like polymers on water absorption and desorption kinetics, with the elevated temperature accelerating the process. Mechanical tests were then carried out on samples at their equilibrium water contents. 3D Fick's model was used to describe the kinetics of water absorption and desorption.

Mode-I interlaminar fracture toughness tests were conducted on BFRP modified with SLP, with samples prepared according to ASTM D5528 and dimensions of $125 \times 25 \times 3$ mm. For low-velocity impact tests, the samples with dimensions of $60 \times 60 \times 1$ mm were fabricated according to ISO 6603-2. Two star-like polymer contents, 0.5 and 1 wt.%, were selected for basalt fibre reinforcement. The laminates were made by hand-layup with five layers of

Department of Mechanical Engineering, Kaunas University of Technology, Studentų g. 56, 51424 Kaunas, Lithuania

² Department of Production Engineering, Kaunas University of Technology, Studentų g. 56, 51424 Kaunas, Lithuania
³ SYNPO a.s., S. K. Neumanna 1316, 530 02 Pardubice, Czech Republic

^{*} tatjana.glaskova-kuzmina@ktu.lt

basalt fibre to achieve a 1 mm thickness. Only the 0.5 and 1 wt.% polymer contents were used, as adding 0.25 wt.% to the bio-based matrix showed no significant effect on the results.

3. Main results and conclusions

Adding 1 wt.% star-like polymers significantly improved the interlaminar fracture toughness of BFRC, enhancing it by 45%. Low-velocity impact tests revealed that the energy absorption of BFRC laminates modified with 1 wt.% of SLP was three times higher than that of unmodified BFRC. The results showed that SLP improved interfacial toughness, providing resistance to delamination and fracture. Additionally, they enhanced energy absorption by increasing the matrix ductility.

However, adding SLP to BFRC increased equilibrium water content and diffusivity by approx. 16-20%, leading to detrimental effects on the mechanical properties of BFRC. The critical load and intralaminar fracture toughness of BFRC decreased by 14% and 33% for neat BFRC and 23% and 48% for SLP-modified BFRC. It was described by the improved wettability of SLP-modified epoxy on the surface of basalt fibres, testified using contact angle measurements.

This study demonstrated the potential of using small amounts of SLP to modify high-bio-content matrices and create novel basalt fibre-reinforced composites with improved mechanical properties. Nevertheless, the environmental stability of SLP-modified BFRC should be further investigated and improved.

Acknowledgements

This project has received funding from the Research Council of Lithuania (LMTLT), agreement No S-MIP-23-134. T.G.-K. is grateful to COST Action CA21155 "Advanced Composites under HIgh STRAin raTEs loading: a route to certification-by-analysis" (HISTRATE).

- [1] Elfaleh, I., Abbassi, F., Habibi, M., Ahmad, F., Guedri, M., Nasri, M., Garnier, Ch., 2023, "A comprehensive review of natural fibers and their composites: An eco-friendly alternative to conventional materials," RINENG, 19, 101271. https://doi.org/10.1016/j.rineng.2023.101271.
- [2] Chen, D., Sun, G., Meng, M., Jin, X., Li, Q., 2019, "Flexural performance and cost efficiency of carbon/basalt/glass hybrid FRP composite laminates," Thin-Walled Struct., 142, pp. 516–31. https://doi.org/10.1016/j.tws.2019.03.056.
- [3] Glaskova-Kuzmina, T., Zotti, A., Borriello, A., Zarrelli, M., Aniskevich, A., 2021, "Basalt fibre composite with carbon nanomodified epoxy matrix under hydrothermal ageing," Polymers, 13(4), 532. https://doi.org/10.3390/polym13040532.
- [4] Grammatikos, S.A., Evernden, M., Mitchels, J., Zafari, B., Mottram, J.T., Papanicolaou, G.C., 2016, "On the response to hygrothermal aging of pultruded FRPs used in the civil engineering sector," Mater. Des., 96, pp. 283–295. https://doi.org/10.1016/j.matdes.2016.02.026.
- [5] Glaskova-Kuzmina, T., Aniskevich, A., Papanicolaou, G., Portan, D., Zotti, A., Borriello, A., Zarrelli, M., 2020, "Hydrothermal aging of an epoxy resin filled with carbon nanofillers," Polymers, 12, 1153. https://doi.org/10.3390/polym12051153.
- [6] Le Gué, L., Davies, P., Arhant, M., Vincent, B., Verbouwe, W., 2024, "Basalt fibre degradation in seawater and consequences for long term composite reinforcement,". Compos. Part A Appl. Sci. Manuf, 179, 108027. https://doi.org/10.1016/j.compositesa.2024.108027. [7] Pinto, R., Glaskova-Kuzmina, T., Žukienė, K., Monastyreckis, G., Novakova, M., Špaček, V., Kovalovs, A., Aniskevich,
- [7] Pinto, R., Glaskova-Kuzmina, T., Žukienė, K., Monastyreckis, G., Novakova, M., Špaček, V., Kovalovs, A., Aniskevich, A., Zeleniakiene, D., 2024, "Effect of star-like polymer on mechanical properties of novel basalt fibre-reinforced composite with bio-based matrix," Polymers, 16(20), 2909. https://doi.org/10.3390/polym16202909

Effect of carbonaceous fillers on interlaminar and compression after impact (CAI) properties of aeronautical CFRP

Aldobenedetto Zotti¹, Simona Zuppolini¹, Anna Borriello¹, Valeria Vinti², Luigi Trinchillo², Mauro Zarrelli^{1,*}

1 Institute for Polymers, Composites and Biomaterials, National Research Council of Italy, P.le Fermi, 1, 80055 Portici, NA, Italy

2 Avio S.p.A., Via Leonida Bissolati, 76, 00187 Roma, RM, Italy

* mauro.zarrelli@cnr.it

Abstract: The effect of different carbonaceous fillers, i.e. graphene nanoplatelets (GNPs), nanotubes (CNTs) and nanofibers (GANFs), on the interlaminar and compression after impact (CAI) properties of CFRP were investigated and discussed. The nanocomposites (NC) obtained by mixing 0.5wt% of fillers into an aeronautical-graded epoxy matrix (HXE75) have shown an improvement of the mode I fracture toughness, except for the NCs loaded with CNTs which show lower values for both K_C and G_C. This behavior is mirrored for mode I interlaminar fracture toughness (G_{IC}) properties of the corresponding composite laminates. CAI apparent modulus and residual strength were evaluated upon barely visible (BVD) damaging event occurring at 32J energy level impact; the recorded CAI results show that addition of GANF reduces the damaged area extension, restoring the value of the residual compression modulus of the corresponding undamaged laminate.

Materials and Methods

1.1. Materials

Three distinct carbon-based fillers, namely graphene nanoplatelets (GNPs), carbon nanofibers (CNFs), and carbon nanotubes (CNTs) were used.

GNPs (G4Nan purchased by Nanesa - Arezzo, Italy) are characterized by an average flake thickness of 8 nm and a specific surface area of approximately 56 m²/g. The CNFs (GANF, purchased by Grupo Antolin - Burgos, Spain), have a fiber diameter of 20–80 nm and a specific surface area of 80–120 m²/g. Lastly, single-walled CNTs (NC7000, purchased by Nanocyl - Sambreville, Belgium), have a diameter and length of 9.5 nm and 1.5 μm , respectively, with an aspect ratio of approximately 1000 and surface area of about 250–300 m²/g.

The epoxy system used for nanocomposites (NC) manufacturing is a patented epoxy resin, labeled HXE75 [1], characterized by a room temperature viscosity of about 10⁴ Pas with a minimum plateau value at 100°C of about 1 Pas. The carbon fibers utilized in the composite fabrication process are Toray T700 UD, which possess a tensile strength of 4900 MPa and a tensile modulus of 230 GPa.

1.2. Composites manufacturing

Each filler undergoes a Fluidized Bed Mixing (FDM) process, which implements high-frequency acoustic waves directly on dry powders to break down solid clusters. A fixed concentration of carbonaceous fillers (0.5wt%) was mixed with the HXE75 epoxy resin by using an industrial high shear rate mixer characterized by a high torque power. The so-obtained NCs were employed to produce modified carbon fiber reinforced composite prepregs by a customized hot melting plant, where uncured resin was first filmed on siliconized paper and then sandwiched on UD carbon fiber layer. Composite prepregs were layered, cured (2h @120°C) and finally machined according to the test standard dimensions (see Fig. 1).



Fig. 1. Modified CFRP manufacturing process.

1.3. CFRP Characterization

The Single Edge Notched Beam (SENB) geometry was employed for evaluation of the NC fracture toughness according to the test standard ASTM D5045 (samples nominal dimensions: $30 \times 7 \times 3.5$ mm³ with a notch depth of 3.5 mm). CFRP were characterized in terms of Mode I Interlaminar Fracture Toughness (GIC) and Compression After Impact (CAI). According to ASTM D5528, the Mode I Interlaminar Fracture Toughness sample geometry was $125 \times 25 \times 4$ mm³ with a pre-crack length, realized introducing a $13 \mu m$ kapton foil during lamination process, of 50 mm. CAI tests were performed according ASTM D7136 standard by inducing a low-speed impact damage (32J impact event) into the composite specimen and later performing a guided compression test (CAI) to assess the residual strength level and apparent modulus. CAI laminates are characterized by a multidirectional stacking sequence, i.e. $[45/0/-45/90]_{4S}$ with nominal dimensions of 150×100 mm. To acquire the laminate deformation, a

Digital Image Correlation equipment (3C Vision Correlated Solution DIC Equip.) was set during the tests to monitor the full deformation field contactless by applying a pattern on a specific area and recording the pattern changes by using a high-definition camera.

2. Results and Discussion

Fig. 2 reports the fracture toughness results of the studied NC; it is evident that GNP and GANF induce a remarkable increase of both $K_{\rm IC}$ (+14% and +12%, respectively) and $G_{\rm IC}$ (+36% and +37%, respectively); conversely, in CNT loaded NC, the carbonaceous filler has a detrimental effect on fracture toughness properties, and that behavior could be attributable to a worst dispersion of CNT in the hosting matrix (compared to GNP and GANF) due to the their larger surface area and consequent higher aggregation tendency. Considering both that the filler content is low (0.5 wt%) and that the $K_{\rm C}$ (1.56 MPa m^{1/2}) and $G_{\rm C}$ (0.68 KJ/m²) neat matrix values are higher compared to most of the commercial DGEBA-based epoxy resins, it results clear that the obtained improvement are significant.

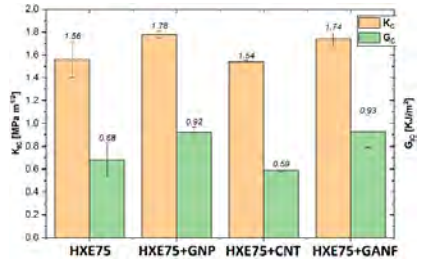


Fig. 2. Fracture Toughness results of carbon-based NC.

Table 1 reports the values of G_{IC} for the composites under investigation. As holding a strong correlation between NC fracture toughness and the corresponding mode I interlaminar fractur toughness, it results clear that G_{IC} values mirror the NC G_{C} behavior: therefore, GNP (+16%) and GANF (+60%) induce an increase of G_{IC} values compared to the unmodified system, while CNT (-5%) have a detrimental effect.

For CAI tests a 32 J impact energy was chosen after preliminary energy impact survey and this value was identified as the most appropriate to induce a BVID (i.e., a non-through indentation with a depth ranging from 0.2 to 0.5 mm) through the laminate; for each damaged sample the extension of the damaged area was evaluated. By DIC technique it has been possible to evaluate the out-of-plane strain map of the laminates, and consequently their residual strength and apparent stiffness.

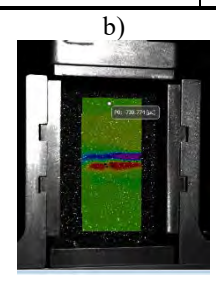
As reported in Table 1, the concentration of GANF remarkably affects both the residual strength, σ^{CAI} , and the apparent modulus, E^{CAI} , of the composite laminate. This is attributable to the smaller damage extension area measured for GANF loaded composites (~110 mm²) compared to the other damaged samples (~410 mm² for the unmodified composite). Compression tests performed on undamaged neat composites have revealed a strength and modulus of about 325 MPa and 55.8 GPa. From tables 1, is worth toing that the GANF concentration hold the initial undamaged composite apparent modulus, highlighting the potential of GANF as filler to limit the delamination.

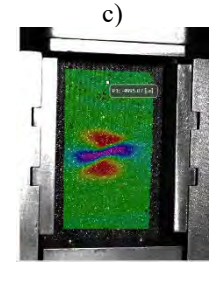
As clear in Fig. 3, the most deformed areas in damaged plates are those closest to the central damage, with a typical local buckling deformation characterized by concave and convex points symmetric respect to the center. Table 1 resumes interlaminar fracture toughness and CAI tests.

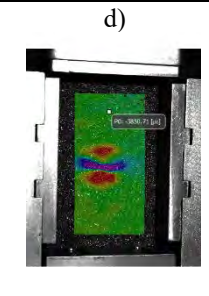
Table 1. CFRP mechanical tests results.					
Sample	G_{IC} [J/m ²]	σ ^{CAI} [MPa]	E ^{CAI} [GPa]		
HXE75-UD_undamaged	-	325±14	55.8±1.0		
HXE75-UD	272±15	170±10	43.8±1.0		
HXE75+GNP-UD	316±18	166±12	45.5±1.7		
HXE75+CNT-UD	258±8	175±7	45.3±0.8		
HXE75+GANF-UD	435±11	188±9	51.6±1.0		

Table 1 CFRP mechanical tests results









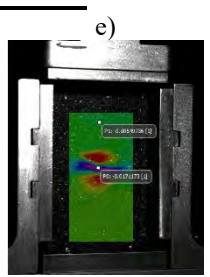


Fig. 3. DIC strain maps of a) undamaged HXE75-UD, b) HXE75-UD, c) HXE75+GNP-UD, d) HXE75+CNT-UD and e) HXE75+GANF-UD.

References

[1] Zotti, A.; Zuppolini, S.; Borriello, A.; Vinti, V.; Trinchillo, L.; Borrelli, D.; Caraviello, A.; Zarrelli, M. Effect of the mixing technique of graphene nanoplatelets and graphene nanofibers on fracture toughness of epoxy based nanocomposites and composites. Polymers 2022, 14, 5105.



Advanced Composites under High Strain Rate Loading A Route to Certification-by-Analysis

2025 Conference 4th – 5th JUNE 2025

Session 3 - Multi-modal sensing for impact detection and damage characterisation (WG5)





Impact damage identification in GFRP structures using the effective boundary approach

Jafar Amraei, 1, * Andrzej Katunin, 1 Chiara Colombo, 2 Antonio Salerno, 3 Andrea Manes 2

Department of Fundamentals of Machinery Design, Faculty of Mechanical Engineering, Silesian University of Technology, Konarskiego 18A, 44-100 Gliwice, Poland

² Politecnico di Milano, Department of Mechanical Engineering, via La Masa 1, 20156 Milan, Italy
³ Politecnico di Milano, Department of Energy, via Lambruschini 4a, 20156 Milan, Italy
* jafar.amraei@polsl.pl

Abstract: Heat accumulation during the non-uniform thermal excitation with a halogen lamp presents a significant challenge in detecting low-velocity impact damage (LVID) of composite plates. This accumulation reduces the temperature contrast between damaged and undamaged areas in the thermograms, making LVID identification more difficult. To tackle this issue, this study utilized the concept of the boundary of effective thermograms (BET) to determine the optimal sequence of registered thermograms, which were subsequently analyzed using the partial least squares regression (PLSR) image processing algorithm to enhance damage identification.

1. Introduction

The growing reliance on composite structures, including glass fiber-reinforced polymer (GFRP), in various engineering sectors, including aerospace, automotive, and marine industries, is driven by their outstanding mechanical properties, such as high strength-to-weight ratio highlights the need for design adaptability. However, these structures are susceptible to low-velocity impact damage (LVID), which can significantly compromise their structural integrity and operational lifespan. Among the various non-destructive testing (NDT) techniques, halogen lamp-based thermography is still employed for assessing impact damage due to its rapid inspection capabilities and non-contact operation.

2. Specimen and testing procedure

The GFRP plate used in this study was fabricated from E-glass fiber-reinforced epoxy composite material, comprising six layers of plain weave fabric with an areal density of 200 g/m^2 , supplied by Izo-Erg S.A. (Gliwice, Poland). The similar mechanical properties of the plain weave reinforcement in two directions allow for the elimination of the effect of fiber orientation on the impact-induced response. The dimensions of the tested GFRP are presented in [1]. To simulate LVID, a custom-designed drop-weight impact test machine was employed [2]. The impactor, labeled as E (see [2] for details), was selected to introduce multiple LVIDs in the GFRP plate. An energy level of 7 J was applied using this impactor. A total of five LVIDs were introduced, with the first impact at the center of the GFRP plate. The remaining four impacts were introduced at the corners of a 50 mm \times 50 mm square, positioned 25 mm from the center along both the horizontal and vertical axes, within the center of the 200 mm \times 240 mm plate.

The testing procedure for evaluating multiple LVIDs in the GFRP plate involved using a continuous halogen lamp (1 kW), model PLC64AL by Proel S.p.a., as the thermal excitation source. The thermal response of the GFRP plate was captured with an IR camera, Titanium by Cedip FLIR LLC, equipped with a cooled InSb sensor having a noise equivalent temperature difference (NETD) of less than 25 mK. The camera recorded thermal transients on the surface of the GFRP plate for approximately 10 seconds at a frame rate of 15 Hz.

3. Results

The registered thermogram captured after 10 seconds of testing, shown in Fig. 1(a), reveals the challenges inherent in halogen lamp-based thermography. Heat accumulation within the GFRP plate caused by the non-uniform thermal excitation from the halogen lamp resulted in a reduced temperature contrast between damaged and undamaged regions. This heat spread across the GFRP surface, diminishing the sensitivity of the technique and complicating the identification of LVIDs. Additionally, environmental factors may further influence the accuracy of the thermal imaging, leading to blurred thermograms. To mitigate this, the thermal response corresponding to the initial condition of the test was subtracted from the registered IR image at the end of testing. The subtracted result is shown in Fig. 1(b). This normalization process allowed for the elimination of thermal noise and environmental influences, thereby making it easier to highlight the damage-induced temperature changes. However, reliance on the raw thermal images, even after normalization, still poses a risk of misinterpreting the extent and location of the LVIDs.

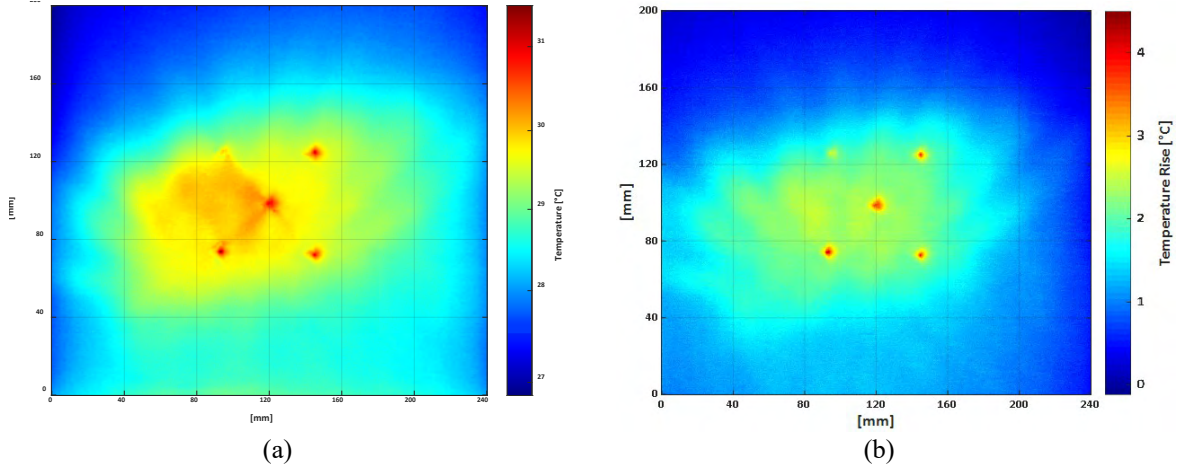


Fig. 1. Registered raw thermogram after 10 sec: (a) before normalization, (b) after normalization.

To enhance the identification of LVIDs, this study implemented the BET concept, a method that determines the optimal sequence of thermograms for identifying LVID in the GFRP plate. Similar to the previously published approach [2], the BET was established at the initial stage of the test, during which the maximum temperature gradient occurred. This dynamic parameter serves as an indicator of the period in which the GFRP plate experiences the highest heat transfer over a short time interval. Fig. 2(a) illustrates the maximum temperature rise observed on the surface of the GFRP plate during testing. The BET was selected by fitting a linear regression to the thermal response curve, and the thermogram corresponding to the point of tangency with this regression line was identified as the optimal BET. These selected thermograms were then analyzed using the PLSR algorithm in MATLAB software. The result of this image processing is depicted in Fig. 2(b), where the enhanced thermogram distinctly differentiates between damaged and undamaged areas, improving the reliability of LVID identification.

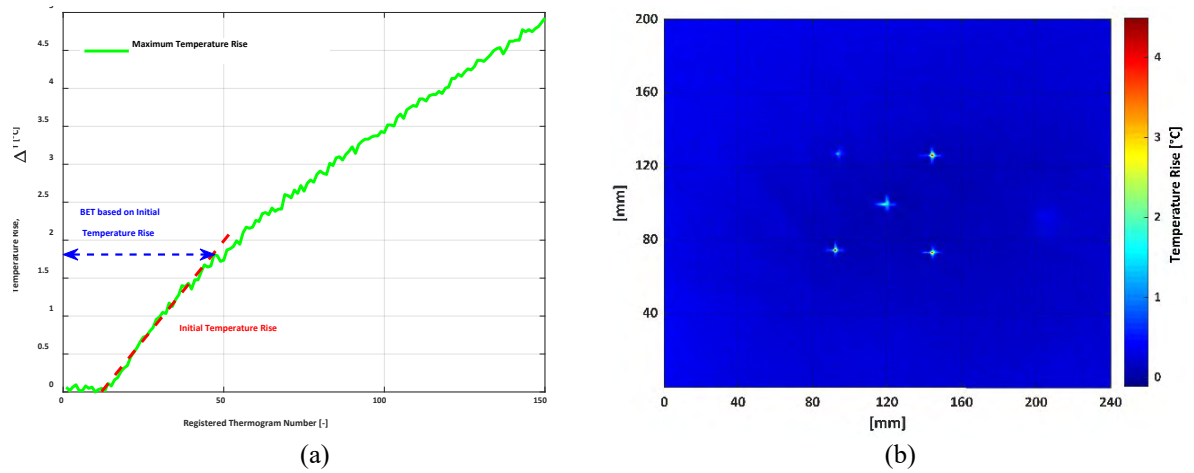


Fig. 2. (a) Optimal BET determined via the initial temperature rise, (b) Enhanced thermogram obtained from BET-based PLSR image processing algorithm.

4. Conclusions

This study demonstrated the challenges of using halogen lamp-based thermography to identify LVIDs in the GFRP plate, primarily due to heat accumulation and environmental influences. Utilizing the BET approach alongside PLSR-based image processing improved the temperature contrast, leading to better identification of LVIDs.

5. Acknowledgements

The first author acknowledges the funding support under the Excellence Initiative – Research University Program of the Silesian University of Technology, with Project Number: 32/014/SDU/10-27-24, year 2024.

- [1] Amraei, J., Katunin, A., Wachla, D., and Lis, K., 2025, "Damage assessment in composite plates using extended non-destructive self-heating based vibrothermography technique," Measurement, 241, p. 115670.
- [2] Katunin, A., Wronkowicz-Katunin, A., and Wachla, D., 2019, "Impact damage assessment in polymer matrix composites using self-heating based vibrothermography," Composite Structures, 214, pp. 214-226.

Full wave field analysis of damage severity for the impacted thermoplastic composites

Paweł H. Malinowski^{1,*}, Luigi Sorrentino²

Institute of Fluid Flow Machinery, Polish Academy of Sciences, 14 Fiszera Street, 80-231 Gdańsk, Poland
 Istituto per i Polimeri, Compositi e Biomateriali, Consiglio Nazionale delle Ricerche, P.le E. Fermi 1, 80055, Portici (NA), Italy
 * pmalinowski@imp.gda.pl

Abstract: This work investigates nondestructive technique of damage assessment based on a laser vibrometer. The vibrometer was used to scan the whole area of the investigated samples to measure the propagating elastic waves excited by a surface bonded piezoelectric sensor. The samples under investigation were polymer composites fabricated from poly(lactic acid) PLA and basalt fibers woven fabrics. The damage introduced in the samples was based on non-perforating impacts introduced with energy ranging between 1 J and 16 J. New approach for extracting the damage location was proposed based on frequency analysis of the measured signals. The impact location and extent were successfully identified.

1. Introduction

There is an increased usage of composites in demanding industrial applications. Recently a strong focus was put on thermoplastic composites and their impact resistance [1]. Their main advantages are the corrosion resistance, cost effectiveness and recyclability [2]. In this work we employed elastic wave propagation phenomena to learn about the structural condition of samples with impact damage. The samples were manufactured from PLA/basalt fiber composites. The whole wave field of propagating waves was measured with a scanning laser Doppler (SLDV) vibrometer, which proved to be an effective nondestructive evaluation (NDE) tool [3]. Based on the gathered data, a damage assessment procedure was developed to investigate the effect of low energy impacts.

2. Samples and measurement procedure

Fig. 1 shows the front (impacted) side of a representative sample (4 consecutive impacts at 4J, namely). The samples were made of PLA (Luminy L175, Total/Corbion NV, the Netherlands) used as matrix and plain weave fabric of basalt fibres (BAS 220.1270.P, Basaltex-Flocart NV, Belgium). The composite sample plate were prepared using film stacking process. Laminates of 10 fabric layer 0/90 were symmetrically arranged [(0/90)5]_s resulting in 1.8 mm thick plates with 45% fibre volume content. For wave excitation a sensor (10-mm diameter and 0.5-mm thickness) was glued at one of the sample edges (sample bottom in Fig. 1). It was excited by a tone burst signal of 100 kHz frequency. The acquisition was made with a single head of the PSV-400-3D vibrometer from Polytec. Thanks to the scanning capabilities of the device the measurements were gathered in 3723 points arranged into a 51x73 rectangular grid. The spacing between grid points was about 2.2 mm. Samples were scanned on the back (measured) side.



Fig. 1. Photo of impacted sample (4J impact × 4) with surface bonded sensor

3. Results and conclusions

The study comprised of the finding of an effective time interval for extracting damage visualization-useful information from the gathered time signals. At each measurement point 1.6 ms-long time signal was gathered. Focusing on smaller time intervals brings the benefit of removing the influence of the signal part that do not carry damage-related information. After the identification of the proper analysis interval, the frequency spectrum was calculated and significant data were extracted after setting a threshold. Finally, the cumulative value from the spectrum is assigned to each measurement point of the sample surface for visualization purposes.

An example of the damage visualization result based on this procedure is shown in Fig. 2. The significant signal was obtained from the 0.43-1.21 ms time window, and the frequency components above 50% of the maximal value were taken into account. Both the single impact at 4J (Fig.2a) and four consecutive impacts at the same energy (Fig.2b) were successfully localized. The damage made at higher energy results in significantly clearer indication.

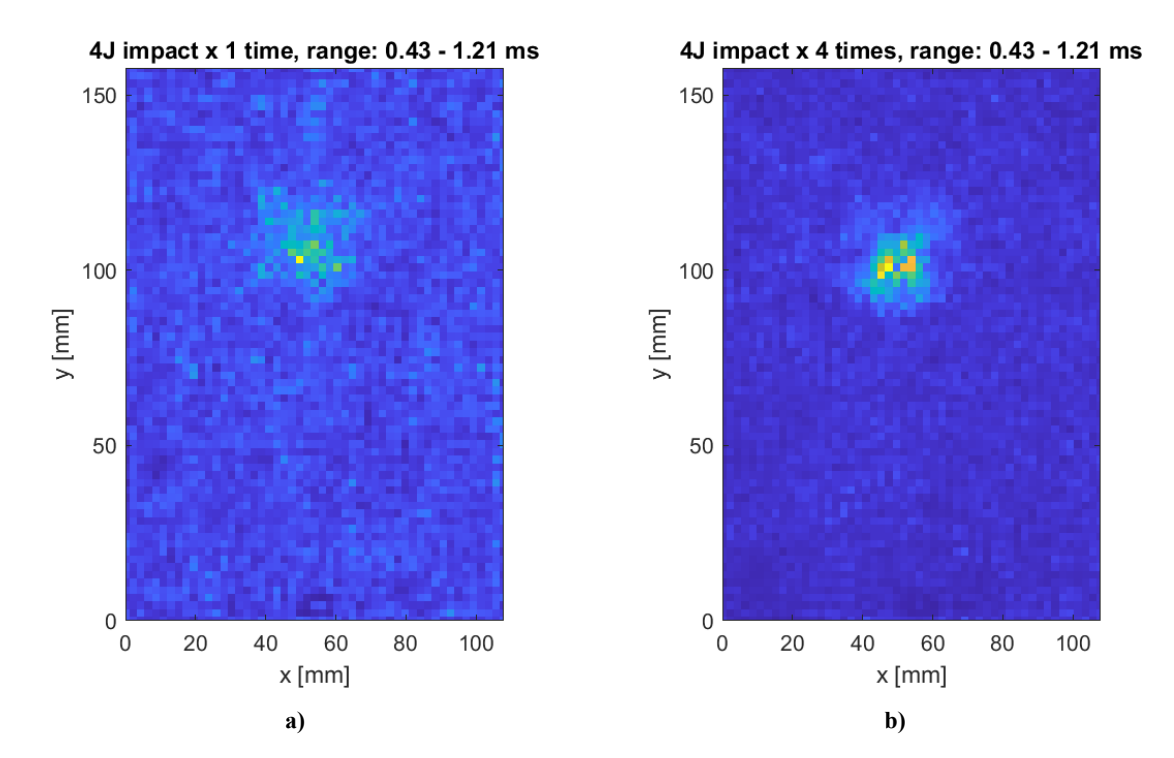


Fig. 2. Result - damage visualization for samples with single impact: a) 4J impact × 1, b) 4J impact × 4

4. Acknowledgments

This study has been carried out within the bilateral collaboration project "Non-destructive evaluations on repaired fibre reinforced composites (REPCOM)" – Biennium Program 2020-2021 between IPCB-CNR and IMP-PAN. The authors would like to thank Mr Fabio Docimo for his contribution to the preparation of all tested samples.

- [1] Shah, S.Z.H., S. Karuppanan, P.S.M. Megat-Yusoff, and Z. Sajid, 2019,. "Impact Resistance and Damage Tolerance of Fiber Reinforced Composites: A Review". Composite Structures, 217, pp. 100–121.
- [2] Sorrentino, L., Silva De Vasconcellos, D., D'Auria, M., Sarasini, F. and Jacopo Tirillò, 2017. "Effect of Temperature on Static and Low Velocity Impact Properties of Thermoplastic Composites", Composites Part B: Engineering, 113, pp. 100–110.
- [3] Malinowski, P.H., Mustapha, S., Fakih, M.A. and Singh, S.K., 2024, January. Employing Guided Wave-Based Damage Localization Techniques for Additively Manufactured Plates with Different Infill Densities. In IMAC, A Conference and Exposition on Structural Dynamics (pp. 33-37). Cham: Springer Nature Switzerland.

Identification of impact damage in sandwich composite structures using high-speed 3D digital image correlation and wavelet analysis

Andrzej Katunin^{1,*}, Róbert Huňady², Martin Hagara³

*andrzej.katunin@polsl.pl

Abstract: Effective techniques for identification of low-velocity impact damage in composite structures are of high demand in applications, especially for sandwich structures, where the presence of impact damage may compromise their stiffness and integrity. In this study, we proposed the modal-based technique for identification of impact damage in structures using high-speed 3D digital image correlation with further post-processing of acquired mode shapes with wavelet transform. A case study for impacted sandwich structure has been demonstrated. This technique is a cost-effective alternative for scanning laser Doppler vibrometry (SLDV), which additionally offers much shorter inspection duration with a comparable sensitivity to SLDV.

1. Introduction

The problem of evaluation of a structural integrity for structures and components after low-velocity impact remain one of the most challenging issues in maintenance, especially for transportation and critical infrastructure. Existing non-destructive testing and structural health monitoring techniques are constantly evolving to improve their sensitivity to various types of damage. Vibration-based methods are among the oldest but also the most promising for structural assessment. Numerous efforts have been made to improve the sensitivity of vibration-based methods in impact damage identification, which are mostly based on processing of acquired mode shapes and modal curvatures to identify damage using advanced processing algorithms [1,2]. Such an approach makes it possible to consider the vibration-based damage identification techniques as local, since due to precise measurements of vibration, mainly by using scanning laser Doppler vibrometry (SLDV), the localization and identification of damage based on processing of mode shapes is possible. The damage identification ability can be assessed as very effective using SLDV, which was demonstrated in previous studies [3]. However, the main limitations of this measurement technique cover long duration of tests (to acquire mode shapes with high resolution, and therefore, identify damage precisely, the grid of measurement points should be dense enough) and high costs of measurement equipment.

In this study, we propose an alternative approach that combines high-speed 3D digital image correlation (DIC) with wavelet analysis of acquired mode shapes for low-velocity impact damage identification in sandwich structures. The study aims to demonstrate the effectiveness of this method in identifying low-velocity impact damage in sandwich structures and to evaluate its potential as a cost-effective alternative to SLDV-based methods.

2. Specimens, Experimental Setup, and Processing Procedure

The tests were performed on square sandwich panels with a side length of 300 mm and thickness of 4.1 mm, manufactured and supplied by PPHU Surfpol. The core of tested panel was 3 mm thick and made of aramid paper impregnated with phenolic resin, while the 0.5 mm thick outer facings made of a glass fiber-reinforced polymer laminate. The manufacturing process and the fundamental properties of these panels are described in detail in [3]. The impact damage was introduced using the custom drop-weight impact testing machine in the center of the tested panels with various impactor geometries and impact energies. The representative case of impacted panel is presented in Fig. 1(a).

The impulse excitation of tested panels clamped on the edges (Fig. 1(b)) was performed using the Brüel & Kjær Type 8206 impact hammer with a hard plastic tip. The vibration response of the panels was captured using the Dantec Dynamic Q-450 correlation system equipped with two Vision Research Phantom v310 cameras (Fig. 1(c)) and the acquired results were pre-processed by the Istra4D software. The details on the testing setup can be found in [4]. The mode shapes were acquired for the frequency range of 0-1.5 kHz and then processed using custom-developed software DICMAN 3D in MATLAB (see [5] for more details).

Department of Fundamentals of Machinery Design, Faculty of Mechanical Engineering, Silesian University of Technology, Konarskiego 18A, 44-100 Gliwice, Poland

² Department of Robotics, Faculty of Mechanical Engineering, VŠB—Technical University Ostrava, 17. Listopadu 2172/15, 708 00 Ostrava, Czech Republic

³ Department of Applied Mechanics and Mechanical Engineering, Faculty of Mechanical Engineering, Technical University of Košice, Letná 1/9, 042 00 Košice, Slovakia

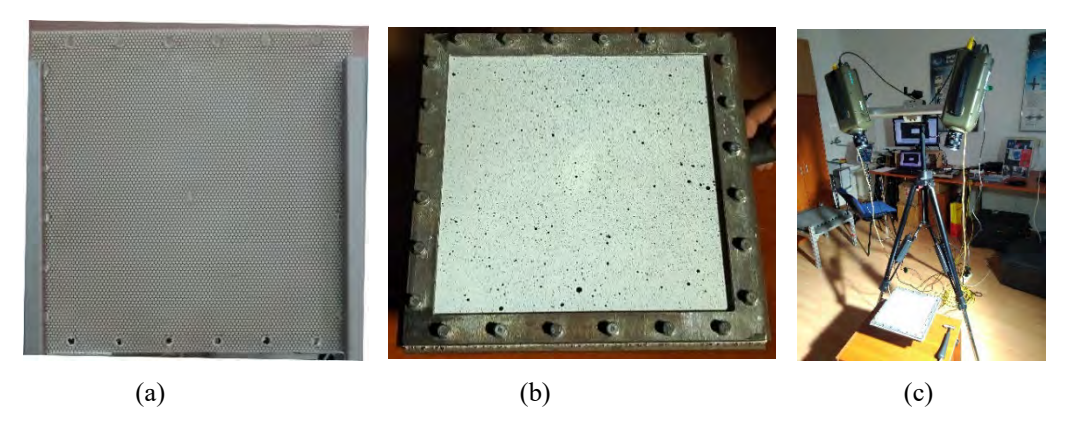


Fig. 1. The representative tested specimen with impact damage (a), the specimen prepared for testing (b), and experimental setup (c).

The acquired mode shapes were then processed using double-density discrete wavelet transform, which ensures enhanced sensitivity to the local disturbances in displacements caused by the presence of impact damage. The resulting wavelet coefficients were scaled and multiplied by entropic weights for each considered mode shape and sets of wavelet coefficients resulting from wavelet analysis, making it possible to improve the detectability of impact damage and to equalize the results of impact damage detection for analyzed mode shapes with various magnitudes. This approach automates the process of selecting the most sensitive mode shapes.

3. Results on damage identification

For the representative case of impact damage introduced with a hemispherical impactor tip of Ø28 mm and impact energy of 15 J four mode shapes with corresponding natural frequencies: 339.8 Hz, 679.7 Hz, 996.1 Hz, and 1195.3 Hz, were acquired. The mode shapes were processed using the described algorithm, and the results for these mode shapes were added up to achieve a single composite image presented in Fig. 2. The colors denote the value of damage coefficient calculated using the presented algorithm. One can notice that the impact damage was successfully identified using the proposed testing and processing procedures.

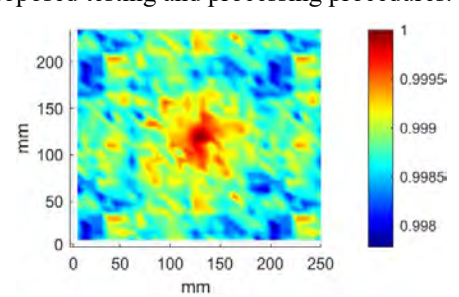


Fig. 2. The result of impact damage identification for a representative case.

4. Conclusions

The presented case study demonstrates the performance of the high-speed 3D DIC enhanced with wavelet analysis in structural damage identification, providing a fast, non-contact and cost-effective approach for identification of impact damage in sandwich structures. This approach can be used as an alternative testing technique with respect to SLDV providing comparative sensitivity to structural damage.

This paper has been supported by the projects VEGA 1/0516/22 and REFRESH–Research Excellence for REgion Sustainability and High-tech Industries project number CZ.10.03.01/00/22 003/0000048.

- [1] Katunin, A., 2015, "Nondestructive damage assessment of composite structures based on wavelet analysis of modal curvatures: state-of-the-art review and description of wavelet-based damage assessment benchmark," Shock Vib., 2015, 1-19. [2] Chaupal, P., Rajendran, P., 2023, "A review on recent developments in vibration-based damage identification methods for laminated composite structures: 2010-2022," Compos. Struct., 311, 116809.
- [3] Katunin, A., 2014, "Vibration-based spatial damage identification in honeycomb-core sandwich composite structures using wavelet analysis," Compos. Struct., 118, 385-391.
- [4] Katunin, A., Huňady, R., Hagara, M., 2024, Damage identification in composite structures using high-speed 3D digital image correlation and wavelet analysis of mode shapes," Nondestr. Test. Eval., in press, doi: 10.1080/10589759.2024.2407893 [5] Huňady, R., Hagara, M., 2017, "A new procedure of modal parameter estimation for high-speed digital image correlation, mechanical systems and signal processing," Mech. Syst. Signal Process., 93, 66-79.

Impedance based Structural Health Monitoring for Multi-Impact Damage Classification in PLA Plates

Paresh Mirgal¹, Daniel del-Río-Velilla², Katarzyna Majewska¹, Paweł H. Malinowski¹

¹ Institute of Fluid-Flow Machinery, Polish Academy of Sciences, 80-231 Gdańsk, Poland
 ² Universidad Politécnica de Madrid, Plaza del Cardenal Cisneros N°3, Edificio A, Madrid, Spain
 * pmirgal@imp.gda.pl

Abstract: Structural health monitoring is critical for ensuring the reliability of additively manufactured structures. This study investigates the impact of structural damage on electromechanical impedance responses using a piezoelectric sensor in Polylactic Acid (PLA) plate. Various damage scenarios, including mass placement and impact-induced cracks at different locations, were analyzed. The Mean Absolute Percentage Deviation (MAPD), Root Mean Square Deviation (RMSD), and Bandwidth Degradation Index (BDI) were used to quantify the damage in the plate. Results show that damage severity and proximity to the sensor significantly affect impedance variations. Cracks closer to the sensor caused higher deviations, while distant impacts had reduced effects. These findings emphasize the importance of sensor placement in structural health monitoring.

1. Introduction

Structural health monitoring (SHM) is crucial for assessing the integrity of engineering structures and preventing catastrophic failures [1]. The electromechanical impedance (EMI) technique, which utilizes piezoelectric sensors, has gained popularity due to its sensitivity to structural changes [2]. This study examines the influence of different damage scenarios on impedance-based parameters, particularly focusing on damage proximity to the sensor placed on PLA plate. Previous research has established that cracks and mass changes affect the conductance signature recorded by piezoelectric transducers [3]. However, the extent to which damage location influences these variations remains an area of interest. By comparing impedance deviations across different impact conditions, this study aims to provide insights into optimal sensor placement and sensitivity to structural damage. The findings contribute to enhancing damage detection strategies in SHM applications, ensuring improved reliability and safety in structural assessments.

2. Methodology

The study considered five different structural conditions to assess the impact of damage on the EMI response. The healthy condition served as the reference, representing the undamaged state of PLA plate. A mass of 100 grams was placed 35 mm away from the PZT to observe its influence without causing actual structural damage to the plate. Impact 1 introduced a single impact (with energy of 5.4 J) at 35 mm from the PZT, while Impact 2 involved a similar impact at the same location, leading to a visible crack. Impact 3 was created by applying an impact at 70 mm from the PZT but at a 90-degree angle from the first impact, which also resulted in a visible crack after second impact similar to impact 2. The experimental set up with impact cases are shown in the Figure 1.



Figure 1. Experiment set up and impact locations

The MAPD, RMSD [3], and BDI [4] were used to quantify the damage. MAPD quantifies the relative deviation between the damaged and healthy conductance curves, providing a percentage-based measure of damage severity. A higher MAPD indicates a greater deviation from the healthy state, signifying more severe structural damage. RMSD measures the overall deviation between the healthy and damaged conductance curves, accounting for squared differences to emphasize larger variations. This metric highlights discrepancies in amplitude between the two signals, making it useful for detecting changes in structural properties. BDI assesses how the bandwidth of the resonance peak changes due to damage, reflecting the loss of structural integrity. A significant reduction in bandwidth indicates material degradation and altered damping characteristics.

3. Results and discussion

The actual conductance responses are compared and impact analysis corresponds to each impact case are presented in Figure 2. The MAPD values indicate the extent of change in conductance due to damage. The mass placement resulted in the lowest MAPD of 1.4583%, as expected, since it did not introduce structural damage but only altered the mass distribution. Impact 1 caused a slightly higher MAPD of 3.2595%, suggesting minor structural alterations. Impact 2, which introduced a visible crack, exhibited a significant increase in MAPD to 14.388%, indicating substantial deviation from the healthy state. Impact 3 caused a slightly higher MAPD of 5.2242%, suggesting minor structural alterations. Impact 4, despite also leading to a visible crack, had a lower MAPD of 6.0731%, likely due to its placement farther from the initial damage site and at a different angle.

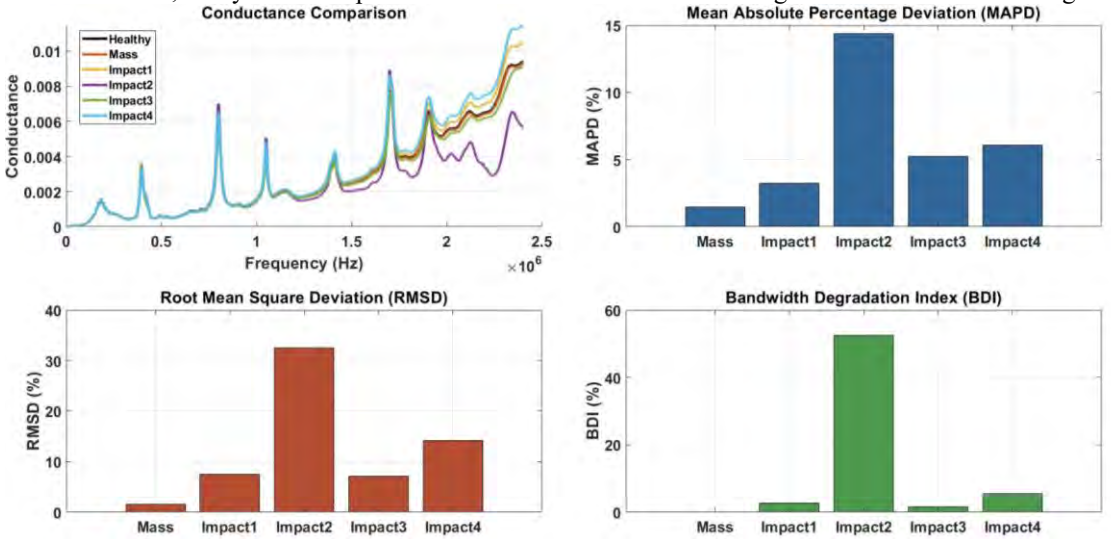


Figure 2. Actual conductance responses and impact analysis

The RMSD followed a similar trend, with the mass placement resulting in the smallest change of 1.5543%. Impact 1 showed a moderate increase in RMSD to 7.498%, while Impact 2 exhibited a large deviation of 32.456%, confirming severe damage. Impact 1 showed a reasonable increase in RMSD to 7.1284%, similar to impact 1. Impact 4 had an RMSD of 14.197%, which, although significant, was lower than Impact 2. This suggests that the relative position of the damage site to the PZT sensor plays a crucial role in the extent of deviation observed in conductance.

The BDI further supported these findings. The mass placement showed no significant degradation (0%), confirming that no damage occurred. Impact 1 resulted in a minor BDI increase to 2.7595%, while Impact 2 exhibited the most substantial degradation at 52.562%, indicating severe structural weakening. Impact 1 resulted in a minor BDI decrease to 1.6426% compare to impact 1. Impact 4, despite causing visible cracks, had a BDI of 5.5191%, much lower than Impact 2. The distance and angle of Impact 3 and Impact 4 from the PZT likely contributed to its reduced influence on conductance and signal degradation.

4. Conclusion

The results highlight the sensitivity of the damage indicators to the severity and location of structural impacts. Damage occurring closer to the PZT, particularly at the same location as previous impacts, leads to significantly higher deviations in conductance-based parameters. Meanwhile, impacts further away or at different angles show relatively reduced effects, even if they cause visible cracks. This underscores the importance of sensor placement in damage detection and monitoring, as the proximity of damage to the sensor greatly influences the detectability of structural changes.

Acknowledgement: The authors acknowledge the funding support provided by the National Science Center, Poland under the OPUS project entitled: Health monitoring of AdDitively manufactured structurES (HADES) (2019/35/B/ST8/00691). The authors are also grateful to TASK-CI for allowing the use of their computational resources.

- [1] Zhang, Y., Li, J. & Xie, X., 2023 "Dynamic analysis of interfacial multiple cracks in piezoelectric thin film/substrate". Acta Mech, 234, pp. 705–727. https://doi.org/10.1007/s00707-022-03390-5
- [2] Malinowski, P. H., Singh, S. K., & Andrearczyk, A., 2024 "Damage detection in 3D-printed plate using the electromechanical impedance method with surface bonded and embedded sensors", In Proceedings of SPIE, 12951, p. 1295111. https://doi.org/10.1117/12.3011812
- [3] Na, W. S., & Baek, J. 2018 "A Review of the Piezoelectric Electromechanical Impedance Based Structural Health Monitoring Technique for Engineering Structures", Sensors, 18(5), 1307. https://doi.org/10.3390/s18051307.
- [4] Wu, B. 2014 "A correction of the half-power bandwidth method for estimating damping", Archive of Applied Mechanics. 85, pp. 315-320. https://doi.org/10.1007/s00419-014-0908-0.



Advanced Composites under High Strain Rate Loading A Route to Certification-by-Analysis

2025 Conference 4th – 5th JUNE 2025

Session 4 - Advanced testing and instrumentation for composites under high strain rates (WG6)





Integration of optical measurements in standard Hopkinson bar data treatment

Marco Peroni1*

¹ European Commission, Joint Research Centre, Via E. Fermi, 2749, 21027 Ispra (VA), Italy *marco.peroni@ec.europa.eu

Abstract: Advancements in high-speed camera performances and the development of new optical hardware as line scan cameras could revolutionise the standard instrumentation adopted in Hopkinson bar based techniques improving the measurements accuracy and providing, in addition, new alternatives for the calibration. This paper presents a strategy to incorporate optical data to integrate, and in some cases substitute, conventional strain-gage measurements in a classical Split Hopkison Pressure Bar (SHPB) experiments. The same methodology could be used to calibrate a SHPB with additional independent measurements and to quantitatively assess the accuracy of the generated data.

1. Introduction

Advancements in high-speed camera performances and the development of new optical hardware as line scan cameras [1] could revolutionise the standard instrumentation adopted in Hopkinson bar techniques. Leverage proficiently innovative instrumentation could be extremely beneficial to rapidly change the equipment bars in relation to tested specimen and for calibration purposes guaranteeing, at the same time, higher levels of measurement accuracy. The objectives of this paper are mainly two: i) present a general strategy to incorporate optical data to integrate conventional strain-gage measurements in a classical SHPB experiments; ii) present an optimized target tracking algorithm specifically developed for high speed imaging in SHPB experiments. In addition, the proposed methodology could be applied to improve the calibration of Hopkinson based equipment introducing two benchmark tests related to optical measurements.

2. Integration of n strain measurements (strain-gages) with p displacement measurements (optical)

Conventional SHPB measurements are normally based on bar strain histories recorded using strain-gage sensors that at the moment remain the only possibility to maintain reasonable noise-to-signal ratios. The adoption of multiple measurement points with a deconvolution algorithm and a Maximum Likelihood approach could improve the accuracy of derived measurements as reported in [2] and automatically reconstruct forces and displacements at specimen ends (since displacement it is often not representative of strain field for composite materials) without additional elaborations (time shifting). On the contrary, this methodology requires a great effort for the installation and calibration of several strain-gage measurement points. Optical measurement techniques at the moment are not able to compute bar strain histories with the same resolution of strain-gages (ohmic and even more semiconductors) but it is feasible to proficiently use optical displacement measurements to increase the accuracy of conventional Hopkinson data elaboration.

Bussac et all [2] showed that it is possible to directly combine n strain measurements with p velocity measurements in the frequency domain to reconstruct forces and displacements applied to specimen ends. Substituting velocities as displacement functions in eq. 21 using $\hat{v}_k(\omega) = i\omega \hat{d}_k(\omega)$, where \hat{v}_k and $\hat{d}_k(\omega)$ are respectively velocity and displacement measurement at k location, i the imaginary unit and ω the circular frequency, the new computation strategy could be directly applied to Hopkinson measurements integrating optical displacement measurements. The new equation gives the possibility to combine an arbitrary number of strain (n) and displacement (p) measurements to reconstruct the forces and displacements applied to the bar ends.

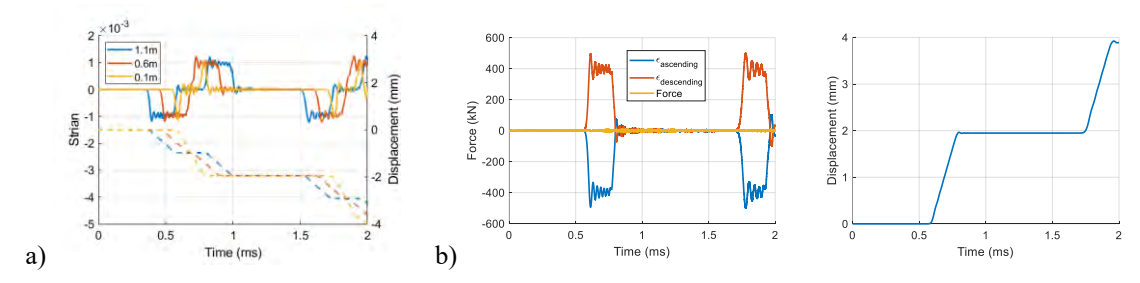


Fig. 1. a) Input signals (numerical simulation) and b) force and displacement reconstructed at the bar end

Fig. 1a shows the input signals generated numerically (strains continuous lines, displacement dotted lines) in a single bar test (Ø 50mm steel bar, striker L=500mm, input bar L=3000mm) and recorded in 3 position (in the

legend the distance from the bar end opposed to the striker). Using the proposed algorithm, it is possible to reconstruct the force and displacement at the end of the bar with at least two of the signals presented in Fig. 1a as reported in Fig. 1b; increasing the number of acquisitions involved in the procedure the reconstructed signals are less affected by measurement systematics errors (that are not present in the simulated signals). The methodology remains still valid when the number of strain measurement points n is zero and measurements are purely optical and provide always the same output: displacements and forces applied by the bars to the specimen ends.

3. Optimized target tracking algorithm for Hopkinson application

From the experimental point of view, the implementation of the algorithm presented in section 2 requires a mixed measuring setup as reported in Figure 2: conventional strain-gage measurements (blue rectangles) are enhanced with several optical displacement measurements obtained with high accuracy multiple tracking techniques.

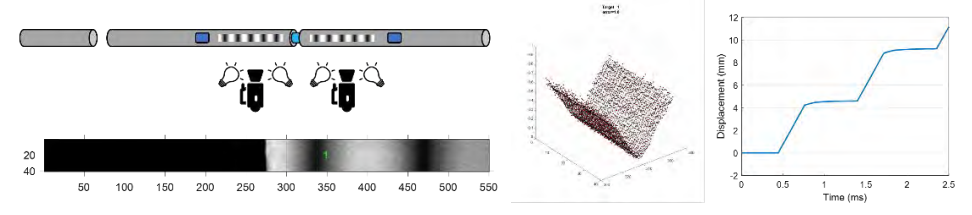


Fig. 2. Experimental setup, grey profile of a 1D Gaussian target and computed displacement.

The tracking techniques is based on targets with a 1D Gaussian profile (in term of greyscale) that present several advantages when applied to Hopkinson experiments: i) the computation is faster than DIC, ii) the particular profile incorporate an intrinsic scale (the σ) to convert displacement directly in mechanical units, iii) cropping the images vertically it is feasible to reach acquisition frequency up to 1MHz with modern high speed cameras and iv) the accuracy could be less than 1 μ m. The number of p displacement measurements can be easily increased without any significant practical effort because targets can be printed on adhesive paper and attached on the adopted bar (making very easy to substitute the bar to face particular requirement due to the specimen geometry/strength).

4. Application to Hopkinson bar calibration

An additional advantage related to the integration of the optical target tracking methodology to conventional Hopkinson measurements could be the application of benchmark tests based on optical data to assess the accuracy of the test results. The idea is to perform two tests with significant boundary conditions to check the accuracy of output data (in term of forces and displacements) and eventually optimize the elaboration procedures. The first benchmark test consists of a test performed on the single incident bar (single bar test). In these conditions there are two precise boundary conditions: the computed force at the end of the bar is zero and the displacement ends can be easily computed with a targets placed at the bar ends. The two constrains can be used to verify the signal computation adopted (and eventually improve it) and to quantitatively assess the accuracy of force and displacement measurements at the input bar – specimen interface. The second benchmark test consist of a test performed with both bars put in contact without any specimen (void test). With this test the calibration of output bar will be assessed using as reference the following boundary conditions: perfect equilibrium between input/output bar and the displacement can be again evaluated with a targets placed at the output bar ends or using the displacement computed by the input bar (when it is in contact with the output bar).

5. Conclusions

In this work the first implementation of a systematic integration of optical measurements in the data processing of conventional Hopkinson data has been presented. The idea is to use a deconvolution algorithm based on multiple measurements obtained by n strain-gages (bar-strain histories) and p optical measurements (displacements of selected bar locations using a proper target tracking technique) in a flexible combination (n or p should be equal to zero). The same methodology could be used to quantitatively evaluate the measurement accuracy of a SHPB or proficiently calibrate a new equipment. Further investigation will be required to understand the actual accuracy of the techniques related to the camera resolution and to find the setup parameters that give best results in term of accuracy (balancing the number and the targets dimensions).

- [1] Roth, C., LeGrelle, F., Tancogne-Dejan, T., Grolleau, V., Gary, G. and Mohr, D., 2024, "Contactless Strain and Velocity Measurements on SHPB: Replacing Strain Gauges by Line Cameras" proceedings 14th Dymat International Conference, pp. 247.
- [2] Bussac, M., Collet, P., Gary, G. and Othman, R., 2002, "An optimisation method for separating and rebuilding onedimensional dispersive waves from multi-point measurements. Application to elastic or viscoelastic bars" Journal of the Mechanics and Physics of Solids 50, pp. 321–349.

Common path polarization Electronic Speckle Pattern Interferometry for dynamic deformation analysis

Violeta Madjarova*, Elena Stoykova, Ginka Ivanova and Branimir Ivanov

¹ Institute of Optical Materials and Technologies, Bulgarian Academy of Sciences, Acad. G.Bonchev Str. 109, 1113 Sofia, Bulgaria
*vdmadjarova@gmail.com

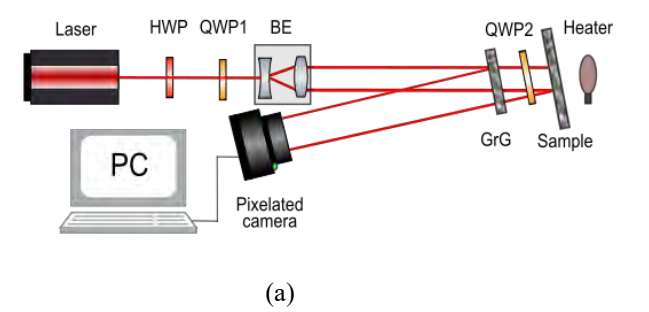
Abstract: In this study, we propose Fizeau type polarization Electronic Speckle Pattern Interferometry (ESPI) for quantitative study of dynamic deformations of sample subjected to thermal expansion. The proposed optical setup is robust to vibrations out-of-plane sensitive polarization ESPI system with pixelated polarization camera as a detector. The setup uses two quarter wave plates to obtain orthogonal circular polarization for the reference and object fields. The signal is recorded by the camera consisting of arrays of linear micro-polarizers in front of the camera pixels. Simultaneously acquired four phase-shifted images permit the implementation of phase shifting algorithm for phase and deformation analysis.

1. Introduction

Electronic Speckle Pattern Interferometry (ESPI) is a widely used optical technique in NDT of diffusely scattering samples due to its robustness, high sensitivity, simplicity and real-time implementation [1]. One of the advantages of ESPI over speckle photometry, for example, is the quantitative evaluation of the deformation and, if some phase shifting algorithm is implemented, this can be done without sign ambiguity [1, 2]. For dynamic deformation studies, conventional phase shifting algorithm that requires a minimum of three phase shifting steps while the sample stays stationary is not applicable. For this reason, a suitable phase-shifting algorithm should be able to provide the phase shifted images simultaneously. One option is to make use of polarization state of the reference and sample beam and a pixelated camera for recording media [3]. In addition, for the case where environmental noise is severe, a common-path ESPI setup should be implemented. In this study we propose common-path polarization ESPI and pixelated camera with linear micro-polarizers for phase shifting.

2. Methods

Figure 1 (a) illustrates the proposed Fizeau type polarization ESPI where the ground glass (GrG) acts as a reference surface and two quarter wave plates – QWP1 and QWP2 - are used to obtain two orthogonal circular polarizations. The light from the laser source (He-Ne laser - LASOS Lasertechnik at λ = 632.8 nm) passes through a half-wave plate (HWP with λ 10 surface accuracy) with fast axis oriented at 45° with respect to the horizontal axis. Following it passes QWP1 (λ 10 surface accuracy) at fast axis oriented at 0° with respect to the horizontal axis to become a left circularly polarized (LCP) field. It is expanded to a beam with diameter 25 mm by the beam expander (BE). The reflected from the GrG field acts as a reference field. The reflected from the ground glass LCP beam becomes right circularly polarized (RCP) field. Part of the beam passes the GrG, QWP2 (λ 10 surface accuracy) at fast axis oriented at 0° with respect to the horizontal axis, reflects from the surface of the sample, passes again QWP2 and the GrG. As a result, the object field remains LCP. At the plane of the pixelated camera, the RCP reference field and the LCP object field are superimposed to interfere. The interference signal is recorded by the camera with linear micro-polarizers in front of each camera pixels oriented at 0, $-\pi/4$, $\pi/2$, $\pi/4$. Figure 1 (b) illustrates four images that correspond to different polarization orientations. Simultaneously acquired four phase-shifted images permit the implementation of a phase shifting algorithm for phase and deformation analysis. The images are captured sequentially during the deformation of the object that is subjected to thermal expansion.



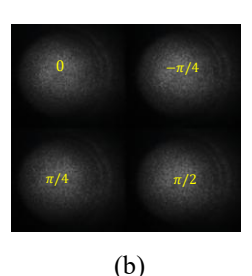


Figure 1. (a) Optical set-up for polarization ESPI. BE – beam expander, $\lambda/2$ – HWP - half-wave plate, $\lambda/4$ – QWP1, QWP2 - quarter-wave plate, GrG – ground glass; PC – personal computer; (b) Structure of a super-pixel in a polarization camera with linear polarizers oriented at $0, -\pi/4, \pi/2, \pi/4$.

To represent the polarization states we use Jones matrices and vectors formalism. The Jones vectors for the reference field \mathbf{R} (RCL) and object field \mathbf{O} (LCL) are expressed as follows:

$$R = E_R exp(i\varphi_R) \begin{pmatrix} 1 \\ i \end{pmatrix}$$
; $O = E_O exp(i\varphi_O) \begin{pmatrix} 1 \\ -i \end{pmatrix}$

The x and y components are not included for simplicity. The reference and object fields pass the polarizers of the camera that are positioned in front of each pixel, as illustrated in Figure 1 (b). The Jones matrix for the polarizers oriented at angle θ = 0, $-\pi/4$, $\pi/2$, $\pi/4$ to horizontal axis are as follows:

The amplitude after passing the polarizer at each pixel is calculated as follows:
$$\theta = 0^{\circ}: P_0 = \begin{pmatrix} 1 & 0 \\ 0 & 0 \end{pmatrix}; \ \theta = 90^{\circ}: P_{90} = \begin{pmatrix} 0 & 0 \\ 0 & 1 \end{pmatrix}; \ \theta = 45^{\circ}: P_{45} = \frac{1}{2} \begin{pmatrix} 1 & 1 \\ 1 & 1 \end{pmatrix}; \ \theta = -45^{\circ}: P_{-45} = \frac{1}{2} \begin{pmatrix} 1 & -1 \\ -1 & 1 \end{pmatrix}$$
The amplitude after passing the polarizer at each pixel is calculated as follows:

$$\begin{split} E(0^\circ) &= E_R exp(i\varphi_R) \begin{pmatrix} 1 \\ 0 \end{pmatrix} + E_O exp(i\varphi_O) \begin{pmatrix} 1 \\ 0 \end{pmatrix}; \ E(90^\circ) = E_R exp(i\varphi_R) \begin{pmatrix} 0 \\ i \end{pmatrix} + E_O exp(i\varphi_O) \begin{pmatrix} 0 \\ -i \end{pmatrix}; \\ E(45^\circ) &= E_R exp(i\varphi_R) \frac{(1+i)}{2} \begin{pmatrix} 1 \\ 1 \end{pmatrix} + E_O exp(i\varphi_O) \frac{(1-i)}{2} \begin{pmatrix} 1 \\ 1 \end{pmatrix}; \\ E(-45^\circ) &= E_R exp(i\varphi_R) \frac{(1-i)}{2} \begin{pmatrix} 1 \\ -1 \end{pmatrix} + E_O exp(i\varphi_O) \frac{(1+i)}{2} \begin{pmatrix} 1 \\ -1 \end{pmatrix} \end{split}$$

Finally, the intensities are represented as follows

$$I(0^{\circ}) = I_1 = E_R^2 + E_O^2 + 2E_R E_O \cos(\Delta \varphi); I(90^{\circ}) = I_4 = E_R^2 + E_O^2 - 2E_R E_O \cos(\Delta \varphi);$$

$$I(45^{\circ}) = I_3 = E_R^2 + E_O^2 + 2E_R E_O \sin(\Delta \varphi); I(-45^{\circ}) = I_2 = E_R^2 + E_O^2 - 2E_R E_O \sin(\Delta \varphi),$$

where $\Delta \varphi = (\varphi_R - \varphi_0)$. The phase can then be calculated using the expression $\Delta \varphi = atan(\frac{I(45^\circ) - I(-45^\circ)}{I(0^\circ) - I(90^\circ)})$

The wrapped $[0, 2\pi]$ in time phase is calculated at each pixel and a 3D matrix for $\Delta \varphi(x, y, t)$ is constructed. The unwrapping is performed in time domain, and two-dimensional deformation is calculated at each instant using the expression $d = \Delta \varphi \lambda / 4\pi$.

Results

The experiments were performed on optical table that was not vibration isolated to test the system under noisy conditions. The sample in the experiments was a plastic glass plate with introduced defects on its back side. The sample was heated with condensed lamp. A sequence of images at 35 fps were acquired for approximately one minute. The phase was calculated using equation for $\Delta \varphi$, unwrapped in time domain and the 2D phase map was obtained. The phase containing the random speckle phase at each pixel was removed by subtracting two phases representing different instants. The obtained in this manner phase was transformed to 2D deformation fields and filtered in space domain to remove the spiky noise. The 2D deformation results are illustrated in Figure 2(a). The location of the defect is clearly visible, marked in Figure 2(a) with an arrow and is further illustrated in Figure 2(b) by the cross sections at the positions of the defect.

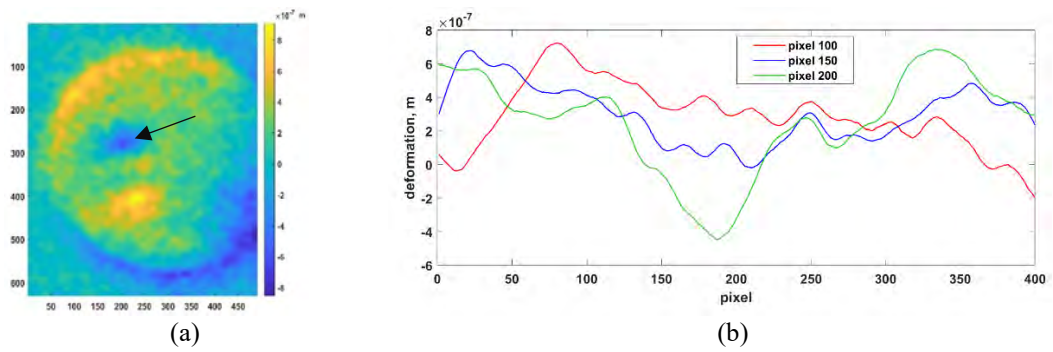


Figure 2. (a) 2D deformation field at 14 seconds after the heating started; (b) Cross-sections for horizontal pixel positions 100, 150 and 200.

Conclusion

In conclusion, we demonstrated a high sensitive and robust Fizeau type polarization ESPI that can be implemented for quantitative studies of samples subjected to thermal expansion under noisy environmental conditions. Hidden defects can be visualized and the change in the 2D deformation field to be followed in time. This research is conducted in the framework of COST Action CA21155 HISTRATE. This work is financially supported by the Bulgarian National Science Fund (BNSF) under project KΠ-06-H88/2.

[1] Zinoviy Nazarchuk, Leonid Muravsky, Dozyslav Kuryliak, 2023, Optical Metrology and Optoacoustics in Nondestructive Evaluation of Materials, Springer Series in Optical Sciences, Springer, Singapore https://doi.org/10.1007/978-981-99-1226-1 [2] Rastogi, P., & Hack, E. (Eds.). 2014, Phase Estimation in Optical Interferometry (1st ed.). CRC Press. https://doi.org/10.1201/b17701

[3] Xing Zhou, Shuhai Jia, Huajian Zhang, Zihan Lin, Bo Wen, Longning Wang, Yunlong Zhang, 2024, "Single-frame fringe pattern analysis with synchronous phase-shifting based on polarization interferometry phase measuring deflectometry (PIPMD)," Optics and Lasers in Engineering, 181, 108406, https://doi.org/10.1016/j.optlaseng.2024.108406.

Next-Generation Dynamic Testing of Composites: A Review

Briek Luyten^{1*} and Patricia Verleysen¹

¹Materials Science and Technology-DyMaLab, EMSME Department, Ghent University, Technologiepark 46, 9052 Ghent, Belgium *briek.luyten@ugent.be

Abstract: Characterizing the complex mechanical behaviour of composites requires a large number of tests due to their intrinsic heterogeneity and anisotropy. In addition, external loading parameters such as strain rate and stress state also affect the material response. This complexity is reflected in the material models, which involve numerous parameters. To enable a more efficient experimental calibration of dynamic composite models, full-field measurement techniques and advanced post-processing methods have gained popularity in recent years. Nevertheless, experimental applications remain rather limited. This review provides an overview of the state-of-the-art, identifying significant potential for applications in high-strain-rate composite testing.

1. Introduction

Because of the anisotropic and heterogeneous mechanical properties of most fibre-reinforced composites, extensive test series are required to characterize their constitutive behaviour. Only identifying the orthotropic elastic properties of laminated composites already necessitates several tensile and compressive tests in different in-plane and through-thickness directions. In the case of non-linear shear behaviour, additional parameters need to be characterized, while damage introduces a further level of complexity. When also taking into account strain-rate sensitivities, the total number of required tests increases exponentially. This severely impedes the characterization and certification of novel composite materials, particularly for high-strain-rate applications.

Recently, efforts have been made to circumvent such extensive experimental campaigns through more efficient test methodologies. These build on a range of different electro-optical techniques for measuring local displacement, slope, or strain fields. These full-field measurements can be exploited to their fullest potential by introducing new sample geometries and experimental techniques that deliberately introduce strain, strain rate, and stress heterogeneities. As a result, each individual test generates a much richer set of data, which can serve as input for inverse identification schemes or other advanced post-processing methods. Ultimately, these novel and highly efficient test techniques allow full mechanical characterization through significantly less tests.

The present review aims to provide a succinct overview of the current state-of-the-art of these next-generation test techniques for composite materials. Section 2 first discusses existing full-field measurement techniques, highlighting those which have been most prominently used in recent years. Section 3 then gives a similar overview of post-processing methods aimed at fully exploiting full-field measurement data, particularly focused on inverse identification techniques. Finally, Section 4 presents specific applications in high-strain-rate testing of composites, pointing towards uncharted potential yet to be explored.

2. Full-Field Measurement Techniques

In their core, electro-optical techniques for measuring full-field deformation or strain maps encode the specimen shape during the experiment into an optical signal. The 'deformed' signal is then compared to an undeformed reference signal, from which displacement or strain information is extracted. For a number of techniques, this comparison is performed by optically interfering both signals, and extracting displacement and strain fields from the imaged interference patterns. Examples include holographic interferometry [1,2], electronic speckle pattern interferometry (ESPI) [1,3], and Moiré interferometry [4,5]. The latter is similar to the geometric Moiré technique, where interference is generated by the superposition of two physical gratings – one deformed and one undeformed [4,6]. While interferometric techniques offer a high resolution beneficial for composite characterization, their implementation can be laborious due to sensitivity to external disturbances. Consequently, their popularity for composite testing applications has noticeable decreased over the past fifteen years, with only some quasi-static applications of Moiré interferometry reported in recent literature [7,8].

The other main branch of full-field measurement techniques does not use in-situ comparison of spatially distinct deformed and reference signals. Rather, deformed images are compared with a temporally distinct reference, i.e., an image of the undeformed sample before the experiment. In the case of speckle photography [9], the sample's diffuse reflection is used as the information carrier, from which deformation is extracted through correlation with the undeformed image. Digital image correlation (DIC) lowers the noise floor of such measurements by working on a multi-pixel level – sacrificing some spatial resolution – typically enhanced by applying a black-and-white speckle pattern to the sample [10,11]. In contrast, deflectometric techniques require a specular specimen surface, in order to reflect the image of a fringe or speckle pattern [12,13]. Finally, grid methods track the deformation of

a regular grid applied to the sample's surface [10,14]. This technique's balance between measurement sensitivity and ease of implementation makes it a popular choice within the field of (dynamic) composite testing. Similarly, DIC methods dominate recent literature despite their relatively limited resolution, primarily due to their straightforward implementation and the availability of commercial solutions.

3. Post-Processing Techniques

Once full-field measurements are obtained, they should be fully exploited in order to identify the composite's mechanical behaviour as efficiently as possible. In its most basic form, this can mean qualitatively comparing the experimental results with numerically [15] or analytically [16] obtained counterparts. If these match closely, the underlying material model can be deemed validated within the tested boundary conditions. If not, modifications or updates are required, either in the general modelling approach, material model, or its parameters. A quantitative method for the latter is the finite element model updating (FEMU) technique [17,18], where material model parameters are iteratively optimized until numerical results converge with experimental data. In literature, this technique has been used to determine in-plane [19] and interlaminar [20] orthotropic elastic parameters, identify Hill's yield criterion [21], and even calibrate a cohesive zone fracture model [22].

Nevertheless, the iterative nature of FEMU techniques imposes a significant computational burden, and may not provide the most efficient solution for each application. Indeed, a large number of studies use an alternative method to inversely identify material model parameters of composites, known as the virtual fields method (VFM) [23,24]. This technique uses virtual fields to establish a set of equations which have the desired material parameters as unknowns. By directly solving this set of equations, the parameters can be obtained in a non-iterative way [25]. Alternatively, virtual fields have also been used to extract other data from full-field measurements, such as acceleration or stress fields [26]. Using this data to construct stress-strain relations, material parameters such as Young's modulus can then be extracted through conventional methods (i.e. slope fitting).

Finally, singular instances can be found in literature where entirely different methods are used to post-process full-field measurements for characterizing composites. Examples include the boundary element method (BEM) [27], the modified constitutive relation error (MCRE) technique [28], or Bayesian identification [7]. The latter results in a probability density function of the estimated parameters, rather than single values.

4. High-Strain-Rate Testing of Composites

The aforementioned test techniques, using full-field measurements and advanced post-processing methods, have seen multiple successful applications in quasi-static testing of various composites – including carbon- and glass-fibre-reinforced polymers (CFRP and GFRP) [29,30], graphite/epoxy [7] and aramid/epoxy [31] systems, as well as wood bio-composites [21,22] and concrete [27]. At the same time, full-field measurement techniques such as DIC [32], deflectometry [12], and grid methods [33] have been demonstrated to reliably capture displacement and strain fields also during dynamic testing of composites. However, the application of post-processing techniques such as FEMU and VFM in high-strain-rate testing of composites remains limited in literature. What follows is an overview of the current state-of-the-art.

As early as 2011, Moulart et al. demonstrated the potential of VFM to extract the Young's modulus and Poisson's ratio of quasi-isotropic GFRP by using the grid method in a single dynamic tensile test with an open-hole geometry [34]. Pierron and Forquin expanded this application to concrete in 2012, obtaining both Young's modulus and tensile strength in a spalling test [35]. A significant advancement came in 2014, when Pierron et al. established foundation for what would later be termed the 'image-based inertial impact' (IBII) test [26]. A quasi-isotropic CFRP specimen was impacted from the side, and VFM was used to extract acceleration and stress data from full-field displacement maps obtained with the grid method. Subsequently, the Young's modulus and Poisson's ratio were determined. Since this initial study, researchers have refined the IBII test technique to determine transverse [33,36], interlaminar [37], and shear [38] properties of CFRP samples. In all tests, measurements obtained with the grid method were processed using VFM.

Despite these advances, to the authors' knowledge no other experimental applications of advanced post-processing techniques for dynamic testing of composites have been reported in literature. Although popular in quasi-static testing, experimental applications of FEMU in this field have not been reported. Similarly, VFM techniques based on alternative measurement systems such as DIC have yet to be demonstrated in dynamic composite testing. While Fu et al. have used numerical simulations to demonstrate the potential of novel specimen geometries designed to deliberately introduce stress/strain heterogeneity [39], experimental applications are currently lacking. Nevertheless, given the range of available full-field measurement techniques and post-processing methods, along with their demonstrated potential in other fields of material testing, significant advances can be expected in the coming years. These developments promise to significantly reduce the number of tests required for fully characterizing the complex dynamic behaviour of composites.

- [1] Jones, R. and Wykes, C., Holographic and Speckle Interferometry, 1989, Cambridge University Press, Cambridge, United Kingdom.
- [2] Schnars, U., Falldorf, C., Watson, J., and Jüptner, W., Digital Holography and Wavefront Sensing: Principles, Techniques and Applications, 2015, Springer, Berlin, Germany.
- [3] Bruno, L., Felice, G., Pagnotta, L., Poggialini, A., and Stigliano, G., 2008, "Elastic Characterization of Orthotropic Plates of Any Shape via Static Testing," Int. J. Solids Struct., 45(3-4), pp. 908-920.
- [4] Post, D., Han, B., and Ifju, P., High Sensitivity Moiré: Experimental Analysis for Mechanics and Materials, 2012, Springer, New York, United States of America.
- [5] Molimard, J., Le Riche, R., Vautrin, A., and Lee, J. R., 2005 "Identification of the Four Orthotropic Plate Stiffnesses using a Single Open-Hole Tensile Test," Exp. Mech., 45(5), pp. 404-411.
- [6] Melin, L.G. and Asp, L. E., 1999, "Effects of Strain Rate on Transverse Tension Properties of a Carbon/Epoxy Composite: Studied by Moiré Photography," Compos. Pt. A-Appl. Sci. Manuf., 30(3), pp. 305-316.
 [7] Gogu, C. et al., 2013, "Bayesian Identification of Elastic Constants in Multi-Directional Laminate from Moiré
- Interferometry Displacement Fields," Exp. Mech., 53(4), pp. 635-648.
- [8] Zhou, M., Xie, H., and Wu, L., 2016 "Virtual Fields Method Coupled with Moiré Interferometry: Special Considerations and Application," Opt. Lasers Eng., 87, pp. 214-222.
- [9] Rastogi, P. K., Optical Measurement Techniques and Applications, 1997, Artech House, Boston, United States of America. [10] Schreier, H., Orteu, J.-J. and Sutton, M. A., Image Correlation for Shape, Motion and Deformation Measurements: Basic Concepts, Theory and Applications, 2009, Springer, New York, United States of America.
- [11] Hao, Z., Ji, X., Deng L., Ke, H., and Liu, L., 2021, "Measurement of Multiple Mechanical Properties for Polymer Composites using Digital Image Correlation at Elevated Temperatures," Mater. Des., 198, p. 109349.
- [12] Miao, C. and Tippur, H. V., 2018, "Measurement of Sub-Micron Deformations and Stresses at Microsecond Intervals in Laterally Impacted Composite Plates Using Digital Gradient Sensing," J. Dyn. Behav. Mater., 4(3), pp. 336-358.
- [13] Xavier, J., Belini, U., Pierron, F., Morais, J., Lousada, J., and Tomazello, M., 2013, "Characterisation of the Bending Stiffness Components of MDF Panels from Full-Field Slope Measurements," Wood Sci. Technol., 47(2), pp. 423-441.
- [14] Longana, M. L., Dulieu-Barton, J. M. and Pierron, F., 2012, "Identification of Constitutive Properties of Composite Materials under High Strain Rate Loading using Optical Strain Measurement Techniques," in Proc. 15th ECCM, Venice, Italy. [15] Tasdemirci, A., Kara, A., Turan, A. K., Tunusoglu, G., Guden, M., and Hall, I. W., 2011, "Experimental and Numerical Investigation of High Strain Rate Mechanical Behavior of a [0/45/90/-45] Quadriaxial E-Glass/Polyester Composite," Procedia Eng., 10, pp. 3068-3073.
- [16] Pagano, N. J. and Halpin, J. C., 1968, "Influence of End Constraint in the Testing of Anisotropic Bodies," J. Comp. Mater., 2(1), pp. 18-31.
- [17] Kavanagh, K. T. and Clough, R. W., 1971, "Finite Element Applications in the Characterization of Elastic Solids," Int. J. Solids Struct., 7(1), pp. 11-23.
- [18] Chen, B., Starman, B., Halilovič, M., Berglund, L. A., and Coppieters, S., 2024, "Finite Element Model Updating for Material Model Calibration: A Review and Guide to Practice," Arch. Comput. Method Eng.
- [19] Genovese, K., Lamberti, L., and Pappalettere, C., 2004, "A New Hybrid Technique for In-Plane Characterization of Orthotropic Materials," Exp. Mech., 44(6), pp. 584-592.
- [20] Seon, G., Makeev, A., Schaefer, J. D., and Justusson, B., 2019, "Measurement of Interlaminar Tensile Strength and Elastic Properties of Composites Using Open-Hole Compression Testing and Digital Image Correlation," Appl. Sci., 9(13), p. 2647.
- [21] Jungstedt, E., Oliaei, E., Li, L., Östlund, S., and Berglund, L. A., 2022, "Mechanical Behavior of All-Lignocellulose Composites - Comparing Micro- and Nanoscale Fibers using Strain Field Data and FEM Updating," Compos. Pt. A-Appl. Sci. Manuf., 161, p. 107095.
- [22] Jungstedt, E., Östlund, S., and Berglund, L. A., 2022, "Transverse Fracture Toughness of Transparent Wood Biocomposites by FEM Updating with Cohesive Zone Fracture Modeling," Compos. Sci. Technol., 225, p. 109492.
- [23] Grédiac, M. and Vautrin, A., 1990, "A New Method for Determination of Bending Rigidities of Thin Anisotropic Plates," J. Appl. Mech., 57(4), pp. 964-968.
- [24] Grédiac, M., Pierron, F., and Surrel, Y., 1999 "Novel Procedure for Complete In-Plane Composite Characterization using a Single T-Shaped Specimen," Exp. Mech., 39(2), pp. 142-149.
- [25] Su, Y., Yao, X., Wang, S., and Ma, Y., 2018 "Simultaneous Determination of Virtual Fields and Material Parameters for Thermo-Mechanical Coupling Deformation in Orthotropic Materials," Mech. Mater., 124, pp. 33-44.
- [26] Pierron, F., Zhu, H., and Siviour, C. R., 2014, "Beyond Hopkinson's Bar," Philos. Trans. R. Soc. A-Math. Phys. Eng. Sci., 372(2023), p. 20130195
- [27] Ferreira, M. D. C., Venturini, W. S., and Hild, F., 2011, "On the Analysis of Notched Concrete Beams: From Measurement with Digital Image Correlation to Identification with Boundary Element Method of a Cohesive Model," Eng. Fract. Mech., 78(1), pp. 71-84.
- [28] Ben Azzouna, M., Feissel, P., and Villon, P., 2015, "Robust Identification of Elastic Properties using the Modified Constitutive Relation Error," Comput. Meth. Appl. Mech. Eng., 295, pp. 196-218.
 [29] Gras, R., Leclerc, H., Hild, F., Roux, S., and Schneider, J., 2015, "Identification of a Set of Macroscopic Elastic
- Parameters in a 3D Woven Composite: Uncertainty Analysis and Regularization," Int. J. Solids Struct., 55, pp. 2-16.
- [30] Lecompte, D., Smits, A., Sol, H., Vantomme, J., and Van Hemelrijck, D., 2007, "Mixed Numerical-Experimental Technique for Orthotropic Parameter Identification using Biaxial Tensile Tests on Cruciform Specimens," Int. J. Solids Struct., 44(5), pp. 1643-1656.
- [31] Jiang, L., Guo, B., and Xie, H., 2015, "Identification of the Elastic Stiffness of Composites using the Virtual Fields Method and Digital Image Correlation," Acta Mech. Sin., 31(2), pp. 173-180.

- [32] Elmahdy, A. and Verleysen, P., 2018, "Challenges Related to Testing of Composite Materials at High Strain Rates using the Split Hopkinson Bar Technique," in Proc. DYMAT 2018, Arcachon, France.
- [33] Parry, S., Fletcher, L., and Pierron, F., 2021, "The Off-Axis IBII Test for Composites," J. Dyn. Behav. Mater., 7(1), pp. 127-155.
- [34] Moulart, R., Pierron, F., Hallett, S. R., and Wisnom, M. R., 2011, "Full-Field Strain Measurement and Identification of Composites Moduli at High Strain Rate with the Virtual Fields Method," Exp. Mech., 51(4), pp. 509-536.
- [35] Pierron, F. and Forquin, P., 2012 "Ultra-High-Speed Full-Field Deformation Measurements on Concrete Spalling Specimens and Stiffness Identification with the Virtual Fields Method," Strain, 48(5), pp. 388-405.
- [36] Fletcher, L., Van Blitterswyk, J., and Pierron, F., 2019, "A Novel Image-Based Inertial Impact Test (IBII) for the Transverse Properties of Composites at High Strain Rates," J Dyn. Behav. Mater., 5(1), pp. 65-92.
- [37] Van Blitterswyk, J., Fletcher, L., and Pierron, F., 2018 "Image-Based Inertial Impact Test for Composite Interlaminar Tensile Properties," J Dyn. Behav. Mater., 4(4), pp. 543-572.
- [38] Van Blitterswyk, J., Fletcher, L., and Pierron, F., 2020, "Image-Based Inertial Impact (IBII) Tests for Measuring the Interlaminar Shear Moduli of Composites," J. Dyn. Behav. Mater., 6(3), pp. 373-398.
- [39] Fu, J., Zhu, K., Nie, X., Tang, Y., Yang, Z., and Qi, L., 2021, "Inertia-Based Identification of Elastic Anisotropic Properties for Materials Undergoing Dynamic Loadings using the Virtual Fields Method and Heterogeneous Impact Tests," Mater. Des., 203, p. 109594.

Elements for a roadmap for standardisation of high strain rate testing of composite materials

Andrei G. Anisimov, 1* Marco Peroni, 2 Tatjana Glaskova-Kuzmina, 3 and Patricia Verleysen 4

¹ Department of Aerospace Structures and Materials, Delft University of Technology, Kluyverweg 1, 2629 HS, Delft, the Netherlands

² European Commission, Joint Research Centre (JRC), Via E. Fermi, 2749, 21027 Ispra, Italy

³ Institute for Mechanics of Materials, University of Latvia, Jelgavas 3, LV-1004, Riga, Latvia

⁴ Materials Science and Technology-DyMaLab Research Group, Faculty of Engineering and Architecture, Ghent University, Technologiepark 46, Zwijnaarde 9052, Belgium

*a.g.anisimov@tudelft.nl

Abstract: One of the objectives for the HISTRATE COST Action is to develop a roadmap for standardising high strain rate testing of composite materials. There is a critical need for uniform, traceable testing guidelines to enable reliable numerical modelling of composite materials in load-bearing structures, particularly under crash or impact conditions. This roadmap seeks to bridge the gap between current academic and industrial efforts and contribute to creating a CEN prestandard.

Introduction

The HISTRATE COST Action aims to improve the standardisation of high strain rate testing for composite materials. Specifically, it was found that a clear understanding of the high strain rate material response, all the way up to failure, is needed to develop a standardised testing protocol that includes rigorous mechanics principles and standardised laboratory instrumentation [1].

COST Actions have already contributed to the early stages of composite material and joint certification. For example, CERTBOND – *Reliable Roadmap for Certification of Bonded Primary Structures* – focused on bonded joints in civil aviation, construction, automotive, and maritime industries [2]. For HISTRATE Action, application industries overlap, focusing mainly on aerospace, automotive, energy and marine.

Based on the general approach for a roadmap development [3-5], the following key aspects have to be considered: the gap analysis, roadmap objectives, proposed actions and milestones, involvement of stakeholders and the implementation plan. This abstract outlines selected elements of the roadmap. Future efforts will address all these aspects to form a complete roadmap of actions.

The gap analysis

Existing testing standards for dynamic material testing, including ISO 26203, ISO 18872 and ISO/DIS 18989, do not cover the complex behaviour of composite materials at high strain rates (up to 10^3 to 10^6 s⁻¹). A detailed review of existing standards is beyond the scope of this abstract. The main identified aspects where uniform testing practices and standardisation are needed:

testing practices and standardisation are needed:
 ■ Complex behaviour of composite materials addressing real loading scenarios: □ Multiaxial load cases instead of uniaxial. □ Multidirectional and woven composites instead of unidirectional. □ Interlaminar fracture toughness dependence on the testing strain rate.
■ Testing efficiency:
☐ Too many parameters are needed to model the material behaviour, leading to an excessive number of tests.
☐ Sustainable and more efficient testing pyramids (methodologies) minimising the amount of material and number of tests.
■ Reach experimental data, observation and measurement efficiency:
☐ Increasing the spatial and temporal resolution to characterise shock wave propagation.
☐ Implementation of full-field techniques instead of single-point measurements.
☐ Fusion of multimodal sensor data.
Roadmap Objectives
■ Short-term goals (1-2 years):
☐ Generalisation of existing best practices and in-house(s) developed procedures.
☐ Overview, comparison and benchmarking of testing and measurement approaches across different laboratories and institutions.

■ Mid-term goals (3-5 years):
☐ Adapting and modifying existing standards to include dynamic loading conditions.
☐ Propose the development of new test methods and specimen geometries.
☐ Propose integrating novel monitoring techniques (e.g., combined full-field imaging and high-speed
point-wise measurements).
■ Long-term goals (5+ years):
☐ Unified testing methodologies across the leading European testing laboratories.
☐ Inputs for a new prestandard (ENV) within the European Committee for Standardisation (CEN) for
high strain rate testing of composite materials.

Stakeholder Involvement and Collaboration

- HISTRATE members represent a diverse community: academic and research institutions, as well as industrial companies, e.g., developers of material modelling software, measurement instrumentation, material developers, designers, and end-users. However, a stronger connection with relevant standardisation societies and certification bodies (CEN, SAE, ASTM) is required to ensure the adoption of standardised practices.
- Collaboration and cooperation:
 - ☐ Internal collaboration within the HISTRATE Action is essential to maintain focus on roadmap objectives. The Action's resources, including targeted Short-Term Scientific Missions (STSM), should accelerate progress.
 - □ Partnerships with external stakeholders, including industrial partners, standardisation societies, and certification bodies, are crucial for obtaining critical feedback and ensuring practical relevance in developing new methodologies.

Proposed Actions

- Drafting good-practices documents related to testing techniques to establish a common foundation (short-term).
- Conducting a round-robin exercise on benchmark tests using reference materials and specimen design to ensure repeatability and comparability (short-term).
- Unifying testing protocols and methodologies across the leading EU testing laboratories to facilitate consistency and data reliability (mid-term).
- Establishing active participation and collaboration with relevant standardisation societies and certification bodies (CEN, SAE, ASTM) to contribute to developing future standards (long-term).

Resources and Support Needed

- Focused work within HISTRATE Action and proactive initiative activities of the Action members to align locally funded research projects with this roadmap.
- Direct use of the HISTRATE resources, e.g. the STSM focused on the roadmap development.

Conclusion

Developing a roadmap for standardising high strain rate testing of composite materials will consolidate current academic activities and industrial needs into coherent, uniform and traceable testing guidelines. These testing guidelines will contribute to developing numerical models that can reliably reproduce the behaviour of composite materials in load-bearing structures where crash or impact scenarios are possible. Furthermore, this roadmap has the potential to pave the way from these testing guidelines to a CEN prestandard.

- [1] COST Action HISTRATE Advanced Composites under HIgh STRAin raTEs loading: a route to certification-by-analysis https://histrate.eu
- [2] Santandrea, F., G. G. Momm, P. Tsokanas, V. Rajcic, D. Skejic, D. Rajnovic, R. Petkovic, and S. Kruse-Strack. "WG6: Review of certification procedures for bonded structures." (2023). https://certbond.eu/wp-content/uploads/CA18120 WG6 D01 Deliverable.pdf
- [3] Garcia, M. L., & Bray, O. H. (1997). "Fundamentals of technology roadmapping." Sandia National Laboratories Report, SAND97-0665.
- [4] Phaal, R., Farrukh, C. J., & Probert, D. R. (2005, July). Developing a technology roadmapping system. In A Unifying Discipline for Melting the Boundaries Technology Management: (pp. 99-111). IEEE.
- [5] Maxwell, J. Research to Standards: Part 2: The Roadmap to Success, https://www.astm.org/news/research-standards-part-2-roadmap-success-ja18?utm_source=chatgpt.com

Overview of available standards on high strain rate testing

Marco Peroni, 1* Andrei G. Anisimov, 2 Tatjana Glaskova-Kuzmina, 3 and Patricia Verleysen 4

¹ European Commission, Joint Research Centre, Via E. Fermi, 2749, 21027 Ispra (VA), Italy

Abstract: In the last decades, significant efforts have been made to improve numerical modelling techniques for several types of loading scenarios. Physical testing remains a fundamental requirement to obtain the material model parameters for reliable and robust simulations. High strain rate testing is largely adopted in all design problems related to impacts and explosions, but it is still not covered by a proper standard for conventional (metals, polymers) and advanced materials (composites, foams, 3D printed). This work summarizes the main standards available in the sector and provides recommendations to improve the situation in the context of HISTRATE action.

1. Introduction

Recently, significant efforts have been made to improve numerical modelling techniques for several loading scenarios. Physical testing remains a fundamental requirement to obtain the material model parameters essential for reliable and robust simulations. High strain rate testing is largely adopted in all design problems related to impacts and explosions but it is still not covered by a proper standard for conventional (metals, plastics) and advanced materials (composites, foams, additively manufactured and 3D printed). The Hopkinson bar is the main testing machine (primarily tension, compression and torsion) that operates in the strain rate range of about $10^2 \div 10^4 \, \mathrm{s}^{-1}$. However, since adopted mainly in the scientific community, related standards are generally incomplete or not updated with the emerging measuring techniques. Some aspects are not covered for lower velocities tests performed with more conventional machines like high-speed servo-hydraulic machines. This work aims to summarize the main standards available in the sector and to provide recommendations to improve the situation in the context of HISTRATE action.

2. Overview of standard available on high strain rate testing

Table 1 gives an overview of standards available on high strain rate mechanical testing: i) the majority relates to metals and polymers and only one to composite materials, and ii) the testing facilities contemplated are mainly Hopkinson bars, servo-hydraulic and drop machines.

	Standard	Relevance to HISTRATE	link
Metals	ISO 26203-1:2018 Metallic materials - Tensile testing at high strain rates. Part 1: Elastic-bar-type systems		https://www.iso.org/stan dard/72573.html
	ISO 26203-2:2011 Metallic materials - Tensile testing at high strain rates. Part 2: Servo-hydraulic and other test systems	A baseline for metals testing at the strain rate up to 10 ³ s ⁻¹ and could inspire similar approaches for composite materials, particularly in defining experimental setups for high	https://www.iso.org/stan dard/46275.html
	ISO/AWI 26203-3 Draft Metallic materials — Tensile testing at high	strain rate shear and tensile testing	
	strain rates. Part 3: Test method at elevated temperature		https://www.iso.org/stan dard/90765.html

Table 1. Overview of standard available on high strain rate testing.

² Department of Aerospace Structures and Materials, Delft University of Technology, Kluyverweg 1, 2629 HS, Delft, the Netherlands

³ Institute for Mechanics of Materials, University of Latvia, Jelgavas 3, LV-1004, Riga, Latvia

⁴ Materials Science and Technology-DyMaLab Research Group, Faculty of Engineering and Architecture, Ghent University, Technologiepark 46, Zwijnaarde 9052, Belgium

^{*} marco.peroni@ec.europa.eu

ers	ISO/DIS 18989 Draft of Plastics — Strain rate dependent tensile tests for thermoplastics at ambient temperature	Test standard for tensile testing of polymers up to 150 s ⁻¹ . It can be used for independent matrix testing	https://www.iso.org/stan dard/85797.html
	ISO 18872:2007 Plastics – Determination of tensile properties at high strain rates	Provides procedures for determining the tensile properties of moulding and extrusion plastics over a wide range of strain rates, including high rates appropriate to impact-loading situations	https://www.iso.org/stand ard/38914.html
Polymers	VDA 287 (03/2022) Strain rate dependent tensile tests for non-fibre reinforced thermoplastics at room temperature, a recommendation of the German Association of the Automotive Industry (VDA).	Guidelines for high strain rate tensile testing of polymers for the automotive industry. The standard specifies testing procedures for unreinforced and reinforced plastics to evaluate their behaviour under dynamic loading conditions.	https://webshop.vda.de/V DA/en/vda-287-032022
	SAE J 2749-2017 High Strain Rate Tensile Testing of Polymers	Addresses high strain rate tensile testing of polymers, covering strain rates between 10 s ⁻¹ and 500 s ⁻¹	https://www.sae.org/stand ards/content/j2749 20170 7/
Composites	ASTM D7136 Standard Test Method for Measuring the Damage Resistance of a Fibre-Reinforced Polymer Matrix Composite to a Drop-Weight Impact Event	Standardized method to evaluate the impact resistance of composite materials under high strain rate conditions	https://store.astm.org/d71 36_d7136m-15.html
Measurements	ISO 22183:2023 Plastics — Validation of force-time curves obtained from high-speed tensile tests	Quality criteria for dynamic force sensors used in high strain rate testing. An example of defining equipment calibration and validation procedures for dynamic tests	https://www.iso.org/obp/u i/#iso:std:iso:22183

Concerning servo-hydraulic and drop test machines, where the test execution or the data elaboration is close to static experiments, standards seem at least sufficiently structured. However, some doubts remain about the specimen geometry and force measurements to be adopted (possible ringing phenomena or data filtering at high velocity). The Hopkinson bar standards are not updated with modern instrumentation (high-speed imaging and more general optical techniques) and provide limited guidelines for testing design and data elaboration procedures (which, in this case, is different from static tests). The procedures presented, for example, in ISO 26203-1, are too simplified to be applied to complex materials like composites. This standard is based on data execution-elaboration procedures related to measuring techniques of more than twenty years ago, totally neglecting high-speed imaging. Moreover, high strain rate testing on composite materials requires peculiar features that sometimes contradict the conventional requirements of Hopkinson bar test on metals and general ductile materials (pulse shaping, fixture requirements, premature failures, etc.).

In addition, emerging experimental techniques like optical-based measurements or laser shock techniques have been uncovered by standards.

Another critical aspect related to high strain rate testing (for all the testing methodologies) is the absence of commonly accepted calibration procedures or benchmark tests to compute a quantitative assessment of measurement accuracy. Leveraging proficiently innovative instrumentation and numerical tools (FEM, AI) that incorporate a statistical evaluation of uncertainties could help to overcome these gaps.

3. Proposals for standard improvements in the context of HISTRATE action

Following the discussion of HISTRATE members in the Athens general meeting 2024, a series of suggestions have been proposed to overcome the lack of standards related to the mechanical characterization at high strain rates of composites that can also be adopted for other material types. Three main actions (probably feasible in the context of HISTRATE) have been individuated and reported in the following paragraphs.

3.1. Draft of good-practices documents related to testing techniques (short-term action)

The main idea in this context is to collect material related to good-practices documents that are available concerning state-of-the-art measuring and testing techniques. Suppose these documents are not available – to draft them. Some material is available, for example, for DIC (i.e.

https://idics.org/guide/DICGoodPracticesGuide_PrintVersion-V5h-181024.pdf) but less for Hopkinson bar technique mainly when applied to complex cases like composites, 3D printed or cellular materials. For each measuring/testing technique involved, details related to test executions and data elaborations could be useful, especially for new users.

3.2. Round-robin exercise on benchmark tests or reference materials (short-term action)

A round-robin exercise related to high strain rate testing could be organized between HISTRATE members with multiple purposes: i) compare experimental data on benchmark or reference material tests to verify the effect of the different execution/elaboration procedures related to involved laboratories; ii) improve good practices documents; iii) share operational tips and tricks related to the selected tests.

Some benchmark tests could be performed simply on the testing facilities to assess the calibration/elaboration procedures adopted (without any specimens) and strengthen the concept of accuracy evaluation of testing machines.

3.3. Try to influence/be present in the standardization process (long-term action)

HISTRATE cost action could contact the CEN-CENELEC organization to confirm the absence of standards related to high strain rate testing in particular on composite materials, and propose to be present/contacted if a new standardization process will start in the following years.

4. Conclusions

This work presents an overview of the standards related to high-strain rate testing, particularly on composite materials. As reported, valuable standards for material characterization at high strain rates are still unavailable at the moment, while at least one standard exists concerning component testing for fibre-reinforced polymer matrix composite [7]. HISTRATE members could improve the situation using three main instruments individuated during the Athens general meeting 2024. In particular, the draft of good practice documents related to high strain rate testing techniques and a series of round-robin exercises seems the most effective until the end of HISTRATE action.

- [1] ISO 26203-1:2018 Metallic materials Tensile testing at high strain rates. Part 1: Elastic-bar-type systems.
- [2] ISO 26203-2:2011 Metallic materials Tensile testing at high strain rates. Part 2: Servo-hydraulic and other.
- [3] ISO 26203-3 Metallic materials Tensile testing at high strain rates. Part 3: Test method at elevated temperature (DRAFT).
- [4] ASTM E209-18 Standard Practice for Compression Tests of Metallic Materials at Elevated Temperatures with Conventional or Rapid Heating Rates and Strain Rates (DRAFT).
- [5] ISO/DIS 18989 Plastics Strain rate dependent tensile tests for thermoplastics at ambient temperature.
- [6] ISO 18872:2007 Plastics Determination of tensile properties at high strain rates.
- [7] VDA 287 (03/2022) Strain rate dependent tensile tests for non-fiber reinforced thermoplastics at room temperature, a recommendation of the German Association of the Automotive Industry (VDA).
- [8] SAE J 2749-2017 High Strain Rate Tensile Testing of Polymers.
- [7] ASTM D7136 Standard Test Method for Measuring the Damage Resistance of a Fiber-Reinforced Polymer Matrix Composite to a Drop-Weight Impact Event.



Advanced Composites under High Strain Rate Loading A Route to Certification-by-Analysis

> 2025 Conference 4th – 5th JUNE 2025

Poster Presentations





Investigation of Strength Properties of Polymer Based Carbon fiber-reinforced plastic (CFRP) and glass fiber-reinforced plastic (GFRP) Composites as Experimental and Numerical

Büşra Osma, 1* Gülşen Akın Evingür²

Department of Naval Architecture and Marine Mechanical Engineering, Institute of Science, Yıldız Technical University, İstanb ul, Turkey
Programme of Mechatronics, Maritime Higher Vocational School, Piri Reis University, İstanbul, Turkey
* busra.osma@std.yildiz.edu.tr

Abstract: The effect of polymer layers into composites used in marine structures was investigated for strength. Polymer materials used as layers were produced by the solution casting method. The composites with a resin/hardener ratio of 10:3 by weight were produced by hand-lay-up technique. The composites' macro scale tensile tests were performed on Instron 8872 model Electromechanical Universal Testing Machine. It was observed that the polymer material used as a layer increased the tensile strength values of the composite materials. The load-dependent deformation changes of the composite materials were numerically compared with the experimental data in ANSYS Static Structural module.

1. Introduction

According to the literature review, polyurethane is so popular thermoplastic materials for sound insulation [1,2]. EVA (ethylene vinyl acetate) can be used for sound insulation [2]. According to the literature study conducted in 2019[4,5], it has been observed that there have been remarkable studies on the sound absorption properties of EVA in recent years. The uniqueness of the study is that EVA materials in the form of film were produced and used as a layer in GRP composite materials. The new type of GRP materials was produced and investigated for acoustic properties and this situation was registered by the Turkish Patent and Trademark Office that it has a new type of material approach [6]. After this research, the mechanical properties of strength properties of polymer-based carbon fiber-reinforced plastic (CFRP) and glass fiber-reinforced plastic (GFRP) composites were investigated with macro scale tensiletests. Within the scope of the BAP (Scientific Research Project) titled "2023-2024-Experimental and Numerical Investigation of Strength Properties of New Type Glass Fiber Reinforced (GRP) Composites", these GRP composite materials were experimentally and numerically investigated in terms of strength properties.

2. Preparation of Composite Materials

EVA copolymer, the weight ratio of vinyl acetate varies between 28% was produced by the solution casting method. The composites with a resin/hardener ratio of 10:3 by weight were produced by hand-lay-up technique at room temperature.

3. Tensile Tests

Tensile tests were performed on CFRP and GFRP composite speciman in Instron 8872 model "Electromechanical Universal Testing Machine" (Figure 1). The capacity of the machine is 100 kN. The test conditions were applied according to ISO 527-4[7] and the test was performed at room temperature.



Fig. 1. Tensile testing of specimens on Instron 8872 model tensile machine

4. Modelling Procedure

The tensile test result data of the layers were used for material identification purposes in ANSYS Data Engineering. ISO 527-4 sample dimensions, the sample model was designed in ANSYS SpaceClaim. Boundary conditions and initial conditions in the tensile test are defined as seen in the Fig. 2.

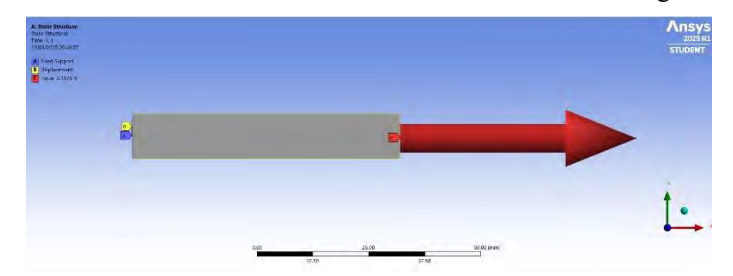


Fig. 2. Defining boundary conditions and initial conditions in ANSYS

5. Conclusion

Modulus (MPa)

The effect of the polymer material used as a layer on the composite material was investigated and this effect cause to increase tensile strength values of composite materials as seen in Table 1.

Composite materials' load-dependent deformation changes were numerically compared to the experimental data in ANSYS Static Structural module. In conclusion, only one-layer tensile test data can be used to determine composite deformation properties depending on load can be investigated numerically. For this reason, this macroscale approach can decrease to manufacturing budget before production of big structure in preliminary design stage.

Table 1. Comparison of the effect of the polymer material used as a layer on the mechanical properties of the composite material

LP-1 without EVA

2535.60472

Tensile Strength(N)		931.46265	862.57245
1.2	rawdata		
1	ansys		
0.8			1
9.0 8.0 8.0 8.0 8.0 8.0 8.0 8.0 8.0 8.0 8			
0.4		A STATE OF THE STA	
0.2	-		
0	50 100) 150 200	250 300 350
0	30 100	100 200 100d(N)	230 300 330

LP-1 with EVA

2437.37294

 LP-3 with EVA
 LP- without EVA

 Modulus (MPa)
 7344.95274
 6805.82265

 Tensile Strength(N)
 6824.92334
 5920.32227

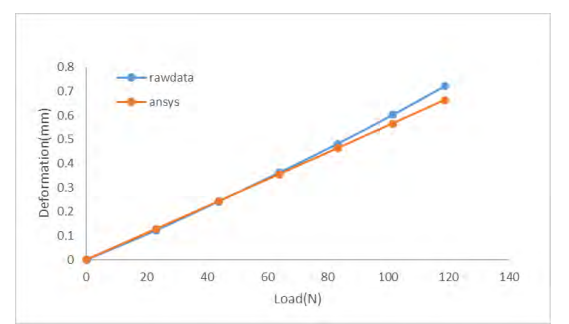


Fig. 3. Deformation(mm)-load(N) graph of tensile test results (raw data) and results obtained by numerical solution (ansys) of LP-7 specimen

Fig. 4. Deformation(mm)-load(N) graph of tensile test results (raw data) and results obtained by numerical solution (ansys) of LP-10 specimen

- [1] Lee, J., Kim, G. H., & Ha, C. S. (2012). Sound absorption properties of polyurethane/nano-silica nanocomposite foams. Journal of applied polymer science, 123(4), 2384-2390.
- [2] Yıldırım, B., Sancak, A., Navidfar, A., Trabzon, L., & Orfali, W. (2018). Acoustic properties of polyurethane compositions enhanced with multi-walled carbon nanotubes and silica nanoparticles: Akustische Eigenschaften von durch mehrwandige Kohlenstoff-Nanoröhren und Silizium-Nanopartikel verstärkten Polyurethan-Verbundwerkstoffen. Materialwissenschaft und Werkstofftechnik, 49(8), 978-985.
- [3] Henderson, A. M. (1993). Ethylene-vinyl acetate (EVA) copolymers: a general review. IEEE Electrical Insulation Magazine, 9(1), 30-38.
- [4] Gong, W., Ma Y.L, Ban D.M., Yin X.G, He L., Fu H., (2019). Study of the Sound Absorption Performance of Ethylene-Vinyl Acetate Foam Material, ISSN 1392-1320 Material Science, Vol.25, No.4.
- [5] Lyu, L., Liu, Y., Bi, J., & Guo, J. (2019). Sound absorption properties of DFs/EVA composites. Polymers, 11(5), 811. [6] Akin Evingür, G., Osma, B., 2024, "A New Laminated Material That Allows To Improve The Sound Insulation Properties Of Submarine Vehicles"
- [7] ISO 527-4:2023- Plastics Determination of tensile properties-Part 4: Test conditions for isotropic and orthotropic fibre-reinforced plastic composites

The effect of laser assisted tape placement processing conditions on flexural strength of in-situ carbon fibre/PEEK laminates

Sara Srebrenkoska ^{1*}, Svetlana Risteska ^{1,2}, Vineta Srebrenkoska ²

¹ Faculty of Mechanical Engineering, Goce Delcev University, Krste Misirkov, No. 10-A Stip, Republic of North Macedonia.

² Faculty of Technology, Goce Delcev University, Krste Misirkov, No. 10-A Stip, Republic of North Macedonia.

*sara.srebrenkoska@ugd.edu.mk

Abstract: Laser-assisted automated tape placement (LATP) has great potential for cost-effective production of thermoplastic parts. The purpose is to investigate how LATP processing conditions affect the flexural strength of laminates made from carbon fibers and polyether ketone (PEEK). The experiments were made by processing the prepreg under different conditions, and the most influential factors were taken into account: laser temperature, compact pressure of the roller, and laser placement angle. Flexural strength tests were performed on all manufactured specimens, and some conclusions regarding process parameters and the ultimate properties of composite specimens were developed based on the experimental data received.

1. Experiment

In this study for the production of the thermoplastic composite laminates, thermoplastic unidirectional prepreg material (UD) was used. Composite specimens with different technological parameters (all possible combinations of the parameters - 8 different samples) were produced with help of laser-assisted automated tape placement head (LATP) (Fig.1). Head is attached to a robot arm, as it is shown in Fig. 2. The tape head consists of: a consolidation roller (outer diameter of 90 mm), a tape feed, guidance, tensioning, and cutting system for UD prepreg tape, an optic lens connected via a fibre-optic cable to a remotely-located 3 kW diodelaser heat source and a temperature sensor (pyrometer) [1-3].



Fig. 1. a) Schematic representation of of automatic tape laying process b) Automatic laser - assisted of UD laying

A tape placement process involves pulling of the thermoplastic prepreg tape from a spool through the feed and guide assembly. On the way to the consolidation roller, the tape is heated on temperature (based of the type of polymer) using a laser. The tape is then placed on the tool and consolidated with a roller [2-4]. During the tape laying, several factors were observed: laser temperature, compact pressure of roller and and laser placement angle, so composite plates with thickness of ~1,5 mm (8 layers prepreg) were manufactured. An investigation of the effect of technological parameters on mechanical properties of laminate panels was performed. The flexural testing was performed according to ASTM D790, using test rupture. Based on the three-point bending test (3pb), prepared specimens were elongated till rupture with help of test fixture and the flexural strength is calculated respectively, according to the standard.

2. Results and discussion

The test results for flexural strength (mean velue of five replications) of each combination are presented in Table 1. The test results indicated an effect of compact pressure of roller and laser temperature on mechanical properties of composite specimens. Namely, the bigger compact pressure of roller and higher laser temperature led to a higher flexural properties of laminate panels. In a polymer composite, each layer has contribution to the whole strength, and when one of the layers in the structure starts to fail, it cracks the matrix around and there appears an increase in the strain. The strain response of the laminate is restored but the load carrying thickness of the panels is decreased due to the failure of one of the layers. As the wall thickness of the laminate panels is decreased, it cannot carry more load anymore, and fails [5,6].

	Sample	Sample designation LATP-UD		
Numb er of exp.	Laser temperature, °C	Laser angle,	Compact pressure, N	Flexural strength, MPa
1	380	25	380	1036,81
2	360	25	380	941,73
3	380	22	380	1011,50
4	360	22	380	927,41
5	380	25	270	903,88
6	360	25	270	858,90
7	380	22	270	921,83
8	360	22	270	892,37

Table 1. Condition of the experiments and flexural test results

Figures 1 shows a typical force - time diagram at ambient temperature for samples (1 and 6) with the highest and lowest values for the flexural strength. The load-time curves of the specimens 1 (five replications) are similar and the laminated samples have a linear behaviour up to cracking of the some layers of samples. The curves have an appearance which is like zigzag at the higher values of the force which corresponds to the cracking of the fiber layers. In the case of the specimens 6 there is a linear behaviour up to cracking of some layers of fibers but the samples are still not destroyed. With continuing of the force, the curves continue to have a view which is like linear up to cracking of the samples.

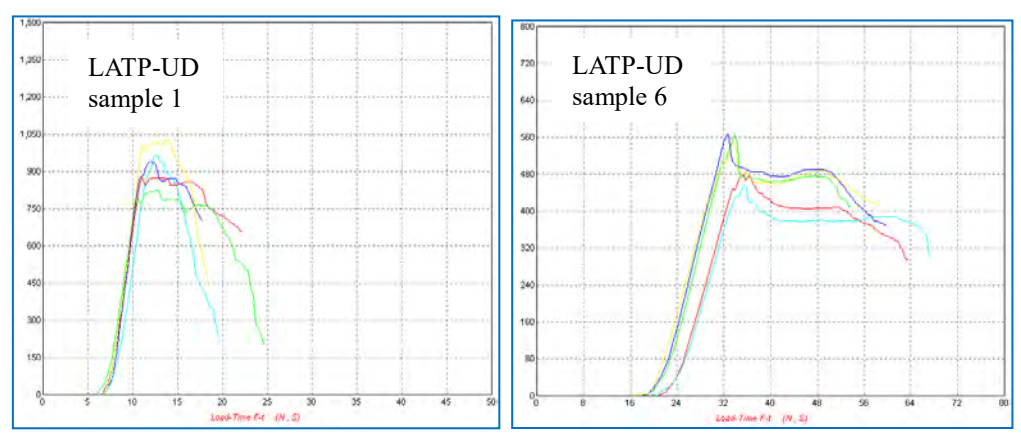


Fig. 2. Load -time diagrams for LATP-UD: sample 1 and sample 6

It can conclude that high quality of laminates made by LATP process depends on the processing parameters fed to the LATP system. Moreover, the compaction force applied during the lay-up process and the laser temperature play a crucial role in achieving of obtaining of defect-free laminates using the thermoplastic UD prepreg materials.

- [1] Stokes-Griffin, C.M., Compston, P., The effect of processing temperature and placement rate on the short beam strength of carbon fibre-PEEK manufactured using a laser tape placement process, Composites: Part A (2015), doi:http://dx.doi.org/10.1016/j.compositesa.2015.08.008C.
- [2] Kaven Croft, Larry Lessard, Damiano Pasini, Mehdi Hojjati, Jihua Chen, Ali Yousefpour, Experimental study of the effect of automated fiber placement induced defects on performance of composite laminates, Composites: Part A 42 (2011) 484–491 Elsevier doi: 10.1016/j.compositesa.2011.01.007.
- [3] Margaret F, Talbott and George S, Springer, The Effects of Crystallinity on the Mechanical Properties of PEEK Polymer and Graphite Fiber Reinforced PEEK, Journal of Composite Materials 1987 21: 1056, DOI: 10.1177/002199838702101104
- [4] Fazil O. Sonmez and H. Thomas Hahn, Modeling of Heat Transfer and Crystallization in Thermoplastic Composite Tape Placement Process, Journal of Thermoplastic Composite Materials 1997, DOI: 10.1177/089270579701000301.\
- [5] Huiran Zou, Weilong Yin, Chaocan Cai, Bing Wang, Ankang Liu, Zhen Yang, Yibin Li and Xiaodong He, The Out-of-Plane Compression Behavior of Cross-Ply AS4/PEEK Thermoplastic Composite Laminates at High Strain Rates, Journal Materials 2018, Vol11, 2312; doi:10.3390/ma11112312
- [6] Lisa Feuillerat, Olivier De Almeida a, Jean-Charles Fontanier , Fabrice Schmidt, Effect of poly(ether ether ketone) degradation on commingled fabrics consolidation, Journal Composites Part A 149 (2021) 106482 https://doi.org/10.1016/j.compositesa.2021.106482

Development of Basalt Based Fiber-Metal Laminates and Analysis of Their Mechanical Properties

Aleksandre Vanishvili, 1* Davit Tsverava, 1 Mariam Gureshidze 1 and Sophiko Kvinikadze 1,

¹ Grigol Tsulukidze Mining Institute, 7 Mindeli St., Tbilisi, Georgia

* Alexandre.vanishvili@gmail.com

Abstract: The aim of this study is to fabricate basalt fabric-reinforced metal-polymer composites and analyze their mechanical properties. Basalt fiber was chosen for its local availability, excellent mechanical and chemical properties, and cost-effectiveness. Within the project, various structured metal-polymer composites reinforced with basalt fabric were produced, and their mechanical properties—tensile and impact strength—were assessed. In this paper, we present the results of our ongoing research.

Introduction:

A composite is a material that is made up of two or more discrete materials that are combined in such a way as to achieve desirable properties [1-2]. Such composite materials include Fiber-Metal Laminate (FML) which consists of layers of metal and reinforcement fiber bonded together with polymer matrix. Basalt fabric was selected as the reinforcing component due to its local production, low cost, and, as well as its outstanding physical and mechanical properties. The choice of basalt fiber is strategic, given its local availability and outstanding chemical composition [3].

The scientists at the Laboratory of Polymer Composites and High-Tech Materials of the G. Tsulukidze Mining Institute are utilizing basalt fibers and advanced fabrication techniques to create FMLs with exceptional mechanical properties [4].

Material and Methodology:

Basalt fiber textile (RB-14-250 mark) was supplied by LLC Basalt Fibers Georgia company, which used as the reinforcement fiber. The polymeric matrix consisted of XRL-ER80AB, a two-component transparent epoxy resin. Aluminum Alloy 1100 sheets were used. RFI (Resin Film Infusion) technology was used to manufacture the metal-polymer composite.

RFI technology involves introducing resin film under vacuum into a pre-prepared composite structure. It is particularly widely used for the production of composites with complex shapes. The process of manufacturing composite materials using RFI technology includes the following stages: preparation and treatment of the surface-mold (selecting glass with a smooth and clean surface and treating the surface with a separating liquid); preparation of the initial components and assembly of the composite layers on the treated glass surface, in the desired sequence; preparation of the vacuum package; preparation and degassing of the matrix polymer; infusion process, followed by curing; opening of the vacuum package. If necessary, thermal treatment of the obtained composite is performed (Figure 1).

In total 5 different composite samples were obtained with different compositions of basalt and aluminum layers (table 1).

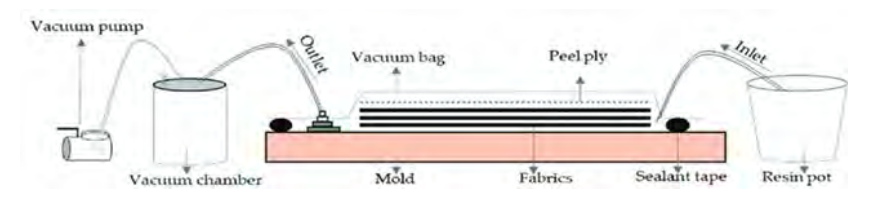


Fig. 1. Schematic of Resin Film infusion (RFI) technology used in production of laminate composite

Low-velocity impact testing was conducted using the Charpy impact tester. The fabricated laminate plates were precisely cut into test coupons with dimensions of 4 mm x 8 mm x 100 mm. During Charpy impact test velocity and energy applied to the sample are maintained at constant values of 7.5 J and 3.5 m/s, respectively. These controlled conditions ensured the precision and reliability of the comparative analysis of the results.

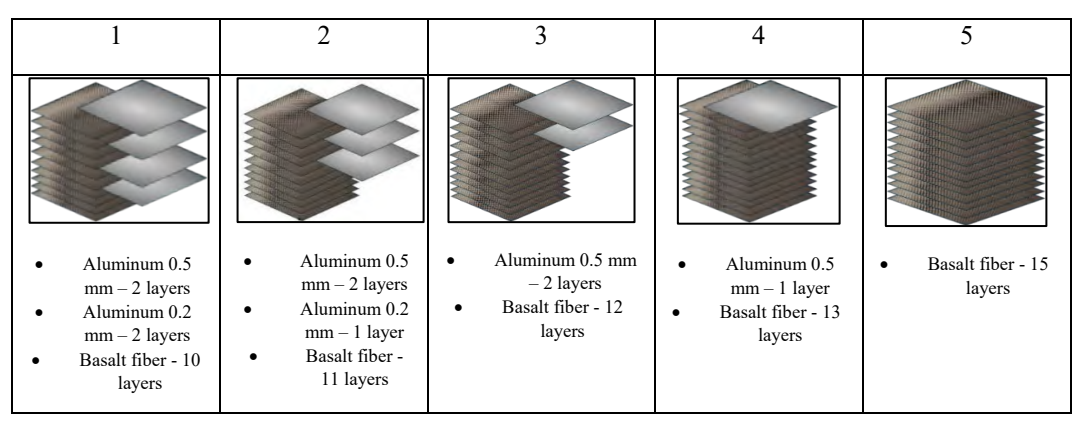


Table 1. layer compositions of test samples.

Results and Conclusion:

The strength assessment of metal-polymer composite samples manufactured using RFI technology was conducted under direct tensile loading using a hydraulic press – a universal testing machine. This equipment is equipped with software that provides "load-deformation" curves. The experiment was carried out at room temperature (24°C), and in all cases, the grip displacement rate was set to 0.2 mm/min.

The Charpy method (Charpy Impact Test) was used to study the impact resistance of the materials, which is widely recognized as one of the primary methods for comparative assessment of the mechanical properties of materials. The use of the Charpy Impact Tester in the research process allows for the determination of the composite's ability to absorb energy during impact (Table 2).

Sample N	Impact resistance test result				
	Fracture energy (kJ/m ²)				
1	5.1				
2	3.6				
3	2.4				
4	2.1				
5	1.6				

Table 2. Impact resistant test results

The research results indicate that the number and arrangement of aluminum layers in metal-polymer composites play a critical role in ensuring impact resistance. Sample 1, which achieved the highest result (5.1 KJ/m²), optimally balances aluminum and basalt layers, providing both impact strength and flexibility. Sample 1 also demonstrated the highest tensile strength (76.0 MPa) and an optimal strain rate (5.4%). The presence of four aluminum layers creates the best balance between strength and relative deformation, allowing the material to withstand high loads while maintaining limited deformation. The project is ongoing, and multiple experiments are planned for future investigation.

Acknowledgments:

This work is in progress with the support of the Shota Rustaveli National Science Foundation of Georgia (SRNSFG) – Grant # AR–22–1445. Title - "Production of multifunctional metal-polymer laminate with high mechanical characteristics and determination of technological parameters"

Reference:

- [1] Hazell, P. J., 2022, Armour: Materials, Theory, and Design, 2nd ed., CRC Press, https://doi.org/10.1201/9781003322719.
- [2] Gibson, R. F., 2010, "A Review of Recent Research on Mechanics of Multifunctional Composite Materials and Structures," Composite Structures, 92(12), pp. 2793-2810.
- [3] Spagnuolo, D. M., Napadensky, E., Sano, T., and Wolbert, J. P., 2011, "Investigation of Basalt Woven Fabrics for Military Applications," Army Research Laboratory, Aberdeen Proving Ground, MD.
- [4] Baliashvili, G., Kvinikadze, S., Iashvili, T., Tsverava, D., and Vanishvili, A., 2024, "Obtaining Metal-Polymer Laminates with High Mechanical Properties," International Multidisciplinary Scientific Geoconference: SGEM, Chapter 6.1, pp. 25-31,

http://doi.org/10.5593/sgem2024/6.1/s24.04.

Influence of some technological parameters on the content of voids on the in-situ thermoplastic composites in Pultrusion, FW and AFP/ATP technologies

Svetlana Risteska^{1*}, Vineta Srebrenkoska¹, Sara Srebrenkoska²

¹ Faculty of Technology, Goce Delcev University, Krste Misirkov, No. 10-A Stip, Republic of North Macedonia.

*svetlana.risteska@ugd.edu.mk

Abstract: The manufacturing processes, such as pultrusion, filament winding and automated fiber/tape placement, have been used conventionally for thermoset composites. The automated processes can be adapted to include in situ consolidation for the fabrication of thermoplastic composites.

In this paper, a detailed review of the factors affecting the in-situ consolidation process is presented for each technology in detail. Experimental tests were performed with changing parameters for the three technologies in order to minimize voids for the fabrication of thermoplastic composites. Optimizing these parameters ensures high-quality composite parts with superior mechanical properties who to be used in many applications.

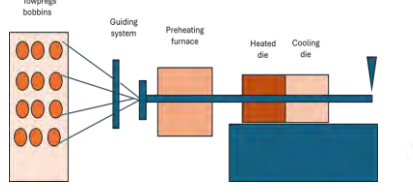
1. Experiment

1.1. Materials

The manufacturing of fiber reinforced thermoplastic polymer (FRP) composites is generally much less time consuming due to their short consolidation cycles. Besides this, FRTP composites also have other advantages over thermoset based FRP composites, including higher toughness, long shelf life, ease of repairing and potential for recycling [1]. For the experiments with pultrusion and FW technology GF/PP was used, that for AFP/ATP technology, GF/PP and GF/PA6 as and other thermoplastics such as PPS/PEEK were used.

1.2. Production of FRTP composites with in-situ consolidation in multiple technologies (Pultrusion, FW and AFP/ATL)

In-situ consolidation relies on heating the thermoplastic polymer matrix rapidly above its melting temperature, followed by fusing the molten surfaces during cooling. This process eliminates a second step of autoclave or hotpress mold consolidation, thereby reducing processing steps and manufacturing expenses.



ROVING HEATING HEATING FIRST HEATED ROLLER

CONSOLIDATION SOLIDATION ROLLER

ROLLER ROLLER

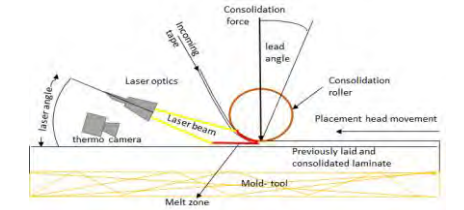


Fig. 1 Schematic layout of designed laboratory pultrusion

Fig. 2 Schematic layout of designed FW laboratory head

Fig. 3 Schematic layout of designed AFP/ATL laboratory head

There are more technologies for In-situ consolidation, they are:

- The term in-situ thermoplastic Pultrusion refers to the use of thermoplastic resins in the pultrusion process. In this case, the thermoplastic resin is introduced directly into the pultrusion process allowing the thermoplastic material to fuse and bond around the reinforcement fibers [2-5].
- In-situ thermoplastic Filament Winding (FW) is an innovative process that combines the benefits of thermoplastic resins with the precise and efficient filament winding technique [6].
- In-situ consolidation in Automated Fiber/Tape Placement (AFP/ATP) enhances the fiber placement process by integrating the resin activation and consolidation directly into the manufacturing workflow.

However, these processes require careful management of key parameters, including temperature, fiber tension, compact pressure and resin flow, to ensure optimal consolidation and part performance. Optimizing these parameters ensures high-quality composite parts with superior mechanical properties. These technologies offer significant benefits across a variety of industries, including aerospace, automotive, defense, and energy, by providing high-performance composite materials with tailored properties [7].

² Faculty of Mechanical Engineering, Goce Delcev University, Krste Misirkov, No. 10-A Stip, Republic of North Macedonia.

2. Results and Discussion

The content of voids in thermoplastic composites produced using pultrusion, filament winding (FW), and automated fiber placement (AFP) technologies is a critical factor influencing the mechanical properties, performance, and durability of the final composite material. The presence of voids can significantly degrade the strength, stiffness, fatigue resistance, and overall integrity of the composite, making it essential to minimize their formation during manufacturing. Various technological parameters in each process can affect void content, and understanding their influence is key to producing high-quality thermoplastic composites Table 1.

Table 1. Technological Parameter Influence on Void Content

Parameter	Pultrusion	Filament Winding (FW)	Automated Fiber /Tape Placement (AFP/ ATP)		
Resin Viscosity	Affects resin flow and fiber impregnation, influencing voids.	Influences resin impregnation and void formation.	Influences resin impregnation and voids.		
Temperature/Heating	Critical for resin melting and consolidation, avoiding voids.	Affects resin melting and cooling rate.	Temperature control ensures proper resin consolidation.		
Pulling/Placement Speed	Too fast reduces impregnation time, causing voids.	Higher speed can lead to incomplete impregnation.	High speed risks incomplete resin impregnation.		
Fiber Tension	Uneven tension causes uneven resin distribution and voids.	Tension controls fiber alignment and resin flow.	Consistent tension ensures uniform impregnation and reduced voids.		
Mandrel/Tool Temperature	Affects resin consolidation, avoiding void formation.	Ensures proper resin solidification on the mandrel.	Uniform mandrel temperature avoids resin issues and voids.		
Layer Overlap and Alignment	Not typically applicable in pultrusion, but fiber alignment affects resin bonding.	Proper layer alignment prevents voids.	Proper layer overlap ensures complete fiber bonding, reducing voids.		

Technological parameters such as resin viscosity, temperature control, fiber tension, speed of processing, and fiber placement alignment all play crucial roles in the formation of voids in thermoplastic composites produced by pultrusion, filament winding (FW), and automated fiber placement (AFP). Understanding and controlling these parameters allows manufacturers to minimize void content and produce high-quality, high-performance composites with optimal mechanical properties. Minimizing void content requires careful attention to each step of the manufacturing process—material selection, resin impregnation, machine settings (e.g., tension and pressure), curing, and post-processing. The results from experiments for void percentages for these technologies are given in Table 2.

Table 2 The lowest percentage of voids from the experiments in all three technologies

Parameter	Pultrusion	Filament Winding (FW)	Automated Fiber /Tape Placement (AFP/ ATP)	
Void contents	1% to 5%	1% to 3%	1% to 5%	

3. Summary

Low void content (< 2%) is generally desired for high-performance applications (e.g., aerospace, automotive) because it ensures better mechanical properties like strength, stiffness, and durability. Higher void content can sometimes be tolerated in less critical applications, though it always comes with trade-offs in mechanical properties.

- [1] Arhant, M.; Davies, P. 2-Thermoplastic matrix composites for marine applications. In Marine Composites; Pemberton, R., Summerscales, J., Graham-Jones, J., Eds.; Woodhead Publishing: Cambridge, UK, 2019; pp. 31–53.
- [2] Huiran Zou, Weilong Yin, Chaocan Cai, Bing Wang, Ankang Liu, Zhen Yang, Yibin Li and Xiaodong He, The Out-of-Plane Compression Behavior of Cross-Ply AS4/PEEK Thermoplastic Composite Laminates at High Strain Rates, Journal Materials 2018, Vol11, 2312; doi:10.3390/ma11112312
- [3] Lisa Feuillerat, Olivier De Almeida a, Jean-Charles Fontanier , Fabrice Schmidt, Effect of poly(ether ether ketone) degradation on commingled fabrics consolidation, Journal Composites Part A 149 (2021) 106482 https://doi.org/10.1016/j.compositesa.2021.106482
- [4] Standard Test Methods for Constituent Content of Composite Materials, ASTM D 3171.
- [5] Tucci, F.; Rubino, F.; Pasquino, G.; Carlone, P. Thermoplastic Pultrusion Process of Polypropylene/Glass Tapes. Polymers 2023, 15, 2374. https://doi.org/10.3390/polym15102374
- [6] Maja Stefanovska, Blagoja Samakoski, <u>Svetlana Risteska</u>, Gari Maneski, "Influence of Some Technological Parameters on the Content of Voids in Composite during On-line Consolidation with Filament Winding Technology" ICMTM Berlin 2014International Conference on Metallurgy Technology and Materials.
- [7] Boon, Y.D.; Joshi, S.C.;Bhudolia, S.K. Review:Filament Winding and Automated Fiber Placement with In Situ Consolidation for Fiber Reinforced Thermoplastic Polymer Composites. Polymers 2021,v 13, pp1951.

Ballistic strength of polyethylene composites based on bidirectional and unidirectional fibers under the high-speed ballistic impact

Vineta Srebrenkoska ^{1*}, Svetlana Risteska ^{1,2}, Sara Srebrenkoska ²

*vineta.srebrenkoska@ugd.edu.mk

Abstract: The purpose is to investigate the behavior of composites made of ultra-high molecular weight polyethylene woven fabrics and unidirectional tapes under the high-speed ballistic impact. Ballistic composites based on bidirectional and unidirectional fibers are manufactured and subjected to ballistics tests. The unidirectional composites have shown superior performance as compared to bidirectional ones due to their lower extent of the reflective impact wave i.e. the ballistic impact wave is transmitted to higher composite area. Due to the crossover points in bidirectional composites, the greater extent of the ballistic wave is reflected, rendering the ballistic impact to smaller composite area.

1. Experiment

1.1. Materials

Plain woven HPPE fabric was used as reinforcement for bidirectional composites and as a matrix polyvinylbutyral (PVB) modified phenolic resin of resole type was used. The impregnation of the fabric with the resin was done on a semi-industrial vertical impregnating machine. The unidirectional tape, which was pre-processed into prepreg, consists of four layers of unidirectional fibers cross plied at $0^{\circ}/90^{\circ}$ orientation, as shown in Figure 1, and sandwiched with a thermoplastic film.

Table 1. The properties of unidirectional and bidirectional prepregs

Property	Unit	Unidirectional	Bidirectional
		prepreg	prepregs
Resin type		thermoplastic	thermoset
			(phenolic resin)
Resin content	%	20±1	20±1
Gel time at 150°C	seconds	-	96
Areal weight	g/m ²	244±7	240±7
Volatiles content	%	<1.5	<1.5

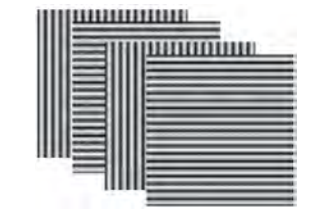


Fig. 1. Construction of unidirectional prepreg

1.2. Molding

The composites were constructed by laying up a multiple number of prepreg plies in accordance with the targeted areal weight and cured at elevated temperature. Each type of composite is manufactured in four different areal weights, 3, 5, 7 and 9 kg/m². This areal range is chosen because it is common for personal ballistic protection. All composites were molded at 130 °C under molding pressure of 10 MPa.

1.3. Ballistic test

Ballistic strength of the composites was assessed by measuring their ballistic strength i.e. V_{50} ballistic limit. V_{50} ballistic limit is a statistical test originally developed by the US military to evaluate hard armor [1,2]. V_{50} testing experimentally identifies the velocity at which a bullet has a 50% chance of penetrating the test object. Fundamental to the concept of ballistic limit is a relationship between probability of penetration of the armor and the striking velocity of the projectile. The projectile-armor relationship satisfies the mathematical conditions of probability distribution i.e. for low velocities probability approaches zero; for high velocities the probability approaches one; and between those extremes of velocity, the probability increases with increasing velocity. When the general model describes physical behavior, probability of penetration can be treated as a probability distribution and is usually described as a Gaussian or normal distribution.

The ballistic test is performed by firing 5.56mm, 1.5 g fragment simulating projectiles on to the composite panel. All test panels (400 mm x 400 mm) prior to testing, are conditioned at 20 ± 2 °C and relative humidity of 65 ± 5 %. At least 14 projectiles are being fired at the test panels and their velocities measured. A projectile which passes through the panel or causes material to be thrown off of the back of the panel is considered complete penetration. All other impacts are defined as being partial penetrations. The V_{50} ballistic limit velocity for a panel is defined as that velocity for which the probability of penetration of the projectile is exactly 0.5. The subscript 50 designates the percentage of that probability of penetration. After a number of projectiles have been fired the V_{50} is calculated as the meaning of the velocities recorded for the fair impact consisting of the seven highest velocities for partial

¹ Faculty of Technology, Goce Delcev University, Krste Misirkov, No. 10-A Stip, Republic of North Macedonia.

² Faculty of Mechanical Engineering, Goce Delcev University, Krste Misirkov, No. 10-A Stip, Republic of North Macedonia.

penetration and the seven lowest velocities for complete penetration providing that all fourteen fall within a bracket of 60 m/s [2].

2. Results and Discussion

The results of the ballistic test are given in Table 2.

Table 2. Ballistic strength of the composites, V_{50} (m/s)

			0	1 ,	50 (
C	Areal weight of composites				
	Composite	3 kg/m^2	5 kg/m^2	7 kg/m^2	9 kg/m^2
	BD-HPPE	319.1	412.9	498.2	557.3
	UD-HPPE	401.1	517.4	601.9	682.1



Fig. 3. Cross-section of UD composite

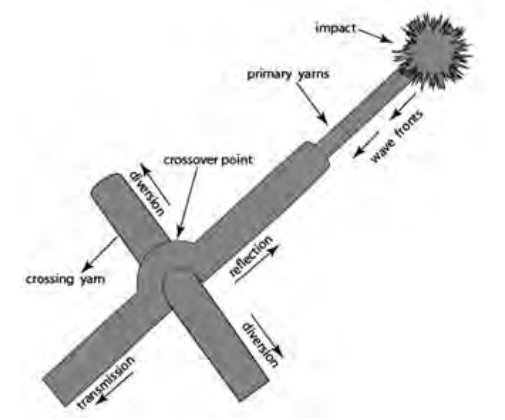


Fig.2. Longitudinal wave propagation in fabric after ballistic impact

In the above table "BD" and "UD" designate bidirectional (fabric) and unidirectional composites respectively. Textiles are used to protect against two categories of ballistic projectiles. Bullets from handguns and rifles form one category. These bullets are designated to deform when they hit a body or another object as this is the most effective way to stop a living being. They use a lot of their kinetic energy in the deformation, so they are relatively easy to stop by e.g. bullet-resistant vest. The other category is formed by fragments from exploding shells and grenades. These fragments are smaller than bullets and they have sharp edges and do not deform. For testing purposes (which was done in the ballistic laboratory of the military contractor "Eurokompozit" from Prilep, Macedonia) we used fragment simulating projectiles (FSP) with a well-defined weight and shape in accordance to NATO standard STANAG 2920 [3]. Analyzing the test results, Table 1, one can conclude that there is a distinct difference in ballistic resistance between woven fabric composites and unidirectional tape composites although these composites are similar in many ways. Unidirectional tape composites have performed much better than their counterparts based on woven fabric. When a projectile hits a woven fabric a shock or strain wave is introduced which spreads through yarns. The primary impacted yarns interact with other yarns by means of couplings at the cross-over points of the fabric. The strain wave can thus spread over a large number of yarns. The positive effect of this mechanism is that energy will be absorbed over a relatively large area. The velocity of the strain wave and of the energy dissipation is directly related to the modulus of fibers [3,4]. The disadvantage of a woven fabric is that the cross-over points reflect part of strain waves and somehow hamper the propagation of the wave, Figure. The cross-over points can be seen as fixed ends. At fixed ends the amplitude of the reflected wave has the same direction as the amplitude of the original strain wave and must therefore be superposed. Thus, a large number of strain waves, travelling in both directions, are introduced into the yarn. The resulting effect is that the elongation in the yarn can reach its maximum, the elongation-at-break, and the projectile can perforate the first few layers. So the effect of cross-over points in fabrics is not always positive. This was the reason for the development of UD materials. In UD material the fibers are laid unidirectional, bonded with a thermoplastic matrix and then crossplied, Figure 1. In this unidirectional construction the yarns have no real cross-over points as in woven fabric. There are cross-over points only between the different layers, Figure 4, but not within a single layer. There is, definitely, an interaction between the cross-plied layers of fibers, but the part of the strain wave that is reflected is much smaller [4-6]. Thus, in UD composites, because of the lack of cross-over points, the strain wave can travel unhampered at a greater distance from the impact point and engage greater surface i.e. mass of the composite in stopping the projectile. This means that the kinetic energy of the projectile will be absorbed over a larger area compared to fabric composites, which results in better ballistic performance by UD composites.

- [1] Silva, M., et al., 2008, "Numerical simulation of ballistic impact on composite laminates", International Journal of Impact Engineering, 31, pp. 289-306.
- [2] Tabiei, A. and Nilakantan, G., 2009, "Ballistic impact of dry woven fabric composites: a review", Applied Mechanical Reviews, 61, pp.115-128.
- [3] NATO Standardization Agency, STANAG 2920-"Ballistic test method for personal armor materials and combat clothing", edition 31 July 2003.
- [4] Gruicic, \dot{M} ., et al, 2013, "A simple model for the prediction of the ballistic limit in thick-section composite laminate", IJERP, 2(2), pp. 84 92.
- [5] Jacobs, M. J. N. and Van Dingenen J. L. J., 2001, "Ballistic Protection Mechanisms in Personal Armour, Journal of Materials Science", 36 (13), pp. 3137-3142.
- [6] X.S. Zeng, X.S., Shim, V.P.W., Tan, V.B.C., 2005, "Influence of boundary conditions on the ballistic performance of high-strength fabric targets", Int. Journal of Impact Engineering, 32 (1-4), pp. 631-642.

Response of sandwich structure containing aluminum honeycomb to the contact explosion

N. Chikhradze, 1, 2* E. Mataradze, 1 and I. Akhvlediani 1

LEPL Grigol Tsulukidze Mining Institute, E. Mindeli Str. #7, 0186, Tbilisi, Georgia
 Georgian Technical University, Kostava Str. #77, 0160, Tbilisi, Georgia
 *e-mail: chikhradze@mining.org.ge

Abstract: A contact explosion occurs when an explosive device detonates on the surface of an object, such as a building, tank, or vehicle, maximizing the explosive impact on a specific target. Therefore, search methods and materials for protection from contact explosions are the actual [1-5]. This paper presents the results of experimental studies of the explosion resistance of a sandwich panel containing steel plates with an aluminum honeycomb intermediate layer. The processes of deformation and destruction of sandwiches during the contact explosion of hexogen charges weighing 5-75 grams were recorded by a video camera at a frequency of 16,000 frames per second. The testing results showed that explosion resistance of a sandwich with a 10 mm thick aluminum honeycomb layer increases by 1.8 times, and with a 30 mm thick layer - by 3 times.

1. Experimental Setup

A series of tests were carried out using the experimental stand, which was a frame made of I-beams. An experimental sandwich panel, measuring 50cmx50cm, was firmly attached to the stand (Figure 1). The tested sandwich panels consisted of two steel plates, one of which was 2 mm thick and another, 3 mm thick; between them was located a 10mm thick aluminum honeycomb layer in one case and a 30mm thick honeycomb layer, in another. For comparison, a two-layer structure made up of two steel plates, one of which was 2 mm and another 3 mm thick, without a protective layer, was tested at a separate stage of the experiments. In both cases, a 2 mm thick steel plate was installed on the blast side. The steel plate had the following properties: density - 7850kg/m³, elastic modulus - 2100,00 MPa, yield stress - 235 MPa, Poisson's ratio - 0.3. The aluminum honeycomb plate consists of 0.8 mm thick aluminum skins (bottom, top), while the core is made up of aluminum honeycombs with hexagonal cells. Panel weight is 6.7-7.7 kg/m², compressive stabilized strength – 2.9 MPa and skin elastic modulus – 68 MPa.



Figure 1. Testing scheme and photo of the stand

During the explosion, deformations of the plates were recorded using a high-speed MIKROTRON Motion video camera. The recording speed at the experiments was 12,000 frames/second. After each explosion, the residual deflection of the plates was measured and the destruction characteristics were visually recorded. The experiments used a cylindrical charge of hexogen with a diameter of 3cm, a bulk density of 1.1 g/cm3 and a detonation velocity of 5800 m/s. The charge was located in the center of the test plate in a paper bag. At different stages of experiments, the mass of the charge varied from 5gr to 75gr. In total, 24 experimental explosions were carried out. The overpressure impulse at the contact surface between the charge and the steel plate is determined according to Baum and Stanyukovich [5].

2. THE TIME RESPONSE OF PANELS

2.1. Response characteristics of steel plates without an aluminum honeycomb layer

Figure 2. presents video frames captured at different time intervals after detonation Based on video recordings, the explosion impact process on the plates developed as follows: $t=36 \mu s$ after detonation: The appearance of craters in both plates; $t=72 \mu s$ after detonation: A crack appears in the upper plate, and the crater on the blast-

side plate expands; $t=468~\mu s$ after detonation: A through-hole forms in both plates; $t=624~\mu s$ after detonation: The through-hole enlarges, and fragments are ejected; $t=780~\mu s$ after detonation: The final stage of deformation and rupture is completed.

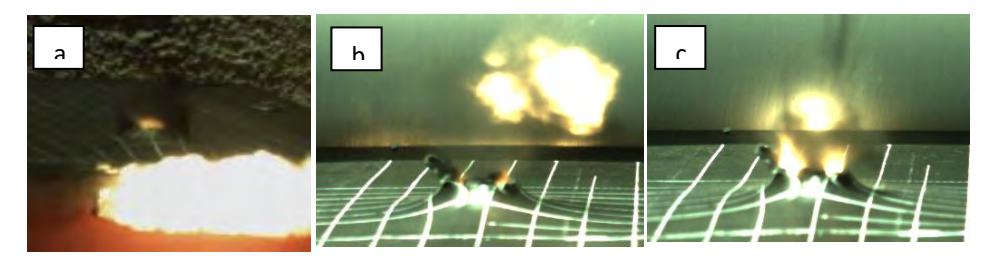


Figure 2. Video frames of the steel plates at different points in time after detonation: a) Crack formation and gas emission (72 μs after the moment of detonation); b) Through hole formation (468 μs after the moment of detonation); c) The ejection of fragments (624μs after the moment of detonation

2.2 Response characteristics of sandwich panels with an aluminum honeycomb layer.

The sequence of deformation and failure in the sandwich panel differs from that of steel plates. In steel plates, cracks initially appear on the side opposite the explosion, whereas in the sandwich panel, they first form on the plate facing the explosion. Additionally, the time required for crack formation and hole development in the sandwich panel was 2.0 to 2.2 times longer compared to steel plates (Figure 3).

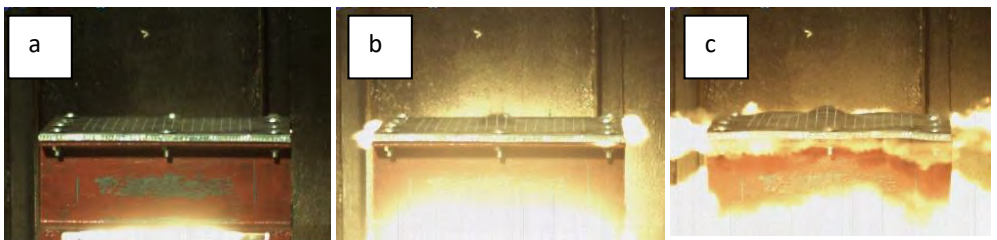


Figure 3. Video frames of the sandwich panel with an aluminum honeycomb layer at different time points after detonation: a) Before detonation; b) Crater formation (79 μs after detonation); c) Through-hole formation (1027μs after detonation)

CONCLUSIONS

- 1. Four modes of deformation and failure were identified for sandwich panels with an aluminum honeycomb layer under contact explosion: I. Residual bending, with all three layers remaining intact; II. Residual bending, with destruction (burnout) of the aluminum honeycomb layer, while both steel plates remain intact; III. Destruction of the steel plate on the explosion side and failure of the honeycomb layer, while the steel plate on the opposite side remains functional; IV: Complete failure of all three layers.
- 2. The explosion resistance of the sandwich panel is determined by the minimum charge mass and overpressure impulse required to cause local rupture and through-hole formation. For sandwich panel with a 20 mm thick honeycomb, the critical charge mass and impulse were 45 grams and 210 kPa·ms, respectively. For the panel with a 30 mm thick honeycomb layer, these values increased to 75 grams and 275 kPa·ms, respectively.
- 3. The time required for crack formation and hole development in the sandwich panel was 2.0 to 2.2 times longer compared to steel plates. In steel plates, cracks initially appear on the side opposite the explosion, whereas in the sandwich panel, they first form on the plate facing the explosion.

- [1] Ma Q, Rejab M, Siregar J, Guan Z. A review of the recent trends on core structures and impact response of sandwich panels. *Journal of Composite Materials*. 2021;55(18):2513-2555. doi:10.1177/0021998321990734
- [2] <u>Hampson P, Moatamedi M. A review of composite structures subjected to dynamic loading. International Journal of Crashworthiness</u>, 2007. DOI: <u>10.1080/13588260701483334</u>
- [3] Jinglin Xu, Jianqing Liu, Wenbin Gu, Xin Liu, and Tao Cao. Shock Wave Attenuation Characteristics of Aluminum Foam Sandwich Panels Subjected to Blast Loading. Shock and Vibration. Volume 2018
- [4] Feng Zhu, Zhihua Wang, Guoxing Lu. The impulsive response of aluminium foam core structures. Int. J. Materials Engineering Innovation, Vol. 1, No. 2, 2009
- [5] Yanghua He et all. The Damage to Thick Steel Plates by Local Contact Explosions. Materials 2023, 16(8), 2966; https://doi.org/10.3390/ma16082966
- [6] Baum F., Stanyukovich, K., Shekhter B. The Physics of Explosion. 1959

Elastomer composites with hybrid carbon fillers

Tuba Evgin,¹ Matej Micusik,^{2,*} Hamed Peidayesh,² Halil Dogacan Koca,³ Alpaslan Turgut,¹ Miroslav Slouf,⁴ Ivan Chodak.²

¹Engineering, Mechanical Engineering Department, Dokuz Eylul University, Izmir, Turkey
² Polymer Institute SAS, Bratislava, Slovakia

³The Graduate School of Natural and Applied Sciences, Mechanical Engineering Department, Dokuz Eylul University, Izmir, Turkey

⁴Institute of Macromolecular Chemistry CAS, Prague, Czech Republic

* matej.micusik@savba.sk

Abstract: Elastomer nanocomposites with three various types of multiwall carbon nanotubes (MWCNTs) were fabricated to investigate the size effect of MWCNTs on the morphological, electrical, thermal, mechanical, and viscoelastic properties, as well as swelling ratio and crosslinking density. Second part of this study was the evaluation of the synergic effect between graphene nanoplatelets (GnPs) and MWCNTs. This synergistic effect is mainly related to the complementary shape of 2D GnPs and 1D MWCNTs forming 3D structure.

Main Text

Elastomer matrices as ethylene propylene diene monomer (EPDM) are of high interest due to its superiorultraviolet, fatigue, moisture, heat, cold, hot tear, oxygen, and weather resistance, cost-effective, good extendibility, low-temperature properties because of its saturated and non-polar backbone. The addition of conductive fillers, such as carbon-based materials as carbon nanotubes makes EPDM electrically conductive to use in microwave absorption, conductive gaskets, EMI shielding, etc. [1]. In addition the mechanical properties are of high importance, because it may influence a manufactured part's effectiveness life. EPDM nanocomposites with three various types of multiwall carbon nanotubes (MWCNTs) were fabricated to investigate the size effect of MWCNTs on the morphological, electrical, thermal, mechanical, and viscoelastic properties, as well as swelling ratio and crosslinking density. MWCNTs enhance electrical, thermal, mechanical, and viscoelastic properties regardless of MWCNT size. The MWCNT size is vital in determining percolation thresholds and thermal conductivity; however, it considerably influences the electrical conductivity in only the percolation threshold region (2–10 phr). The diameter of MWCNTs is a more regulating factor for nanocomposites' electrical properties than length. The EPDM nanocomposites, including MWCNTs with a longer length, low diameter, and higher specific surface area (SSA), show a better thermal conductivity enhancement (95%) due to forming more easily thermally conductive networks. The size of MWCNTs is a negligible key factor for mechanical and viscoelastic properties [2].

Second part of this study was the evaluation of the synergic effect between graphene nanoplatelets (GnPs) and MWCNTs. The synergistic effect is mainly related to the complementary shape of 2D GnPs and 1D MWCNTs forming 3D structure. We used two types of GnPs with different SSA and two MWCNT with different aspect ratios. GnPs with higher SSA show better compatibility and adhesion between GnPs and MWCNTs or EPDM matrix, resulting in better results in the electrical conductivity of samples.

References

[1] A. A. Athawale and A. M. Joshi, "Electronic Applications of Ethylene Propylene Diene Monomer Rubber and Its Composites," in, eds. D. Ponnamma, K. K. Sadasivuni, C. Wan, S. Thomas, and M. A.-A. Al-Ma'adeed (Cham: Springer International Publishing, 2016), 305–333.

[2] Tuba Evgin, Matej Micusik, Halil Dogacan Koca, Hamed Peidayesh, , Alpaslan Turgut, Miroslav Slouf, Ivan Chodak. "Evolution of Morphological, Electrical, Thermal, and Mechanical Properties of Elastomer Nanocomposites With Different Sizes of MWCNTs" J Appl Pol Sci, 2025; 142:e56628.

Acknowledgement

This research was partially funded by the Slovak agency VEGA grant number 02/006/22. The authors would like to acknowledge the contribution of the COST Action CA21155 (HISTRATE).

Thermo-reversible Diels-Alder polyurethane adhesives for sustainable composite bonding Ana C. Restrepo-Montoya^{1*}, Katrien V. Bernaerts², Ainara Saralegi¹, Arantxa Eceiza¹,

Abstract:

This study investigates a reprocessable polyurethane as adhesive designed to address industrial materials selection challenges. By integrating thermo-reversible Diels-Alder adducts, the study enables the creation of composites with on-demand debonding and reshaping capabilities (Figure 1)[1]. This innovation demonstrates potential benefits in emissions reduction. The synthesized adhesive exhibits flexural moduli ranging from 1 to 2 GPa, with 60-80% modulus recovery observed post-reprocessing. This characteristic provides a pathway to meet application of the adhesive in wood, metal, and plastic composites, serving as a practical use case, highlighting the potential of sustainable, high-performance materials to enlighten industrial materials selection[2].

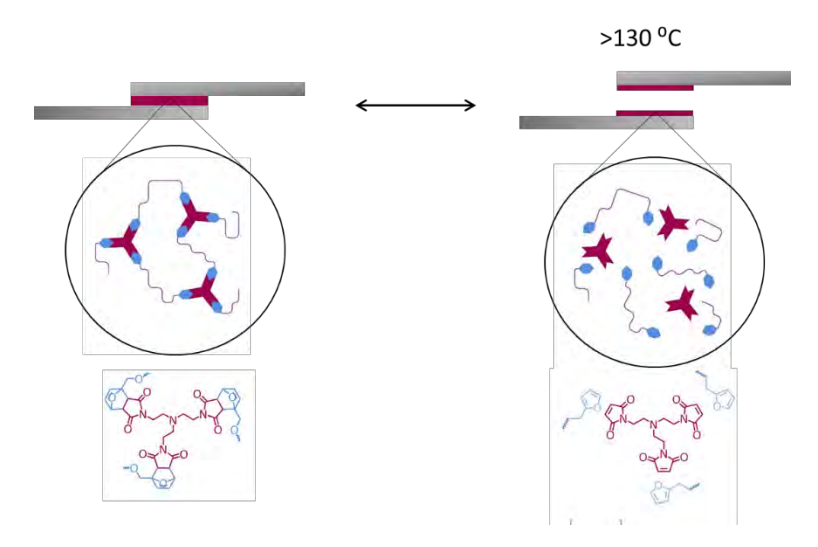


Figure 1 Scheme of the bonding-debonding test of polyurethane adhesive with dynamic bonds.

- [1] A. C. Restrepo-Montoya, I. Larraza, O. Echeverria-Altuna, I. Harismendy, A. Saralegi, and A. Eceiza, "Emerging Reprocessable and Recyclable Biobased Cross-Linked Polyurethanes Through Diels-Alder Chemistry," *ACS Appl. Polym. Mater.*, pp. 0–11, 2023, doi: 10.1021/acsapm.3c03070.
- [2] J. Liu, A. Pich, and K. V. Bernaerts, "Preparation of lignin-based vinylogous urethane vitrimer materials and their potential use as on-demand removable adhesives," *Green Chem.*, vol. 26, no. 3, pp. 1414–1429, 2023, doi: 10.1039/d3gc02799f.

¹ Group 'Materials + Technologies', Department of Chemical and Environmental Engineering, Faculty of Engineering of Gipuzkoa, University of the Basque Country UPV/EHU, Plaza Europa 1, Donostia-San Sebastian 20018, Spain.

²Maastricht University, Faculty of Science and Engineering, Aachen-Maastricht Institute for Biobased Materials (AMIBM), Sustainable Polymer Synthesis Group, Brightlands Chemelot Campus, Urmonderbaan 22, 6167 RD Geleen, the Netherlands

NEW COMPOSITE MATERIALS WITH ENHANCED MECHANICAL PROPERTIES

Jadranka Blazhevska-Gilev*, Marija Prosheva

Faculty of Technology and Metallurgy, Ss. Cyril and Methodius University in Skopje, 1000 Skopje, R.of N.Macedonia

* jadranka@tmf.ukim.edu.mk

Abstract: The study of the effect of the type of hybrid CNT/graphenic filler, either G or rGO, on the properties and performance of polymer composites, which were synthesized by in-situ miniemulsion polymerization, showed that G/CNT(graphene/carbon nanotubes)-based composites exhibited improved film morphology due to better filler distribution and a more organized film structure than that of rGO/CNT composites. Consequently, the G/CNT/polymer composites presented an order of magnitude increased Young's moduli. The water resistance as well was much better than that of rGO/CNT based composites, especially for 10:1 ratio of the G/CNT, which presented 60% lower water absorption than neat polymer. The water resistance of both type of the composites was compromised probably due to the presence of hydrophilic functional groups that facilitated water diffusion into the film.

1. Experimental part

G/CNT hybrids and rGO/CNT hybrids in three different weight ratios (G:CNT of 10:1; 1:1; and 1:10) respectively (rGO:CNT of 10:1, 1:1, and 1:10) were prepared by by sonication under continuous stirring with magnetic stirrer of 200 rpm. The resulting G/CNT hybrids were dispersed in water using sodium dodecyl sulfate as a surfactant. In order to obtain reduced graphene oxide, the GO/CNT hybrids were subjected to reduction with PVP. Then ascorbic acid was added with the ratio of solids to reductant of 5:1. After the reduction, all three samples were subjected do dialysis to remove the excess of PVP. Two series of composites were synthetized by in-situ miniemulsion, one of them based on 1 wt% of the G/CNT hybrids, and the other based on 1 wt% of the rGO/CNT hybrids.

The mechanical properties of the composites were determined by tensile testing, following ASTM D3039. The tensile testing was carried out with a TA.HD plus texture analyzer (Stable Micro Systems Ltd., Godalming, UK). Using Microsoft Excel functions, Young's modulus and Offset Yield were estimated.

The water uptake of the neat polymer and the composites was investigated following ASTM D570-98.

1. Results and Discussions

In order to investigate the influence of G/CNT and rGO/CNT filler on the mechanical properties of the polymer based composites films, tensile measurements were performed, including the neat polymer film, synthesized under the same conditions as the composites. The stress-strain curves for the neat polymer and the various composites are presented in Figure 1.

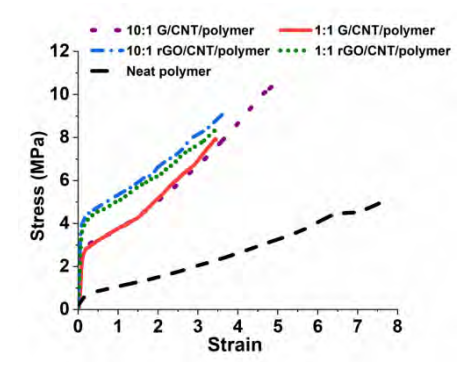


Fig.1 Stress-strain behavior of the neat polymer and different composite films.

Table 1 shows the modulus and other mechanical properties. By adding a small amount (1 wt%) of hybrid filler, much stronger composites were produced. The Young's moduli of the G/CNT polymer composites improved fivefold, while the same amount of rGO/CNT hybrid resulted in one order of magnitude higher moduli. This difference is likely a result of the compatibility between the hybrid filler and the polymer matrix. The presence of residual oxygen functional groups on rGO physically and chemically interacted with the polymer matrix, as we demonstrated previously, even introducing covalent crosslinking [1]. On the other hand, this crosslinking reduces the mobility of the filler in the matrix.

	1 ,		
Sample	Stress at	Young's	Offset Yield
Sample	break [MPa]	modulus [MPa]	stress [MPa]
Neat polymer	4.93	0.010	0.51
10:1 G/MWCNT/polymer	10.54	0.0557	2.32
1:1 G/MWCNT/polymer	7.93	0.0405	2.27
10:1 rGO/MWCNT/polymer	9.15	0.11	3.32
1:1 rGO/MWCNT/polymer	8.44	0.09	3.18

Table 1. Mechanical properties of the neat polymer and different composite films

It is worth mentioning that the 10:1 G/CNT/polymer composites present a very high elongation at break. Although the composites are less flexible than the neat polymer as shown in Figure 1, the flexibility lost is negligible for this composite, considering the much higher moduli. The much higher value of the Young's moduli of the composites compared to the neat polymer suggests that the hybrid effectively restricts the movement of the polymer chains making the samples less flexible as well as the stress is efficiently transferred from the polymer matrix to the filler. The neutralized strain of the composites is 4.5 times higher than the neat polymer for G/CNT samples and 6 times higher for rGO/CNT samples. This means that the composites will undergo permanent deformation at higher stress. In general, a higher Young's modulus and offset yield stress suggest that the material will be durable and more resistant to applied mechanical stress. The strengthening effect of the carbon nanomaterial incorporated into the polymer matrix is due to the high ratio of carbon nanomaterials that allows for efficient stress transfer from the polymer matrix to the carbon nanomaterials that are known for their excellent mechanical properties. The efficient stress transfer is related to the distribution of the filler as well as its chemical characteristics. In this regard, the good dispersion of the 10:1 G/CNT hybrid throughout the polymer matrix improves the stress distribution leading to this composite having better properties than the 1:1 G/CNT composite, where agglomeration of the filler was observed. In the case of the rGO/CNT/polymer composites, it can be seen that these sample materials have better mechanical properties compared to the G/CNT/polymer. This is due to the fact that the rGO structure contains defects as well as oxygen functional groups that increase the compatibility of the filler with the polymer. The improved compatibility results in the formation of stronger interactions between the two phases and a consequent improvement in stress transfer. Along with high mechanical resistance, low sensitivity to humidity and water is an important property that can determine the application of polymer composites. It was evaluated by immersing the composite film in water and following the change in weight, which resulted in water uptake by the film. Figure 2 shows the results of measuring the water uptake, i.e. the change in weight in relation to the immersion time.

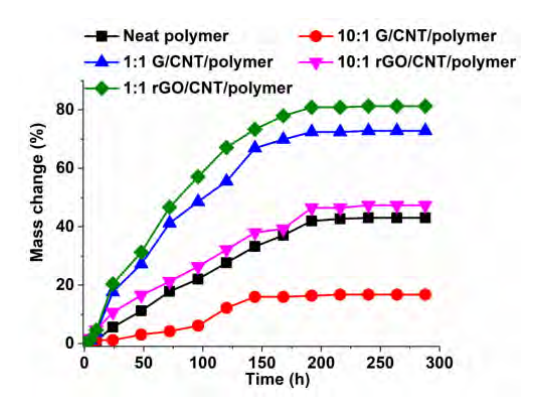


Fig. 2 Mass change (%) in relation to the immersion time for the neat polymer and the different composite films.

As shown in Figure 2, all the compounds present increased water uptake compared to the neat polymer, except for the 10:1 G/CNT based composite. These results are quite surprising. In water films, due to the presence of surfactant and hydrophilic moieties of the initiator, water uptake is usually high, as can be seen for the neat polymer which presents 40% water absorption in 300 h. It was expected that the fillers would introduce a kind of barrier to water diffusion, even in the case of the rGO-based hybrid. However, the present results show that the water absorption of the composite films is higher, indicating the presence of hydrophilic pathways or networks that facilitate water diffusion. This could be on the one hand due to the high presence of hydrophilic oxygen groups in the case of rGO, and on the other hand due to irregularities in the film formation resulting from the formation of various microcracks as the water evaporates. To examine the reduction in water uptake in

the case of 10:1 G/CNT/polymer composites compared to neat polymer, the weight change (%) of neat polymer and 10:1 G/CNT/polymer was compared in Table 2.

Tab.2 Reduction of water uptake for 10:1 G/CNT/polymer compared to the neat polymer.

Immersion time (h)	48	96	144	192	240
Reduction of water uptake (%)	72	72	52	61	61

The results show that the incorporation of 1 wt% 10:1 G/CNT hybrid filler into the polymer matrix significantly reduced water uptake within the first 100 hours of the aging process, as the reduction in water uptake was slightly more than 72%. Before the saturation stage for both samples, the reduction in water uptake was reduced to 51%-61%. Under saturated conditions, the water uptake reduction was 61%. Most likely, the good distribution of the 10:1 G/CNT hybrid throughout the polymer matrix, contributes to the filler acting as a barrier that prevents water from penetrating the material, while at the same time contributing to the formation of a quality film during water evaporation. The 10:1 G/CNT/polymer composite was previously reported to possess radical scavenging character, thus introducing it into a (meth)acrylic polymer film enhances its photostability [2]. This characteristic combined with improved mechanical resistance and reduced water absorption make this composite a promising material for future application as a protective coating for outdoor use.

2. Conclusion

In this work, a facile and rapid method for the synthesis of G/CNTs and rGO/CNT-based aqueous polymer composites is presented. The main objective of the work was to compare different types of graphene G and rGO and to study their influence on the properties and performance of the obtained aqueous polymer composite.

As a consequence of such structures, G/CNT-based composites presented improved mechanical properties and an order of magnitude higher Young's moduli, without a significant decrease in elongation at break. The obtained results show that miniemulsion polymerization is an excellent method of choice for the in situ synthesis of aqueous polymer composites. According to the mechanical performance, as well as the reduced water absorption, it can be concluded that these films have great potential to be used as protective coatings.

- [1] Kim J-Y, Kim TY, Suk JW, et al. Enhanced dielectric performance in polymer composite films with carbon nanotube reduced graphene oxide hybrid filler. Small. 2014;10:3405-3411.
- [2] Prosheva M, Aboudzadeh MA, Leal GP, Blazevska Gilev J, Tomovska R. High-performance UV protective waterborne polymer coatings based on hybrid graphene/carbon nanotube radicals scavenging filler. Part Part Syst Charact. 2019;36:1800555.

Thermomechanical Properties of Electrospun Polyacrylonitrile Nanofibers with Embedded Magnetic Nanoparticles in a Magnetic Field

A.Sezai Sarac *

Istanbul Technical University, Polymer Science & Technology, 34469 Maslak, Istanbul, Turkey
* sarac@itu.edu.tr

Abstract: In this study fabrication, thermomechanical deformation, and characterization of polyacrylonitrile composite nanofibers incorporating magnetic metal oxide nanoparticles are performed. Electrospinning was utilized to generate nanofibrous structures with homogeneously dispersed nanoparticles. Dynamic mechanical analysis under applied magnetic fields demonstrated substantial enhancements in the composite properties, particularly around the glass transition temperature

1. Experimental

Polyacrylonitrile (PAN, average Mw 150 000), N,N0-dimethylformamide(DMF \$ 99.8%) were obtained from Sigma Aldrich. Iron oxide nanopowder (γ -Fe2O3, 99.9%, 10 nm average diameter, near spherical) and MnZn ferrite (MnZnFe₂O₄, 99.99%, size diameter 28 nm, near-spherical) nanoparticles were obtained from US Research Nanomaterials. The electrospinning setup included a grounded collector placed within a syringe, a high voltage direct current (DC) power source capable of producing positive DC voltage up to 50 kV and a syringe pump with a feeding rate ranging from 5.5 mL h⁻¹ to 400 mL h⁻¹. Dynamic mechanical analysis (DMA) experiments were performed using PerkinElmer DMA-8000 in the temperature range 300 K–800 K with a heating rate of 5 K min–1 and measured in tension mode at different frequencies with the applied sinusoidal force of 0.5, 5 and 15 Hz.

The morphological characteristics and chemical composition analysis of the produced nanofibers were examined by scanning electron microscopy (SEM) and integrated energy-dispersive X-ray (EDX) analysis, respectively. Surface features were investigated on a Hitachi S-4800 SEM at 2 kV acceleration voltage on samples coated with Au/Pd (5 nm) using secondary electron (SE) mode

2. Results and Discussions

Electrospinning leverages electrostatic forces to produce micro- and nanofibers from polymeric solutions [1,2]. This versatile technique facilitates the creation of diverse fibrous architectures. The high porosity and substantial specific surface area of electrospun nanomaterials render them ideal candidates for a wide array of nanotechnological applications, including filtration, biotechnology, sensing, energy storage, and catalysis.

Electrospun polyacrylonitrile composite nanofibers incorporating metal nanoparticles are exhibited enhanced thermomechanical properties. Dynamic mechanical analysis reveals significant increases in stiffness and shifts in glass transition temperatures in the composites compared to the pristine polymer (Fig.1). These modifications are attributed to strong interfacial interactions between the nanoparticles and the cyano groups of polymer matrix, resulting in altered polymer chain dynamics. High-resolution scanning electron microscopy (HRSEM), X-ray diffraction (XRD), spectroscopic techniques (FTIR, Raman, XPS), and thermomechanical data collectively elucidate the mechanisms of interaction between the nanoparticles and the polymer matrix, confirming the uniform dispersion of nanoparticles and providing insights into the underlying mechanisms [3].

MnZn ferrite shows a greater shift in glass transition temperature (Tg) compared to Fe_2O_3 because it interacts more strongly with the applied magnetic field. This stronger interaction is due to MnZn ferrite's higher magnetic permeability and lower coercivity. These properties arise from its complex spinel structure and the presence of Mn^{2+} ions, which promote stronger magnetic coupling than the Fe^{2+}/Fe^{3+} interactions in the simpler structure of Fe_2O_3 . Fe_2O_3 's lower permeability and susceptibility result in a minimal shift in Tg, as it interacts weakly with the magnetic field.

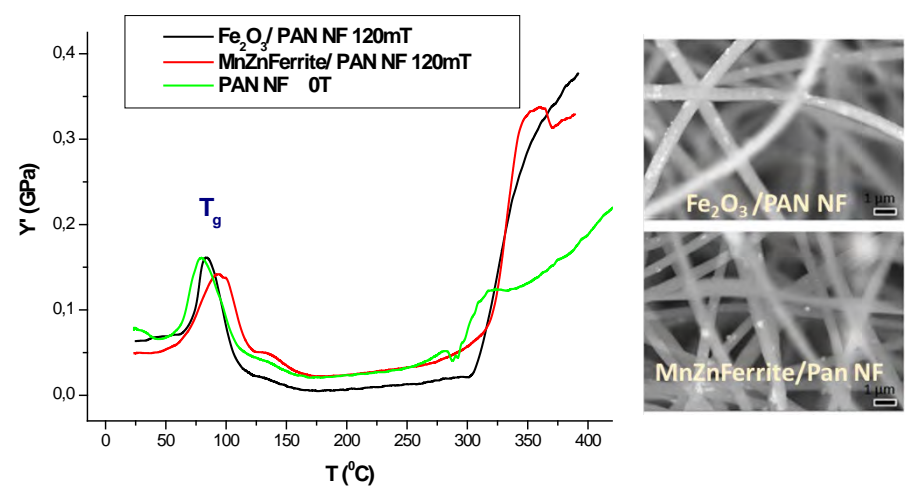


Fig.1.Thermomechanical and morphological results of composite nanofibers (Reproduced from Ref.[3] with permission from the Royal Society of Chemistry)

2 Conclusions

SEM imaging and EDX mapping indicate NPs are well dispersed in PAN composite nanofibers with minimum bead formation. Fe₂O₃ and MnZn ferrite nanoparticles embedded in the polymer matrix hinder cross-linking throughout the network and enhance the inter-chain interactions. These findings demonstrate the potential of these composites for applications demanding tailored mechanical properties and responsiveness to external stimuli, such as magnetic fields.

References

[1]Huner, K., Sarac, B., Yüce, E., Rezvan, A., Micusik, M., Omastova, M., Eckert, J., Sarac, A.S., Mol. Syst. Des. Eng., 8, 2023, pp. 394-406

[2] Nanofibers of Conjugated Polymers. A.S.Sarac, 2016, 1st ed. Jenny Stanford Publishing, Singapore

[3] Sarac, B., Soprunyuk, V., Herwig, G., Gumrukcu, S., Kaplan, E., Yüce, E., Schranz, W., Eckert, J., Boesel, L., and Sarac, A.S., Nanoscale Adv., 6, 2024, 6184-6195

Impact Localization in a CFRP Plate with unknown Material Properties

Rohan Soman, 1,* Tim Baetzel, 2 Andreas Hornig^{2,3,4} and Maik Gude²

¹ Institute of Fluid Flow Machinery, Polish Academy of Sciences, Gdansk, Poland

² Institute of Lightweight Engineering and Polymer Technology (ILK), Technische Universität Dresden, Dresden, Germany

⁴Department of Engineering Science, University of Oxford, Parks Road, Oxford OX1 3PJ, United Kingdom

*rsoman@imp.gda.pl

Summary: Impact detection and localization remain very important aspects of the structural health monitoring system especially for composite structures. Composite structures typically have low damage tolerance and an impact may lead to barely visible or internal damage not visible in ordinary visual inspections. Hence a system that is able to detect and localize impact is invaluable for non-destructive testing inspectors. Such a system allows inspection of only the identified region which reduces downtime and inspection costs. Several techniques have been developed for impact detection. The problem with the localization is that most techniques depend on the time of arrival of the impact-induced waves and need information on the velocity of propagation of those waves for localization which is a challenge in an anisotropic composite. Furthermore, due to the structural complexity of the component, the velocity of propagation is not constant and it changes based on the ambient conditions. Hence, this work deploys a specially designed network which allows impact localization without knowing the velocity of propagation and in-turn without knowing the material properties. The work is carried out on carbon fiber-reinforced polymer composite subjected to hammer impacts.

1. Introduction

Structural health monitoring (SHM) is of significant interest to infrastructure owners as it reduces the lifecycle cost of structures. An important aspect of the SHM system is the ability to detect and localize impacts. Impacts are a common occurrence in the aerospace industry stemming from tool drop during maintenance or hail strikes. There are two key challenges in the detection and localization of impact events. Firstly, the determination of the exact time of arrival (TOA) of the acoustic waves is a challenge. Several techniques based on the amplitude as well as the frequency content of the waves have been identified, but this aspect continues to be a challenge [1]. The second challenge, even if the time of arrival of the wave is determined accurately, is transforming this information for localization needs the accurate information of the velocity of the propagation of the wave. This wave velocity is a function of the material of the structure, the thickness, as well as the ambient conditions. Most composite structures have orthotropic properties and the wave velocity is affected by the material properties in different directions. Thus it is an extremely difficult task to convert the TOA information to the space domain for localization. This work employs a novel strategy for impact localization using two L-shaped arrangements of the piezo-transducers [2]. Impact localization is achieved without knowing the velocity of propagation of the acoustic wave or the material properties. The method is applied for impact localization in a carbon fiber reinforced polymer plate (CFRP) with known geometry but unknown material properties.

2. Experimental Setup and Methodology

For the impact study, a CFRP plate with dimensions $300 \times 150 \times 6$ mm³ was instrumented with six PZT sensors as shown in Fig 1. Ten impacts were introduced at the marked locations with a hammer. The impact forces were not measured, as in real in-service conditions the impact energy is not known. The CFRP plate was clamped at one end (cantilever). The data was collected using an oscilloscope. The time of arrival (TOA) was estimated based on the Akaike information criterion (AIC) [3]. The AIC was computed using equation 1.

$$AIC(k) = k \ln[var\{U(1:k)\}] + (K - k - 1) \ln[var\{U(k + 1:K)\}]$$
 (1)

where, k is the serial number of sample corresponding to time t, K denotes the total number of collected samples, U is the amplitude of the signal captured, and var indicates the variance of the signal in the given sample/time window. The metric is based on the fact that prior to the arrival of the waves the signal is mostly noise, while after the arrival of the waves there is a sudden change in the frequency content, which can be utilized for TOA determination. Once the TOA is determined the change in the TOA of the sensors is calculated, which may be used for determining the angle of incidence (θ) using equation 2. The θ for both the clusters is determined and their point of intersection is the predicted impact location.

$$\theta = \tan^{-1}(\frac{\Delta t_{13}}{\Delta t_{12}}) \tag{2}$$

³ Center for Scalable Data Analytics and Artificial Intelligence (ScaDS.AI) Dresden/Leipzig, TUD Dresden University of Technology, Dresden, Germany

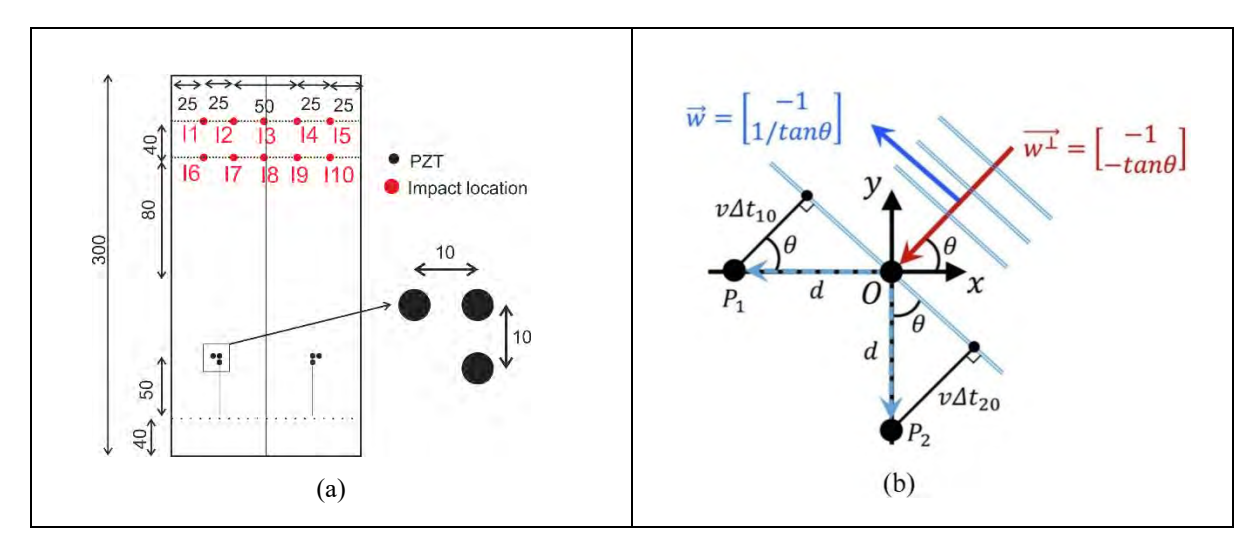


Fig. 1. Setup and methodology a) Schematic of the sample b) Concept for impact localization (from [2])

3. Results

The Fig. 2a shows the AIC plot for the impact 1 case. It can be clearly seen that there is a valley, the minima point is identified as the TOA for each sensor. Based on equation 2, the θ is determined for both sensor clusters and the impact can be located as can be seen in Fig. 2b. Similar results were also obtained for the other impact locations.

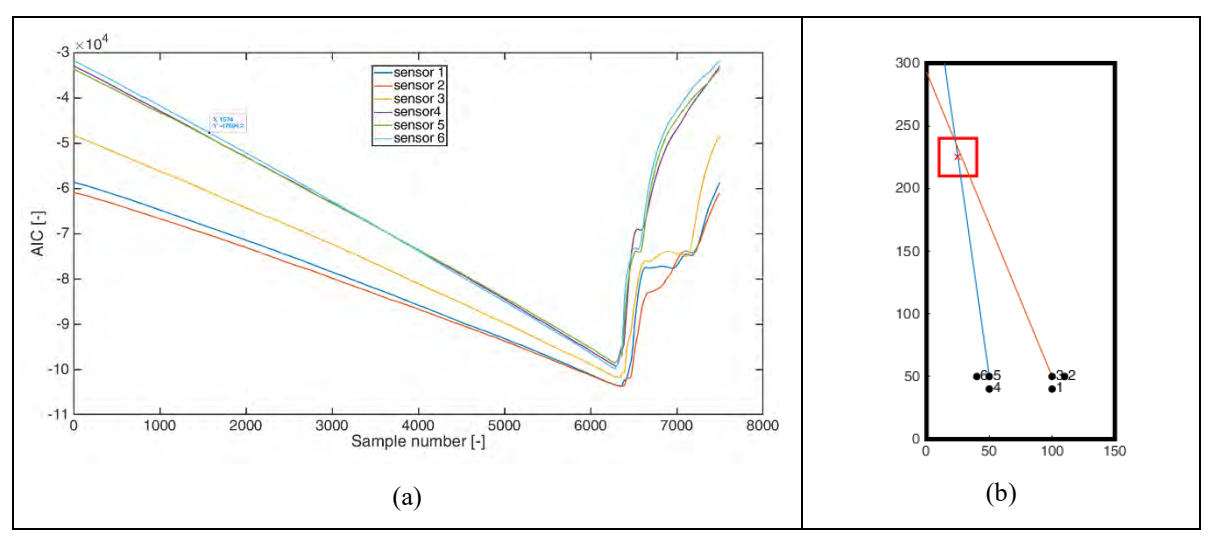


Fig. 2. Results for localization of impact a) AIC for all sensors b) Localization using eq 2.

4. Conclusions

As shown in Fig. 2b, the impact location was accurately localized without knowing the velocity of wave propagation or the material properties. The applicability of this method for different sensor systems will be investigated in the future.

References

- [1] Capineri, L., & Bulletti, A. (2021). Ultrasonic guided-waves sensors and integrated structural health monitoring systems for impact detection and localization: A review. Sensors, 21(9), 2929.
- [2] Ma, C., Zhou, Z., Liu, J., Cui, Z., & Kundu, T. (2023). Acoustic source localization using L-shaped sensor clusters: A review. Ultrasonics, 132, 107020.
- [3] Sen, N., Gawroński, M., Packo, P., Uhl, T., & Kundu, T. (2021). Square-shaped sensor clusters for acoustic source localization in anisotropic plates by wave front shape-based approach. Mechanical Systems and Signal Processing, 153, 107489.

Acknowledgements

Dr Rohan Soman acknowledges the funding support of National Science Center, Poland, grant number: 2020/39/D/ST8/00188. The collaboration was made possible through the STSM funded by the COST Action CA21155 (HISTRATE).

Delamination detection in complex composite laminates using guided wave mode conversion tracking

Kai Zhu, ¹ Tomasz Wandowski, ¹ and Maciej Radzieński ^{1,*}

¹ Institute of Fluid-Flow Machinery Polish Academy of Sciences, Fiszera 14 St, Gdansk, 80-231, POLAND

* maciej.radzienski@imp.gda.pl

Abstract: Guided waves are highly sensitive to discontinuities such as delaminations in composite materials and are widely applied in structural health monitoring. In the proposed approach, the antisymmetric mode, which converted from the symmetric mode upon encountering damage, is tracked and fused to characterize the damage. The methodology consists of three key steps: mode filtering, precise mode tracking employing a velocity-based tracking mask, and damage feature fusion through root mean square integration. Experimental validation on a stiffened glass fiber reinforced polymer plate successfully identifies multiple delamination regions, demonstrating the effectiveness of proposed method in accurately detecting and locating structural damage.

1. Introduction

Composite laminates are widely used due to their high strength-to-weight ratio and corrosion resistance [1]. However, these materials are prone to damage, making efficient non-destructive testing (NDT) methods essential. Among various NDT approaches, guided wave inspection has proven effective for detecting damage in composite laminates. It is particularly advantageous in critical applications due to its ability to propagate over long distances with minimal energy loss and its high sensitivity to changes in material properties.

Compared to traditional single-point measurements [2], full-wavefield data provides more comprehensive information about wave patterns and anomalies caused by structural damage. Recent literature highlights significant advancements in damage imaging methods utilizing full-wavefield data. Notably, the guided wave mode conversion technique offers higher contrast and clearer edge detection without requiring reference data or prior knowledge of material properties [3]. However, this technique faces significant challenges related to local mode coupling, thus requiring more precise modal tracking methods.

To address these issues, an improved Guided Wave Mode Conversion Tracking (GW-MCT) method is proposed.

2. Guided Wave Mode Conversion Tracking

As shown in Fig. 1 (a), when the fastest-propagating S0 mode (solid black line) encounters damage, it converts partially into other wave modes (red dashed line). The guided wave mode conversion tracking (GW-MCT) proposed in this research is schematically illustrated in Fig. 1 and includes three key steps: S0 mode filtering, mode tracking, and damage feature fusion. All time-frequency transformations employed in this paper are based on the three-dimensional Fourier transform.

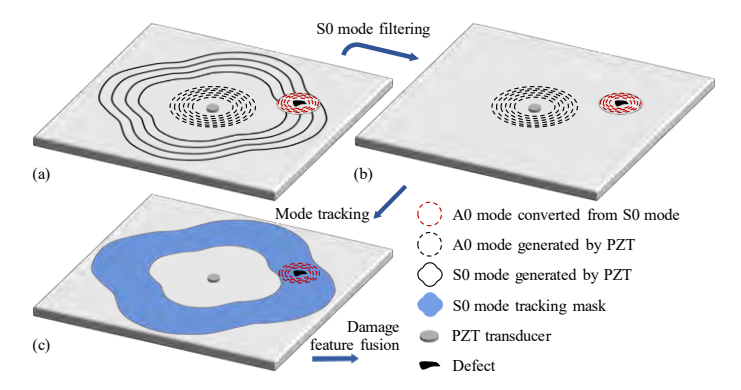


Fig. 1. Schematic representation of GW-MCT: (a) mode conversion behaviour, (b) mode conversion after mode separation, (c) isolated A0 mode from S0 mode conversion.

2.1. S0 Mode Filtering

In the presence of localized damage, the original S0 mode and the damage-induced A0 mode (converted from the S0 mode) may coexist. To effectively extract detailed damage features, a dispersion curve estimation method is adopted as the initial step in the proposed approach, illustrated in Fig. 2. Specifically, as depicted in Fig. 2, the result is obtained by multiplying the data in the wavenumber–frequency domain $V(k_x, k_y, f)$ (Fig. 2 (a)) with the S0 mode filtering mask $w(k_x, k_y, f)$ (Fig. 2 (b)). The filtering mask is defined such that the S0 mode region is assigned a value of 0, while all other regions are set to 1, with Gaussian blur applied to smooth the transition between regions.

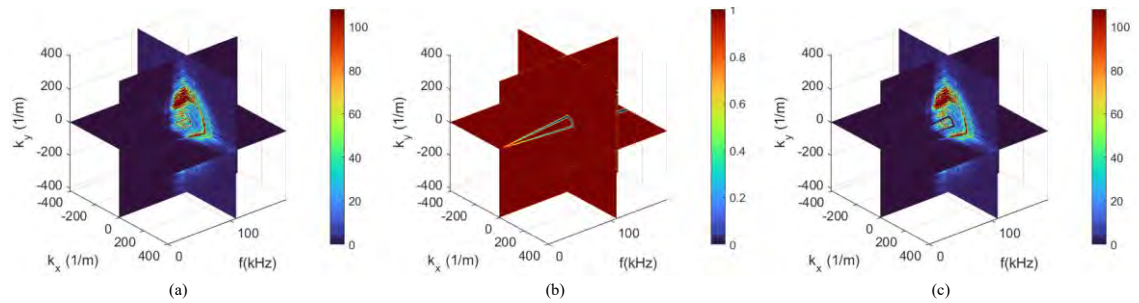


Fig. 2. Wavenumber-frequency domain data and S0 mode filtering mask: (a) experimental data before filtering, (b) S0 mode filter, (c) experimental data after applying the A0 mode filter.

2.2. Mode Tracking

To further enhance the extraction of detailed damage features, a more precise S0 mode tracking mask is proposed. In this method, the velocity $v(\theta)$ of the S0 mode at various angles is obtained using a semi-analytical approach. The tracking mask for the S0 mode is defined as follows:

$$M(d,t) = \begin{cases} 1 & v(\theta) \cdot t - H/2 \le d \le v(\theta) \cdot t + H/2, \\ 0 & other \end{cases}$$

where d is the distance from the guided wave excitation point, and H represents the width of the tracking mask, as illustrated in Fig. 1 (c).

2.3. Damage Feature Fusion

Following the application of the mode tracking, the GW-MCT is synthesized using the root mean square function, effectively integrating the A0 mode, converted from the S0 mode, into a coherent mapping, as shown below:

$$MCT = \sqrt{\frac{1}{N} \sum_{t=t_1}^{t=t_N} \widetilde{u}(x, y, t)},$$

where N represents the total number of wave frames used to track the A0 mode converted from the S0 mode.

3. Experimental Results

The glass fiber reinforced polymer plate specimen, featuring cross stiffeners and three delamination regions, is illustrated in Fig. 3 (a). As shown in Fig 3 (b), the final MCT mapping of the wavefield accurately identifies both the locations and sizes of the delaminations, even in a complex specimen containing multiple stiffeners. The highlighted region near the center, indicating the location of the bonded piezoelectric transducer actuator, has been excluded from the final mapping for clarity.

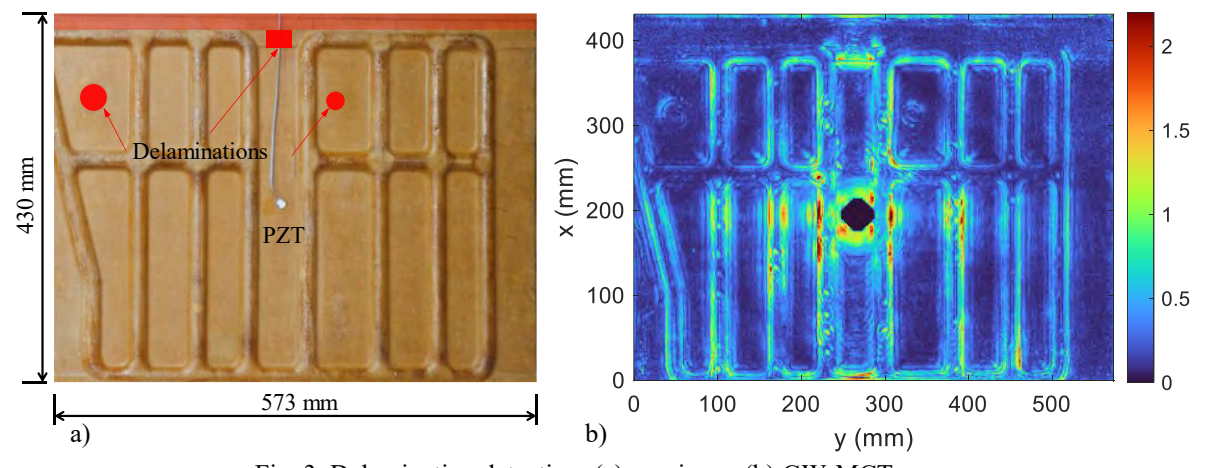


Fig. 3. Delamination detection: (a) specimen, (b) GW-MCT map.

- [1] D.K. Rajak, D.D. Pagar, R. Kumar, C.I. Pruncu, Recent progress of reinforcement materials: a comprehensive overview of composite materials, J. Mater. Res. Technol. 8 (2019)
- [2] M. Cao, Q. Ren, A.E. Pizhong, Q. Ae, Improved hybrid wavelet neural network methodology for time-varying behavior prediction of engineering structures, (2009).
- [3] T. Wandowski, M. Radzienski, P. Kudela. Lamb wave S0/A0 mode conversion for imaging the internal structure of composite panel, Composite Structures, (2025).

Detection of Subsurface Damage Caused by Impact in CFRP Composites Using an Eddy Current Sensor

Tomasz Rogala, 1* Grzegorz Tytko², Andrzej Katunin¹,

¹ Department of Fundamentals of Machinery Design, Silesian University of Technology, 44-100 Gliwice, Poland
² Faculty of Automatic Control, Electronics and Computer Science, Silesian University of Technology, 44-100 Gliwice, Poland
* Tomasz.Rogala@polsl.pl

Abstract: This study provides insights into the evaluation of subsurface damage in carbon fiber-reinforced polymer (CFRP) materials by utilizing eddy current sensor. The implemented sensor has a compact, single potcore coil design with a straightforward structure, operating effectively within the range of 109-113 kHz. CFRP specimens with barely visible impact damage (BVID), resembling damage encountered during an aircraft's operational lifespan, were examined. The inspection results demonstrated high sensitivity in detecting impact-induced damage, compared to ultrasonic testing outcomes. The proposed sensor effectively identified BVID caused by a 15 J impact and allows to detect subsurface damage. Detailed investigations shows that approximately 20% of the change in the resistance value is attributed to subsurface damage.

1. Introduction

Impact damage in CFRP composites is often invisible, worsens with environmental exposure, and requires rigorous non-destructive inspections for safety. Non-destructive testing (NDT) ensures the safety and reliability of aircraft composite structures by detecting and monitoring damage without material compromise. Among various NDT methods, eddy current testing (ECT) and ultrasonic testing (UT) are the most widely used because of their accuracy and repeatability. ECT detects damage in conductive materials through electromagnetic induction, where changes in coil impedance might indicate damage. Although modifications are often required for effective CFRP inspection due to its anisotropic conductivity. UT, using high-frequency waves, excels at detecting internal damage but faces challenges with subsurface damage detection. This study presents an application of an eddy current sensor with a pot-core coil [2,3,6] for detecting subsurface damage induced by impact damage in CFRP composites, validated by computed tomography (CT) and UT. Detailed numerical results quantify the change in coil resistance (dR) caused by subsurface damage.

2. Materials, testing procedures and reference results

The CFRP specimens, provided by Dexcraft s.c. (Poland), were fabricated using Vacuum Assisted Resin Transfer Molding with 60% volumetric fabric content, LG700 epoxy resin, and T700 carbon fabric, resulting in 2.5 mm thick sheets cut into 100×100 mm samples. To evaluate NDT performance, barely visible impact damage (BVID) was introduced using a drop-weight impact machine with steel hemispherical impactors of varying diameters of 28, 22 and 16 mm, denoted as B, C, and D, and different energy levels (15 J, 17.5 J, 20 J) [1,5].

Reference measurements were conducted to relate the ECT results to UT on barely visible impact damage (BVID) specimens. Inspections were carried out with a Boeing® MAUS® V automated scanner, utilizing a 5 MHz transducer at 0.254 mm/pixel resolution. Time-of-flight (ToF) C-Scans were performed to assess damage size and location based on the resolution information, material speed of sound and signal ToF. To estimate the fraction of the ECT scalar result and to attribute its fraction to the subsurface damage part, an additional CT scans were performed as well for some of the specimens' artificial damage in the form of flat bottom holes (FBH) were tested. FBHs were introduced using a 3 axis CNC milling machine with positioning accuracy > 0.01 mm using a VHM type milling cutter. These specimens were specifically designed to test the performance of NDT techniques. We selected 4 FBHs with a diameter of 2, 3, 4 and 7 mm with four depths of FBH of 0.5, 1, 1.5, 2 mm [4]. The eddy current test stand included a sensor, an LCR meter, and a computer. The sensor featured a 740-turn coil within a 14±0.2 mm F-1001 ferrite pot-core, protected by epoxy resin. Resistance values were measured using a Keysight E4980AL LCR meter (±0.1% accuracy) over a 70–120 kHz range, with 1 kHz increments for optimal sensitivity. Measurements, averaged over three trials, were controlled via Keysight BenchVue software. The sensor was moved in 0.5 mm steps across the specimen.

3. Results and evaluation of fraction of subsurface damage

A minimum resistance change dR of 5% was established as the damage detection threshold to balance the sensitivity to subsurface and small damage while minimising false positives. For barely visible impact damage (BVID), the optimal ECT frequency was 109-111 kHz, allowing reliable detection in all cases, including 15 J impacts. Changes in the resistance value dR of the eddy current coil obtained for specimens with BVID are presented in Figure 1. Direct estimation of subsurface damage using an EC sensor is challenging since impacts affect both subsurface and bottom surfaces and the result is represented by the scalar value. Therefore the analyses

of CT scans and known EC sensor outcomes from FBH specimens were performed to isolate the sensor's response to subsurface damage in CFRP specimens. ECT results were analysed to assess the impact of damage depth on sensor response. A consistent frequency of 111 kHz was used for both FBH and impact-damaged specimens. The results showed a proportional relationship between the resistance change and the damage size, leading to the development of a power model to estimate the sensor response based on the damage depth.

The analysis of ECT results for impact-damaged specimens requires additional data, as subsurface damage influences resistance changes along with deeper structural layers, making direct estimation challenging. To address this, CT scans were used to map the internal damage distribution, providing a detailed reference to correlate EC sensor responses with structural alterations. A data-driven approach was implemented, using morphological damage features such as eccentricity and solidity, extracted from CT images at different depths.

A power model established for damage depth based on FBH together with a model that correlates EC sensor responses with structural alterations were used estimate changes of value in resistance across specimen depth, allowing identification of trends in subsurface damage effects. The developed model was cross-validated by comparing its predictions with empirical ECT data, achieving an RMSE within acceptable limits. The results indicate that approximately 20% of the total resistance change is attributable to subsurface damage, which remains undetectable by UT scans. This demonstrates the ability of ECT to provide additional diagnostic insights, particularly to identify internal damage beyond the detection range of conventional ultrasonic techniques. The fraction of the ECT response attributed to subsurface damage is presented as the crossed areas in the Figure 1.

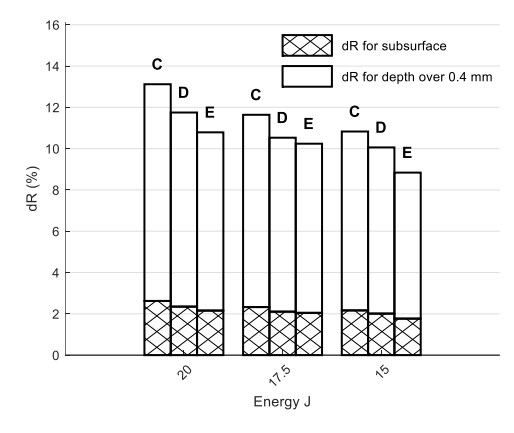


Fig. 1. Changes of resistance values for grouped for different energy levels and impactor diam. C, D, E.

4. Conclusions

The eddy current sensor with a pot-core coil effectively detects damage, including barely visible impact damage (BVID), with validated repeatability and a sensitivity threshold of $dR \approx 5\%$. Optimal detection was achieved within a frequency range of 109–113 kHz, enabling accurate assessment of surface and subsurface damage. The sensor's sensitivity to damage edges, particularly in BVID, enhances its capability for aircraft skin inspections and other composite structures where early damage detection is critical. The study highlights the complementary role of ECT alongside UT. By integrating CT scan data and a data-driven model, the contribution of subsurface damage to ECT responses was quantified. The results indicate that 20% of the resistance change in BVID specimens corresponds to subsurface damage beyond UT detection limits.

This work was supported in part by the Excellence Initiative—Research University Program implemented with the Silesian University of Technology, in 2024, under Grant 02/150/SDU/10-21-01.

- [1] Katunin, A. Wronkowicz-Katunin, and K. Dragan, 2020 "Impact damage evaluation in composite structures based on fusion of results of ultrasonic testing and X-ray computed tomography", Sensors, vol. 20, no. 7, p. 1867
- [2] Praphaphankul, N., Akutsu, A., and Sasaki, E. 2023 "Numerical study for development of subsurface crack detection using pulsed eddy current and swept frequency eddy current", Struct. Infrastruct. Eng., vol. 1, pp. 1–16
- [3] Tytko, G., Dziczkowski, L., Magnuski, M., Zhang, Z., and Luo, Y., 2023, "Eddy current testing of conductive discs using the pot-core sensor", Sens. Actuators A, Phys., vol. 349, Art. no. 114060.
- [4] Tytko, G., Rogala, T., Katunin A. and Yin, W. 2024 "Damage Detection in Carbon Fiber-Reinforced Composite Structures Using Eddy Current Pot-Core Sensor," in IEEE Access, 12, pp. 123609-123620.
- [5] Wronkowicz, A. "Non-destructive evaluation of composite aircraft elements based on ultrasonic testing and image analysis," Ph.D. dissertation, Dept. Fundamentals Machinery Des., Silesian Univ. Technol., Gliwice, Poland, 2018.
- [6] Zhang, S., 2024 "Analytical model of an E-core driver-pickup coils probe applied to eddy current testing of multilayer conductor", Appl. Comput. Electromagn. Soc. J. (ACES), vol. 38, pp. 914–921

Numerical simulation tool for speckle-based NDT systems: ESPI, shearography and laser speckle photometry

Elena Stoykova^{1*}, Violeta Madjarova¹, Ginka Ivanova¹, Branimir Ivanov¹, Nataliya Berberova-Buhova^{1,2}

¹Institute of Optical Materials and Technologies, Bulgarian Academy of Sciences, Acad. Georgi Bonchev Str., Bl.109, 1113 Sofia, Bulgaria ²University of Chemical Technology and Metallurgy, 8 St. Kliment Ohridski Blvd, 1756 Sofia, Bulgaria

*elena.stoykova@gmail.com

Abstract: Speckle-based non-destructive testing (NDT) for materials characterization is intensively developing area. This paper presents a simulation tool for numerical analysis of systems for electronic speckle pattern interferometry (ESPI), shearography and laser speckle photometry (LSP). The tool facilitates studying the impact of speckle properties, including temporal correlation, and existing noise sources for various optical designs on phase retrieval accuracy and process monitoring efficiency. Performance of an ESPI system is analyzed for the raw data capture by a polarization camera ensuring four steps phase-shifting.

1. Introduction

Speckle-based NDT techniques offer high sensitivity and full-field measurement capabilities, enabling detection of deformations and providing rapid, contactless inspection of critical components in aerospace, automotive, and manufacturing industries [1]. These advanced techniques support quality control and maintenance. Developing a simulation tool for speckle-based systems by numerical modelling of complex speckle patterns guides design and optimization of the measurement setups, enhances understanding of noise and error sources, and improves data interpretation in NDT applications. This paper presents a simulation tool elaborated in MATLAB and Python with a graphical user interface for accuracy analysis of measurements based on ESPI, shearography, and LSP. An ESPI system is analyzed to illustrate the tool's options using raw data generated for a polarization camera which provides four-step phase shifting.

2. Simulation tool - combined ESPI/LSP measurement

The developed simulation tool can be used for analysis of three types of measurements. For each of them, it includes the following blocks: i) generation of raw data, ii) extraction of relevant information, iii) accuracy evaluation. The first block implements computer generation of subjective speckle patterns with given speckle properties (size, contrast, evolution) taking into account the measurement principle to encode the sample change into phase information and adding temporal speckle correlation and noise sources. The second block comprises algorithms for phase retrieval and dynamic speckle analysis and includes filtering options. The third block is dedicated to quality assessment of the output results by using various metrics.

For description of the developed tool, we propose and prove by simulation ESPI measurement performed using a polarization camera. We consider an out-of-plane displacement for a sample with a rough surface, e.g. a subjected to heating plate of a composite material. The sample is illuminated by a laser light at wavelength $\lambda = 0.6328~\mu m$. The phase, $\varphi = \varphi_{sp} + \varphi_d$, of the complex amplitude, U_s , of light on the sample surface is composed by the speckle phase, φ_{sp} , uniformly distributed from 0 to 2π , and phase, $\varphi_d = 4\pi d/\lambda$, related to displacement d. Both φ_{sp} and φ_d depend on spatial coordinates and time. Temporal correlation in phase φ_{sp} is introduced following the normalized temporal correlation function, $\rho(\tau)$, where the time lag, τ , may vary in space and time. A vibration noise can be also added. The complex amplitude can be generated for an arbitrary intensity distribution in the illuminating laser beam. The complex amplitude of the light field on the sensor aperture is $U_{cam} = FT^{-1}\{H \cdot FT\{U_s\}\}$ where $FT\{\cdot\}$ denotes Fourier transform and H is a *circ* function in the Fourier domain with a cut-off frequency equal to $N_x \Delta D/(2\lambda f)$, where Δ , D and f are the pixel pitch, the diameter and the focal distance of the camera objective and we assume that numbers of pixels $N_{x,y}$ along x and y axes are equal. By varying the parameters of the cut-off frequency, patterns with different speckle size and contrast are generated. An option for introducing a shot noise at detection is envisaged.

An array of linear micro-polarizers in front of the camera pixels forms a structure of super-pixels of size $2\Delta \times 2\Delta$ (Fig. 1 top). The polarizers are oriented at 0° , -45° , 45° , 90° and provide simultaneously four phase-shifted images i_1, i_2, i_3, i_4 when the object and reference beams interfering on the camera's aperture are orthogonal circularly polarized beams. The set i_1, i_2, i_3, i_4 is formed from the image I of size $N_x \times N_y$, that is recorded by the camera at moment $t = s\Delta t$, (where Δt is the time interval between two consecutive images, $s = 1, 2 \dots S$). The following relations are valid: $i_1(k, l, s) = I(2m + 1, 2n + 1, s), i_2(k, l, s) = I(2m + 1, 2n + 2, s), i_3(k, l, s) = I(2m + 2, 2n + 1, s), i_4(k, l, s) = I(2m + 2, 2n + 2, s), k, l = 1 \dots N_{x,y}/2; m, n = 0 \dots N_{x,y}/2 - 1$. The obtained intensity distributions are given by the equations $i_1 = I_R + I_O + 2\sqrt{I_R I_O} cos \varphi$ and $i_4 = I_R + I_O - 2\sqrt{I_R I_O} cos \varphi$, $i_2 = I_R + I_O + 2\sqrt{I_R I_O} sin \varphi$ and $i_3 = I_R + I_O - 2\sqrt{I_R I_O} sin \varphi$ where I_R and I_O are the intensities of the

reference and the object beams (in the case of shearography, these are the intensities of both sheared beams). Such speckle patterns can be formed experimentally by using e.g. Fizeau interferometer for ESPI or Michelson interferometer for shearography. The speckle phase in the reference beam remains constant in time. For the ESPI simulation, we used the model of displacement given by $d(x = p\Delta, y = q\Delta, t = s\Delta t) = s\varepsilon h(p, q) p, q = 1..N_{x,y}$ and $h(p,q) = exp \left\{ -\left[(p - N_x/2)^2 + \left(q - N_y/2 \right)^2 \right] / \sigma^2 \right\}, \sigma = N_x/\alpha$. We assume that the displacement is accompanied by correlated in time evolution in speckle described by $\rho(\tau) = exp(-\tau/\tau_{corr})$ at $\tau_{corr}(p,q,s) =$ $au_{max} - s\epsilon \Delta th(p,q)$, where au_{max} is the constant maximal correlation radius. The simulated experiment included generation of S=200 speckle images at $N_{x,y}=1024$, $\tau_{max}/\Delta t=200$, $\alpha=3$, $\varepsilon=0.1$, $\epsilon=0.9$. The ESPI results are shown in Fig. 1 bottom and Fig.2. The absolute difference of $i_1(k, l, 36)$ and $i_1(k, l, 6)$ shows typical correlation fringes formed under uniform illumination at the beginning of the observation. Temporal variations of intensity $i_1(128,128,s)$ and $i_1(256,256,s)$ show that the correlation fringes in time for the modelled decreasing τ_{corr} are rather distorted. The recorded sequence of images permits temporal unwrapping to be applied to the phase at each pixel. The restored displacement at the end of the experiment (s = 200) for the speckled output is rather noisy. It can be substantially improved after applying a Gaussian filter to the unwrapped phase map. The deviation of the filtered output from the model is from --0.06 μm to 0.03 μm , which shows stable reconstruction despite the differences in I_0 values at a given pixel (k, l) of the composed images i_1, i_2, i_3, i_4 .

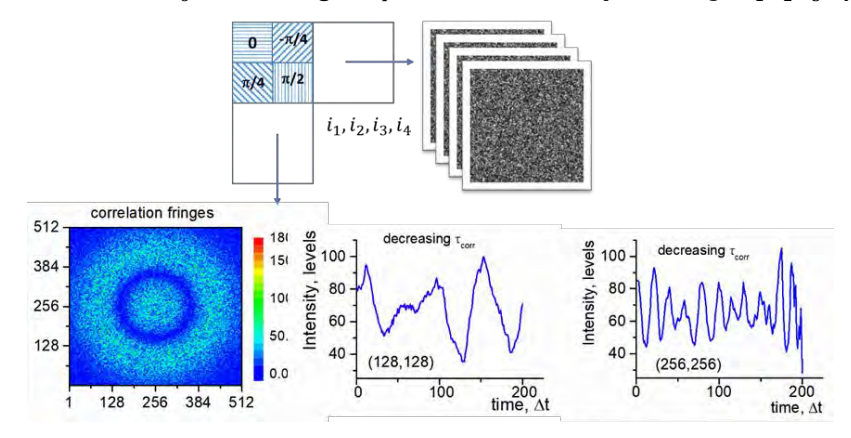


Figure 1 *Top:* structure of a super-pixel in a polarization camera with linear polarizers oriented at 0° , -45° , 45° , 90° . *Bottom*: correlation fringes at subtraction of the 36^{th} and the 6^{th} i_1 images, intensity i_1 at pixels (128,128) and (256,256) as a function of time.

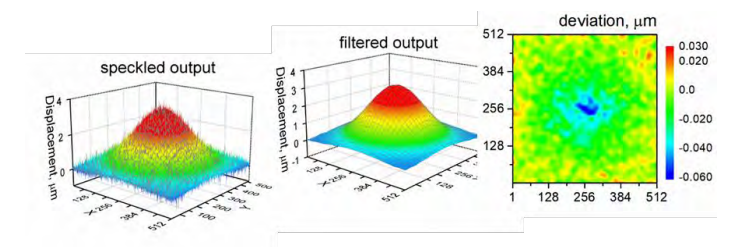


Figure 2 Displacement extracted from the speckled and filtered phase maps, and deviation of the filtered output from the model.

In summary, we presented a numerical simulation tool for analysis of speckled-based NDT systems that allows for studying their design, accuracy and options for quality improvement. Using this tool, we have proven that recording speckle images with a polarization camera illuminated by orthogonal circularly polarized reference and object beams facilitates ESPI measurement.

Acknowledgement

This research is conducted in the framework of COST Action CA21155 HISTRATE. This work is financially supported by the Bulgarian National Science Fund (BNSF) under project KΠ-06-H88/2.

References

[1] Zinoviy Nazarchuk, Leonid Muravsky, Dozyslav Kuryliak, 2023, *Optical Metrology and Optoacoustics in Nondestructive Evaluation of Materials, Springer Series in Optical Sciences*, Springer, Singapore https://doi.org/10.1007/978-981-99-1226-1

A Study on Specimen Dimension for Standardization of the Split Hopkinson Pressure Bar Test

Ozgen Colak*1,2, Hamdi Jmal², Samuel Berthe², Yuksel Cakir^{2,3} and Nadia Bahlouli²

¹Yıldız Technical University, Department of Mechanical Engineering, Turkey

²Strasbourg University, ICUBE, Strasbourg, France

³Istanbul Technical University, Department of Electronics and Communication, Turkey

* ozgen@yildiz.edu.tr

Abstract:

The Split Hopkinson Pressure Bar (SHPB) test is widely used to characterize the dynamic behavior of materials, yet it lacks a standardized testing protocol. This study investigates the influence of specimen dimensions on SHPB results using polypropylene (PP) specimens of varying sizes. Experimental results reveal that specimen dimensions have impact on test accuracy and the length-to-diameter (L/D) ratio of the specimen is crucial for ensuring accurate stress-strain measurements. These findings offer a critical step toward standardizing SHPB testing, improving the reliability and consistency of dynamic material characterization, particularly for polymeric materials like PP.

1. Introduction

In various practical applications, particularly in industries like aerospace and automotive, critical components often experience high strain rate loading due to events such as collisions, impacts, bird strikes in aviation, and lightning strikes. The Split Hopkinson Pressure Bar (SHPB) test is a widely used technique for determining the dynamic mechanical properties of materials under high strain rates. However, unlike other mechanical testing methods (such as tensile or compression tests, which follow ASTM or ISO standards), SHPB lacks a universally accepted standard. This lack of standardization introduces variability in specimen geometry, strain rate control, data processing, and experimental setups, making it difficult to compare results across different studies.

This work aims to identify the most influential parameters affecting SHPB results. By determining that specimen dimensions have impact, this research contributes to establishing fundamental guidelines for SHPB standardization. Future efforts should focus on developing an internationally recognized testing protocol to enhance the reliability and repeatability of SHPB experiments across different laboratories.

2. Split Hopkinson Pressure Bar (SHPB) Test Principle

SHPB test is a well-established method for determining the high strain rate behavior of materials. It is based on wave propagation theory, where a compressive stress wave travels through a specimen to evaluate its dynamic mechanical response. The SHPB apparatus consists of three main bars: striker, incident (input) and transmitted (output) bars. Striker bar is a projectile launched using a gas gun to generate an impact. Incident bar receives the impact and transmits a stress wave toward the specimen. Transmitted bar records the transmitted wave after it passes through the specimen, [1, 2]. A cylindrical polypropylene (PP) specimen is placed between the input and output bars. The elastic strain generated in incident and transmission bar are used to calculate the stress-strain in the sample. The nominal strain rate in sample is proportional to the reflected strain and inversely proportional to the length of specimen and is calculated as

$$\dot{\varepsilon}(t) = -\frac{2C_0}{L} \varepsilon_r(t) \tag{1}$$

where C_0 is the wave velocity of the bar material, L is the initial length of the specimen, $\varepsilon_r(t)$ is the time-resolved strain associated with the reflected pulse in the incident bar. Considering the elasticity modulus (E) and density (ρ) of the bars, the wave velocity of the bar is $C_0 = \sqrt{E/\rho}$. The nominal stress is calculated as,

$$\sigma(t) = \frac{A_t}{2A_r} E[\varepsilon_i(t) + \varepsilon_r(t) + \varepsilon_t(t)]$$
 (2)

where A_s and A_t are the cross-section areas of the specimen and transmission bar respectively, $\varepsilon_i(t)$ is the time-resolved strain associated with the incident pulse in the incident bar, $\varepsilon_t(t)$ is the time-resolved axial strain in the transmission bar and E is Young's modulus of the bar. True strain and stress are identified from nominal measurements as

$$\varepsilon_t(t) = -\ln(1 + \varepsilon_n(t))$$

$$\sigma_t(t) = \sigma_n(t)[1 - 2\nu\varepsilon_n(t)]$$
(3)

3. Experimental Results

Different specimen slenderness ratio (λ =L/D, L: thickness of the specimen, D: diameter of the specimen) are considered. 5 different slenderness ratios are used, however, here only results about two different specimen dimensions are given. Strain rate versus time and stress- strain curves are depicted in Fig. 1a, b.

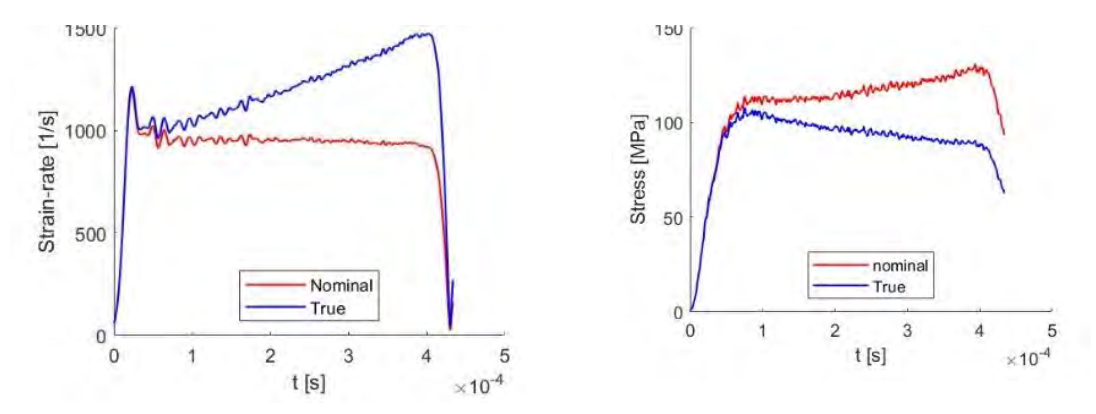


Fig. 1. Strain rate versus time and stress versus time curves (engineering (nominal) and true) for λ =0.5 (diameter of the specimen is 8 mm)

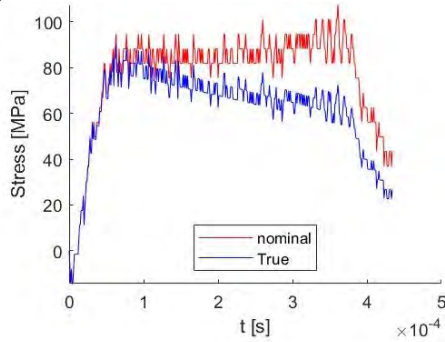


Fig. 2. Stress versus time curves (engineering (nominal) and true) for $\lambda=1$ (diameter of the specimen is 4 mm)

As seen in the Fig. 2, there is oscillations in the stress strain curves. The smaller diameter specimen (D=4 mm) shows a much lower peak stress and fluctuates considerably, indicating instability or higher sensitivity to experimental conditions.

4. Conclusions

The SHPB test results indicate that specimen size significantly affects the mechanical response. Lower slenderness ratio specimens provide higher peak stress and more stable deformation behavior. Higher one shows lower stress and significant oscillations, suggesting that they may be less reliable for precise mechanical property evaluation. For SHPB compression tests, an L/D ratio between 0.5 and 1.0 is commonly used to balance stress uniformity and minimize end effects. However, the optimal ratio may vary based on material behavior and testing conditions.

- [1] Siviour, C. R. and Jordan, J. L., 2016, "High strain rate mechanics of polymers: a review", Journal of Dynamic Behavior of Materials, 2, pp.15–32.
- [2] Kolsky, H., 1949, "An investigation of the mechanical properties of materials at very high rates of loading", Proc. Phys. Soc. Sect., B 62, 676.